ISSN 0110-3326

EARTHQUAKE RESISTANT PRECAST CONCRETE BUILDINGS: SEISMIC PERFORMANCE OF CANTILEVER WALLS PRESTRESSED USING UNBONDED TENDONS

by

Dr A M Rahman
and
Dr J I Restrepo

Department of Civil Engineering
University of Canterbury
Christchurch, New Zealand

Research Report 2000-5
August 2000

Sponsored by the Public Good Science Fund,
Foundation for Research, Science and Technology
Contract UOC 808

TABLE OF CONTENTS

ABSTRACT

The magnitude of the economic losses sustained by communities subsequent to recent moderate and large earthquakes has prompted the need for seismic design philosophies and construction methods aimed at minimizing structural and non-structural damage. In this project, the use of unbonded prestressing tendons as a connection mechanism in precast concrete construction is investigated for New Zealand materials and conditions.

Vertically stacked precast wall units are post-tensioned together by means of prestressing strands, which are passed through vertical ducts inside the walls. As the walls are subjected to lateral displacements, gaps form at the base of the walls. The gaps reduce the system stiffness. As long as the prestressing strands are kept within the elastic limit, they can provide a restoring force which will return the walls to their initial position. Thus, the lateral force-displacement response may be idealised by a non-linear elastic relationship. The integrity of the walls is maintained as no plastic hinges form in the wall units and there are no residual post-earthquake deflections.

Three half-scale precast wall units were tested individually in this study. Two specimens (Units 2 and 3) incorporated energy dissipation devices in the form of dog-bone milled reinforcing bars cast into the foundation beam and grouted into the walls at the horizontal construction joints. In addition, gravity load effects were simulated in Unit 3 by means of external post-tensioning bars bolted to the strong-floor. The walls were subjected to drift (lateral displacement-to-height of actuator from wall base) levels reaching 4%. Damage was limited to concrete spalling at the ends of the walls. A linearly elastic response was effected in Unit 1 while a flag-shaped hysteresis response was observed in Units 2 and 3. The energy dissipators in Units 2 and 3 provided up to 14% equivalent viscous damping.

The Public Good Science Fund of the New Zealand Foundation of Research, Science and Technology provided funding for this project under contract UOC 808.

ACKNOWLEDGEMENTS

Funding for this project provided by the New Zealand Foundation of Research, Science and Technology (FRST) under the Public Good Science Fund is gratefully acknowledged.

The following companies kindly provided material for construction of the specimens: Firth Industries Ltd., Hurricane Wire Products Ltd., and Construction Techniques Ltd.

The assistance of Mr P. Murphy in construction and testing of the specimens is acknowledged. A debt of gratitude is owed to Mrs M. Callahan, Mrs A. Roberts, and Mr T. Holden for the effort in preparing this report.

The authors would also thank the following individuals for their useful contribution, constructive and interesting discussions and valuable advice: Prof. M.J.N. Priestley, University of California at San Diego; Prof. J. Stanton, University of Washington at Seattle; Dr M. Rodriguez, National University of Mexico; Dr R.C. Fenwick, Dr J. Ingham, Mr P. Laursen, University of Auckland; Mr D.K. Bull, Holmes Consulting Group Ltd.; Mr R.W. Irwin, Mr R. Robinson and Mr P. Wilby, Construction Techniques Ltd. and to Mr G. Banks, Alan Reay Consultants Ltd.

LIST OF FIGURES

LIST OF TABLES

NOTATION

Roman Symbols

a = Depth of equivalent rectangular stress block in the stress distribution profile of a concrete section, mm.

A_g = Wall cross section area, mm^2.

A_{ps} = Total area of prestressing strands, mm^2.

A_{sd} = Area of reduced segment of energy dissipator, mm^2.

A_{ps} = Area of prestressing tendons, mm^2.

A_r = Aspect ratio of wall = H_w/L_w.

b = Beam width, mm.

b_e = Effective width of concrete element without concrete cover, mm.

b_w = Wall width, mm.

c = Distance from extreme compression fibre to neutral axis in the stress distribution profile of a concrete section, mm.

c_c = Concrete cover, mm.

C = Resultant internal compressive force acting at the ends of the wall, N.

d_{ed} = Location of energy dissipator furthest from wall edge in compression, mm.

d_{ps} = Distance of prestressing tendon furthest from neutral axis depth from the extreme compression fibre at the toe of the wall, mm.

D_m = Coefficient determining the contribution of higher mode effects to the base shear, as a function of effective first and second mode masses and mass assigned to the wall.

E_D = Dissipated energy as measured by the area under the hysteretic response, N.mm.

E_{ps} = Elastic modulus of a prestressing tendon, MPa.

E_c = Elastic modulus of concrete= $6900 + 3320\sqrt{f'_c}$, MPa.

E_{so} = Maximum strain energy, N.mm.

f_c = Compressive strength of concrete, MPa.

f'_c = Compressive strength of concrete, MPa.

f'_{cc} = Axial compressive strength of confined concrete, MPa.

f_{cr} = Modulus of rupture in concrete $= 0.8\sqrt{f'_c}$, MPa.

f_{psu} = Ultimate tensile strength of a prestressing tendon, MPa.

f_{psi} = Initial stress in prestressing tendons after losses, MPa.

f_{psy} = True limit of proportionality of a prestressing tendon, MPa.

f_{slp} = Nominal limit of proportionality of the prestressing tendon corresponding to 0.2% strain offset, MPa.

$\bar{f}_{su}$ = Mean ultimate tensile strength of reinforcement used in the manufacture of the energy dissipator, MPa.

f_{su} = Ultimate tensile strength of non-prestressed reinforcement, MPa.

f_y = Lower characteristic yield strength of non-prestressed reinforcement, MPa.

F = Force due to friction between the precast concrete wall components or between the wall and foundation, = $\mu_f P$, N.

F_{ed} = Ultimate tensile force of an energy dissipator, N.

F_{edy} = Yield strength of an energy dissipator, N.

F_{lp} = Tensile in a prestressing tendon corresponding to the nominal limit of proportionality, N.

F_{psi} = Prestressing force in tendons after losses, N.

h_b = Overall beam depth, mm.

H = Height of the resultant static lateral force from base of wall, mm.

H_w = Wall height, mm.

H_1 = Height of the resultant of the dynamic lateral inertial forces from base of wall, mm.

I_g = moment of inertia of the gross cross section, mm^4.

k = Concrete strength enhancement coefficient due to confinement.

L_e = Length of milled segment of energy dissipator, mm.

L_p = Plastic hinge length, mm.

L_{ps} = Total unbonded length of prestressing tendon, mm.
= 4800 mm for Units 1 and 2.
= 4840 mm (for Unit 3).

L_w = Length of wall, mm.

M = Bending moment at base of wall due to lateral forces, N.mm.

M_g = Bending moment at which separation of the beam and column initiates, N.mm.

M_{lp} = Bending moment corresponding to the wall's limit of proportionality, N.mm.

M_{max} = Maximum base moment found from a static push-over analysis based on an assumed vertical distribution of equivalent lateral forces., N.mm.

M_u = Moment at the collapse prevention limit state, N.mm.

M_w = Mass assigned to a wall, equal to th total building mass divided by the number of walls, kg.

M_1 = Effective first mode mass, kg..

M_2 = Effective second mode mass, kg.

n = Number of storeys in a building.

N^* = Concentric axial load due to gravity loads, N.

p_s = Volumetric confinement ratio at wall toes.

p_t = Ratio of transverse reinforcement in wall units.

p_l = Ratio of longitudinal reinforcement in wall units.

P = Total axial compressive force in wall, which is represented by the initial post-tensioning force in the prestressing strands and any gravity loads, N.

$\ddot{u}_{o,max}$ = Peak acceleration for the design level ground motion, mm/s^2.

V = Lateral force acting on the wall, N.

V_{cr} = Lateral force in actuator associated with the development of first flexural cracking in a wall, N.

V_g = Lateral force in actuator at which separation between the wall toe and foundation beam initiates, N.

$V_{H,max}$ = Contribution of higher response modes to base shear, N.

V_{lp} = Lateral force at "yield" (limit of proportionality) of system, N.

V_{max} = Maximum base shear demand, N.

V_{rock} = Equivalent static lateral force resulting in rocking, N.

V_{slide} = Equivalent static lateral force resulting in sliding, N.

V_u = Lateral force at the collapse prevention limit state, N.

$V_{1,max}$ = Base shear derived from the first mode of response assuming a vertical distribution of equivalent lateral inertia forces, N.

$\bar{x}_1$ = The resultant height of the equivalent inertia forces assuming a vertical distribution of these forces, mm.

Z = Elastic section modulus, = $b_w L_w^2 / 6$, mm^3.

Greek Symbols

α, β = Parameters defining the equivalent compression stress block in confined concrete.

Δ_{ed} = Elongation of energy dissipator, mm.

Δ_h = Horizontal displacement of wall, mm.

Δ_{ps} = Elongation in prestressing tendon due to wall rocking, mm.

Δ_{psd} = Elongation of the prestressing tendon at the design lateral drift of 2.5%

Δ_{psy} = Elongation of prestressing tendon corresponding to nominal yield strain, mm.

Δ_v = Vertical displacement of wall, mm.

ΔF_{ps} = Variation of post-tensioning force in prestressing tendon due to wall rocking, N.

ε_{ed} = Average strain in energy dissipator.

ε_{su} = Uniform strain of Grade 430 reinforcement ≈ 0.16.

ε_y = Yield strain of Grade 430 reinforcement ≈ 0.003.

ζ_{eq} = Equivalent viscous damping ratio.

η = Averaging factor for the forces in the prestressing tendons.

θ = Rotation of wall = Δ_h / H.

θ_{lp} = Lateral drift of the wall at "yield" (limit of proportionality).

θ_p = Plastic rotation due to a lateral force defined as the total curvature between two points.

θ_u = Wall drift at collapse prevention limit state = 2.5%.

μ_f = Coefficient of friction.

ϕ = Curvature of wall defined as the variation of the rotation over a unit length.

ψc = Vertical distance at the ends of the wall over which rotations are assumed to occur, expressed as a fraction of the neutral axis depth, mm.

ω_v = Dynamic shear magnification factor designating the location of the resultant of the lateral inertial forces including higher mode effects.

1. EXECUTIVE SUMMARY

The use of precast concrete construction in New Zealand has been developing at a notable pace for the past twenty years. In this country, the seismic design of precast concrete wall units has followed the "emulation" concept in which the wall units are designed to perform in a manner similar to cast-in-place monolithic construction. This is achieved by providing connections of sufficient strength so that the inelastic response expected of the system is effected by means of the formation of plastic hinges. While this guarantees performance commensurate with that stipulated in the relevant New Zealand design standards for cast-in-place concrete construction, the advantages of precast concrete construction are not fully utilized. Increased on-site labour is necessary to achieve the detailing that is required in emulation type precast construction, especially with regard to the continuity of vertical reinforcement passing through horizontal joints where plastic hinges are expected to develop.

The aim of this project is to increase the economic benefits of precast concrete construction in seismic environments. This can be achieved by developing systems that limit post-earthquake damage in the precast elements and eliminate the post-earthquake residual lateral displacements in the system. The use of unbonded prestressing tendons as the connection mechanism between precast concrete wall units is ideal in the realization of this aim. Continuity of the vertically stacked precast wall elements is achieved by post-tensioning the unbonded prestressing tendons so that an effective load path is maintained at large drift levels. The horizontal shear force must be transferred through the horizontal connection. Sliding shear must be prevented by ensuring a suitable shear transfer mechanism. For example, shear can be transferred solely by a friction mechanism or in combination with shear keys or vertical dowels. When reliance is placed only on friction, the aspect ratio (height/length) of the wall determines the manifestation of sliding in the response of the wall. Therefore, this value must be selected such that rocking is the predominant deformation mode. The post-tensioning force in the prestressing strands provides the precast concrete components with a self-centering capability. Thus, post-earthquake residual drifts may be practically eliminated even after large lateral displacement demands. The response of the system may therefore be described by a non-linearly elastic relationship in

which the change of system stiffness is associated with the development of a gap between the rocking wall and the supporting foundation or between the vertically stacked walls.

In recognition of the potential of this system, and in order to introduce this system to the New Zealand construction industry, a series of tests were designed and conducted at the University of Canterbury. In addition to the use of local material and construction practices, some additional low-cost features were added to improve the energy dissipation capacity of the system. Three half-scale precast concrete wall units were subjected to a quasi-static reversed cyclic load regime. The reinforcement details of the wall panels, prestressing strand arrangement and loading regime were similar in all three units. The prestressing strands were close to the wall mid-length. A simple energy-dissipation device in the form of a standard reinforcing bar with a reduced diameter over a specific length (dog-bone) was incorporated in two of the units. Gravity load effects were simulated in one unit by means of external post-tensioning bars. Conventional rectangular ties and longitudinal bars provided confinement in the wall toes where the rocking mechanism of the wall against the foundation was expected to result in large concrete compressive strains. High drift levels (exceeding 3%) were attained in the three units with only minor damage concentrated in the toes of the walls. This damage is much less than would be experienced by a monolithic cast-in-place wall designed for full ductility. Near elastic behaviour of the prestressing strands was maintained even at high drift levels. This resulted in the absence of residual drifts. The dog-bones proved to be very effective in providing energy dissipation to the linearly elastic response of the system, resulting in equivalent viscous damping ratios of up to 14%.

2. INTRODUCTION

2.1 General

Since the mid-1980s the use of precast concrete as a construction material has increased rapidly in New Zealand. Ease and speed of erection, high quality control and a wide range of aesthetic finishes have been factors that have contributed to the appeal of precast concrete with architects, developers, designers and contractors. However, research into the seismic performance of precast concrete elements and their connections has not kept pace with their increased use. In New Zealand, research has been mainly directed towards verification of existing designs, detailing practices and construction techniques [M2, R1]. A study group was formed in 1988 to outline the needs of the precast industry, recommend topics requiring further research and define recommended practice in New Zealand [G1]. Among the topics requiring further research was the design and behaviour of precast concrete structural wall systems.

The design of precast concrete structural walls may be categorised into two approaches: emulation and jointed. In the former, the strength of the connections between the precast units is such that the inelastic response is restricted to specifically detailed regions within the wall units. These regions correspond to the plastic hinges in monolithic construction. While this allows designers the freedom to apply the well-established guidelines of monolithic construction, post-earthquake repairs are expected due to the damage associated with the development of plastic hinges.

The "jointed" design philosophy allows for the connections between the wall units to provide the energy dissipation mechanism at large lateral displacements. While the relevant New Zealand design standard [S2] allows for both types of construction, the jointed type of construction is not widely applied and has been restricted to structures with limited ductility demands. This is due to the fact that the ductility capacity of the system is limited by the geometry of the connection. In connections designed and manufactured according to conventional practice, large ductility demands concentrate within a limited distance thus imposing excessive strains on the connections.

Therefore, a construction technique is required which would combine the ease of installation of jointed systems with the ductility capacities associated with emulation type construction.

A collaborative USA-Japan research programme (PREcast Seismic Structural Systems, PRESSS) [P3] was initiated in 1990 to recommend guidelines for the seismic design of precast concrete buildings. As part of this programme, investigations have been conducted into both precast moment-resisting frame and precast structural wall systems which incorporate partially unbonded prestressing tendons as a connection mechanism between the precast elements. The fundamental performance criteria of these connection mechanisms are:

- The integrity of the precast concrete elements is maintained as the structure is subjected to large lateral displacement demands,

- The post-earthquake residual drifts are minimised.

These objectives are achieved by means of the unbonded prestressing tendons in which the unbonded length, location and initial prestressing force are such that the tendons maintain their elastic characteristics even at drift levels corresponding to the expected maximum seismic demand.

2.2 Current Design Criteria

While the New Zealand concrete structures design standard, NZS 3101:1995 [S2], includes some provisions for the design of precast concrete structures, no guidelines exist for the use of unbonded prestressing strands as connections in precast concrete walls. The use of partially unbonded tendons in beam-column joints is allowed if designed in accordance with the recommendations given by Priestley and Tao [P4].

Tentative design guidelines for precast concrete walls connected by partially unbonded prestressing strands that achieve the suggested performance objectives will

be presented here within the context of the New Zealand Loadings Standard, NZS 4203: 1992 [S1].

The performance of structures in the above standard is intended to fulfil two limit states based on the expected seismic demand:

a) The serviceability limit state defines the acceptable levels of deformations and deflections within which the appearance or function of buildings are maintained during a 10-year average return period seismic event.

b) The ultimate limit state stipulates the preservation of the strength, and stability of any part of the building. Seismic loading levels for this limit state correspond to earthquakes with a 475-year average return period.

The design objectives of the proposed system, in accordance or above the current requirements, may be enumerated as follows:

a) Spalling of cover concrete at the ends of the walls shall be the only acceptable level of damage under a serviceability loading level.

b) The integrity of the wall toes above the horizontal connection must be preserved at the collapse prevention limit state (which corresponds to a 2500-year average return period event). Confinement of the wall toes must be provided to ensure crushing of the concrete does not occur within the expected compressive strains.

c) The prestressing tendons must remain elastic even at lateral displacement levels corresponding to the collapse prevention limit state for the following reasons:

   i) In order to preserve the restoring capability of the prestressing strands, thus eliminating post-earthquake residual drifts of the structure,
   ii) The clamping action provided by the prestressing tendons is maintained. This clamping force contributes to the shear resistance and is necessary for structural stability through the preservation of an effective load path.

2.3 Performance-Based Design

The engineering community has recently started to perceive the need to review code definitions of acceptable structural performance due to the magnitude of the economic losses sustained by communities after recent seismic events. At present, the performance of structures is designated by two limit states expressed in terms of the probability of exceedence of a seismic event of a certain magnitude occurring within a specific exposure. The objectives of specifying these limit states, as stipulated in NZS 4203: 1992 [S1], are:

- To sustain all loads to be encountered during the life of the building with an adequate margin of safety.

- To limit deformations of the structure within allowable limits.

- To avoid structural damage and the limitation of other damage during an event that occurs occasionally.

- To prevent collapse and irreparable damage and to minimize the probability of injury due to loss of life of people in and around the building during an event that occurs rarely.

Thus, while the issues of life safety and collapse prevention during a large magnitude event are clearly addressed, the limitation of structural damage during such an occasional event is not. Current research trends [P2] have focused on the latter aspect with the resulting development of design philosophies and construction techniques that place greater emphasis on reducing the economic impact of earthquakes on communities.

The fundamental goal of the proposed system is the prevention of damage to the precast concrete wall units designed as the lateral load resisting system in a building. This is achieved by the preclusion of plastic hinge development. The lateral displacement demands are attained through the development of gaps at the

horizontal joints between the precast wall units, see Figure 2.1 (a). The system performance may be described as non-linearly elastic with gap formation at the horizontal joints between the precast concrete wall units. This gap results in a reduction in stiffness which is recovered as the elastic prestressing tendons restore the walls to their original positions, see Figure 2.1(b).

The prevention of inelastic deformations in the prestressing tendons is a primary objective, as this will preclude post-earthquake residual drifts and affects the overall system response. In addition, the post-tensioning forces in the prestressing tendons provide a clamping force that contributes to the prevention of sliding of the walls. The initial post-tensioning force, location of the prestressing tendons within the length of the wall, unbonded length and seismic demand are factors which must be considered to achieve this performance criterion.

The concrete at the wall toes immediately above the horizontal connection will be subjected to relatively large strains during wall rocking. Adequate confinement should be provided to ensure that crushing of the concrete in these regions does not impair the overall wall response.

The lateral force-deformation response of the proposed system can be determined from first principles, in a similar fashion to the monolithic cast-in-place system. Thus, the response of the proposed system to lateral deflections may be assessed from characteristic stress-strain relationships of the constituent materials. The amount of detailing required in the proposed system to achieve the expected lateral displacement demands is minimal compared to monolithic cast-in-place construction.

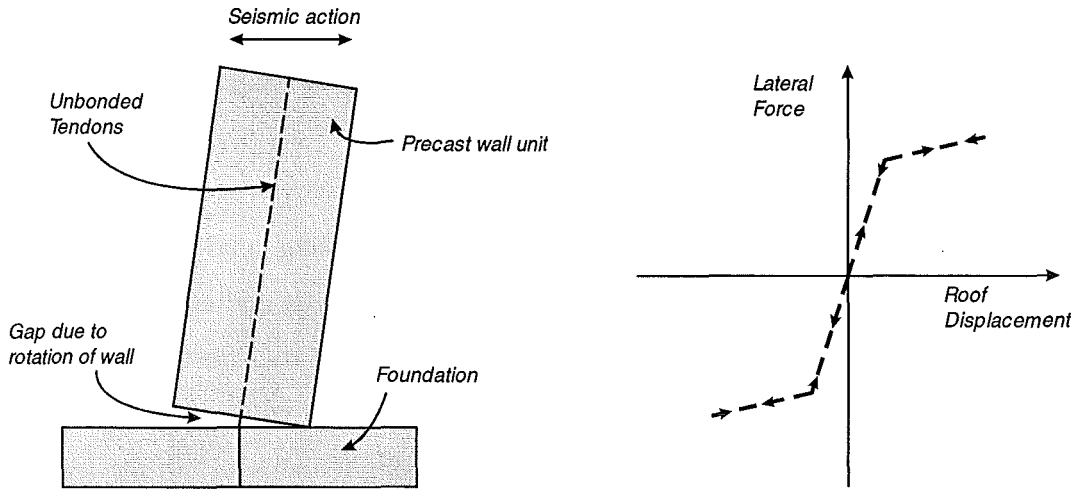

Figure 2.1: Schematic representation of proposed system with lateral force displacement behaviour.

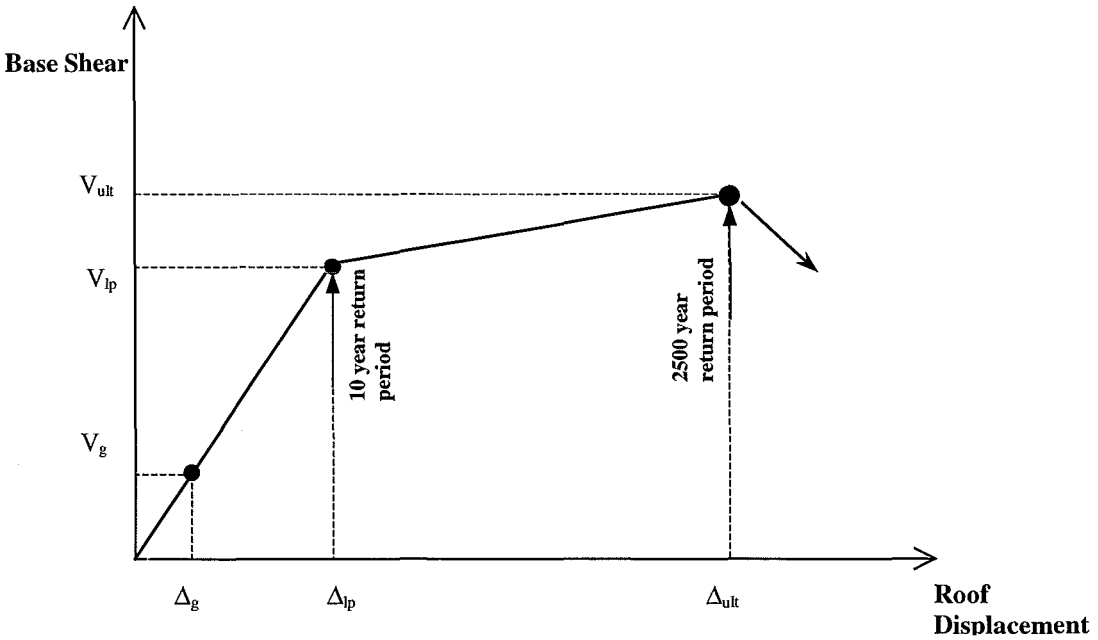

Figure 2.2: Performance limits of proposed system.

The recommended performance of the proposed system is shown in Figure 2.2 in which the important properties are as follows:

- The point (V_g and Δ_g) represents the stage at which separation of one end of the wall from the supporting wall or foundation occurs (lift-off).

- Limit of Proportionality (V_{lp} and Δ_{lp}): The non-linear response of the wall resulting from its separation from the base is limited. Pronounced non-linear response will commence at stress levels corresponding to non-linear behaviour of constituent materials. In a properly designed wall this is defined as the point where non-linear behaviour of the concrete in compression is initiated, at a compressive stress in the extreme edge of the wall equal to $0.5f'_c$. The lateral force and lateral displacement of the wall corresponding to this stress level are V_{lp} and Δ_{lp}, respectively.

- Yielding of the prestressing tendons (V_{ult} and Δ_{ult}): The lateral force level at which the prestressing tendons attain a tensile stress level corresponding to their limit of proportionality. This limit state represents failure of the precast post-tensioned wall.

The two points (Δ_{lp}, V_{lp}) and (Δ_{ult} ,V_{ult}) define the bilinear representation of the response of precast concrete walls with partially unbonded tendons.

2.4 General Characteristics of the Proposed System

The proposed connection mechanism aims to address the need of limiting the economic impact of earthquakes through reducing the post-earthquake damage and rehabilitation. The use of unbonded prestressing tendons for connecting precast concrete wall units enhances the seismic performance of precast construction while maintaining its economic benefits.

The main attributes of the proposed system may be enumerated as follows:

- A robust system is achieved which is insensitive to the detailing at the horizontal joints of the precast wall units as no main vertical reinforcement passes through that joint except for the prestressing strands.

- Non-linear response of the system is effected by means of the development of gaps at the horizontal joints between the precast concrete units and not by means of conventional plastic hinges as in monolithic cast-in-place construction. Thus, the integrity of the units is maintained resulting in a reduction of post-earthquake reconstruction and repairs, thereby allowing the rapid resumption of businesses and essential services.

- The preclusion of conventional plastic hinges eliminates the post-earthquake residual drifts that are expected from monolithic cast-in-place construction that is subjected to equivalent levels of lateral displacement levels. The prestressing tendons must remain elastic in order to achieve this attribute.

- The basic lateral force-deflection characteristics of the proposed system may be represented by a non-linearly elastic idealisation, see Figure 2.1. The gap at the horizontal connection between the precast units results in a softening of the system stiffness. Limited non-linear concrete behaviour in the compression regions also contributes to the non-linear response of the system. Most of the initial stiffness of the system is regained upon closing of the gaps between the precast units.

- The absence of conventional energy dissipation mechanisms (i.e. plastic hinges) may result in large lateral drift demands in addition to an increased number of response cycles. These increased displacement demands are effected as rotations at the base of the walls and not as a result of increased interstorey drift.

- The increase in fundamental natural period of the structure at separation between the precast units often results in a reduction in lateral force demands. This partly compensates for the lack of energy dissipation in the system.

- Load paths are not affected by the response of the system to large lateral drift levels. This is due to the restoration of the initial elastic stiffness of the system provided the prestressing steel has maintained its elastic properties. Strength degradation even at drift levels corresponding to the ultimate limit state is expected to be negligible.

While the non-linear elastic characteristic of the proposed system guarantees the integrity of the walls units after a seismic event, no effective means of energy dissipation exists in the proposed system. This places excessive deformation demands on the non-structural elements of the structure in which the proposed system is incorporated. Damping of the system with some form of energy dissipation device ensures that the large lateral drift capacity of the proposed system does not result in excessive deformation demands on the non-structural elements. In the present study, the supplementary damping is in the form of dog-bones manufactured from standard 20 mm diameter reinforcing steel bars.

2.5 Objectives

Recent research trends are directed towards the limitation of post-earthquake damage in structures [P2]. Investigations into the use of unbonded prestressing strands as a connection mechanism in precast construction, for both moment resisting frame and wall systems, for seismic regions has shown extremely promising results [C1, E1, K1-K3, M1, P1, P4, P5]. Due to the extensive use in New Zealand of precast concrete wall units as a lateral force resisting system, the feasibility of this system for New Zealand construction practices and conditions has been the main objectives of the present study. Reducing the seismic damage sustained by precast concrete structures will enhance the economic benefits of this type of construction.

3. LITERATURE REVIEW

3.1 General

The literature pertaining to this construction method is limited, as the merits of precast construction post-tensioned with partially unbonded tendons have only recently been recognised. The bulk of research has emanated from the United States where a four phase research programme (PREcast Seismic Structural Systems, PRESSS) was initiated in 1990 to recommend guidelines for seismic design of precast concrete buildings [P3]. Extensive analytical and experimental investigations have already been conducted under this programme and are described below. These studies culminated in the large-scale test of a 60%-scale model of a five-storey building which incorporated a number of lateral load resisting systems [N1, P5]. Research conducted to date is summarised in the following sections.

It is to be noted that while most of the research under the PRESSS programme has been conducted on precast concrete frame systems, the principles are similar for precast concrete wall systems.

3.2 University of California at San Diego

In a numerical investigation conducted by Priestley and Tao [P4] on precast concrete frame construction, prestressing strands were used to connect precast concrete beams to precast concrete columns spanning several floors. These strands were unbonded for some distance on either side of the beam-column joint. A 2% volumetric ratio of spiral confinement was suggested at the beam end regions with a spiral pitch not exceeding one-fourth of the spiral diameter. Extensive dynamic inelastic time-history analyses were conducted and the results were compared to monolithic cast-in-place construction. The bi-linear idealisation of the lateral force-displacement characteristics shown in Figure 3.1 was used in the analyses. Tao and Priestley associated the limit of proportionality (Δ_y, F_y) shown in Figure 3.1 with twice the force required to decompress the post-tensioned beam. The ultimate point, (Δ_u, F_u), was associated with the limit of proportionality of the tendons.

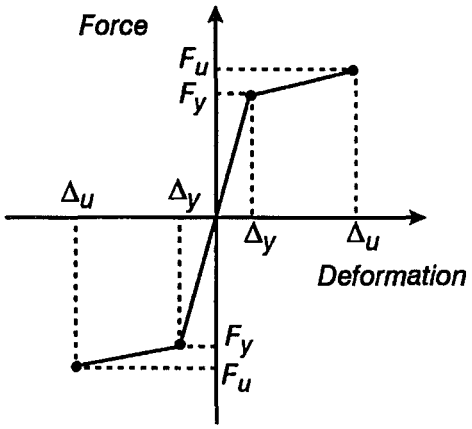

Figure 3.1: Bilinear representation of lateral force-displacement assumed by Priestley and Tao [P4].

The authors concluded that partially unbonded post-tensioned connections in precast frame construction would not only reduce the post-earthquake residual drifts but also reduce the requirements for shear reinforcement at the beam-column joints. This is due to the clamping action of the post-tensioning force, which would assist in transmitting joint shear forces by means of a direct strut action in the joint. These benefits are provisional on the elastic response of the post-tensioning steel which is determined by the unbonded length, the location of steel within the section and the initial prestressing force.

An experimental study of two precast beam-column subassemblages representing exterior and interior joints was subsequently conducted [M1] to verify the conclusions of Priestley and Tao [P4] and to outline the requirements of a more extensive experimental study within the PRESSS programme. Spiral reinforcement extending a distance equal to the beam depth was used to confine the concrete in the segment of the beam adjacent to the column, see Figure 3.2. Reduced beam-column joint shear reinforcement was provided to investigate the transfer of forces in this region.

Epoxy grout was used during the assembly of the precast segments and multi-strand tendons were post-tensioned in oversized ducts. Despite the low reinforcement content in the beam-column joint no failure occurred and the cracks were well distributed. Inelastic compression of the concrete in the beam at larger ductility levels resulted in a reduction in stiffness. However, the extent of overall damage was minimal and easily repairable.

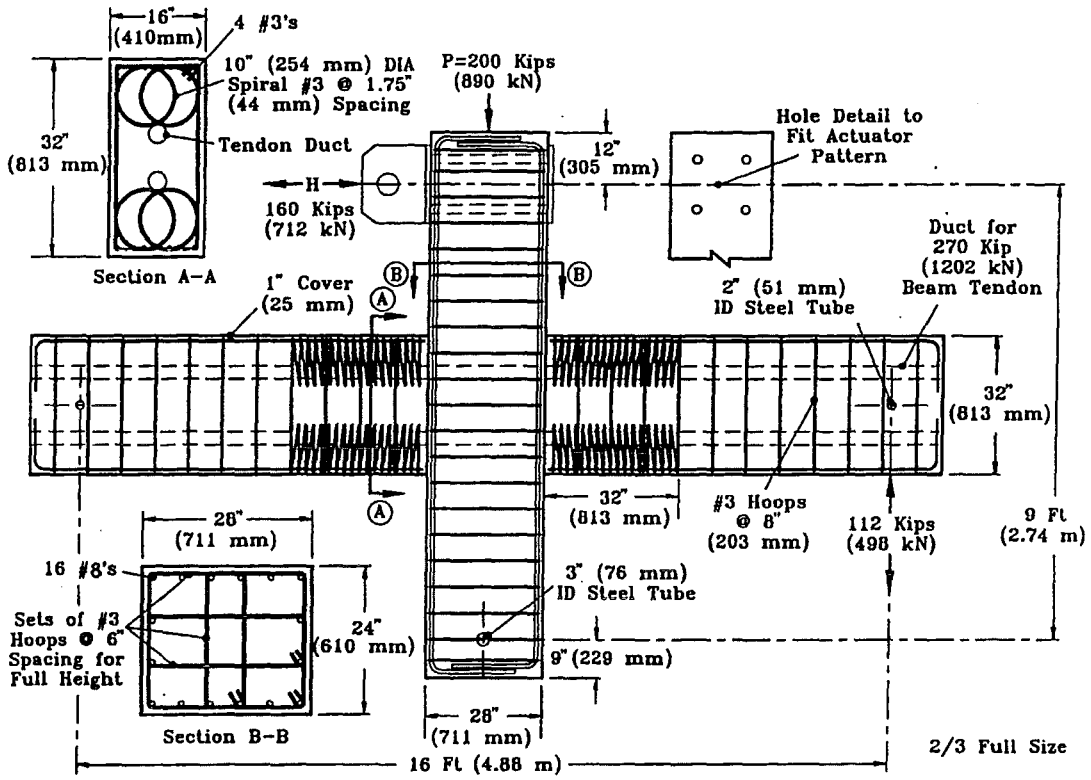

(a) Interior Joint.

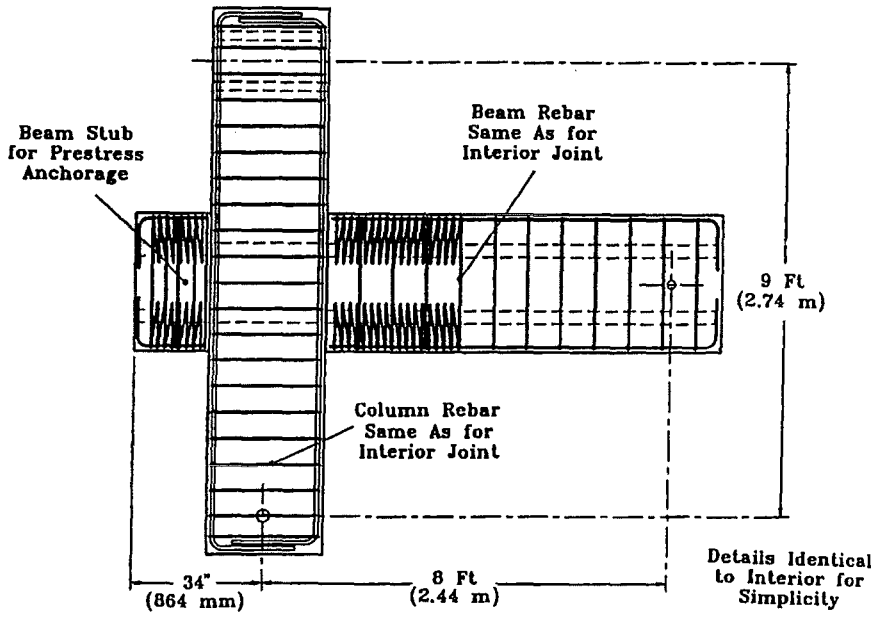

(b) Exterior joint.

Figure 3.2: Precast concrete beam-column subassemblages of MacRae and Priestley [M1].

The final phase of the PRESSS programme culminated with the construction and testing of a 60% scale five-storey precast concrete building at the University of California, San Diego [N1, P5]. The test building was based on a prototype building with floor plan dimensions of 30.5 m x 61 m. The use of a pseudo-dynamic testing procedure permitted the construction of the building with a reduced floor plan area of 4.6 m square, see Figure 3.3. Two moment resisting frames provided the lateral force resistance in one direction whereas coupled structural walls provided the resistance in the orthogonal direction.

Four lateral force resisting systems, see Figure 3.4, were employed in the construction of the frames. One frame incorporated the systems shown in Figures 3.4 (a) and (b) while the other frame was constructed using the systems shown in Figures 3.4 (c) and (d). Details of these systems and their seismic performance are given elsewhere [N1, P5].

Figure 3.5 shows the elevation of the coupled precast structural walls. The walls were constructed using four two-and-a-half storey high panels. Unbonded post-tensioning threaded rods were employed to connect the wall panels vertically and to connect the walls to the foundation beam. Welded U-shaped stainless steel strips were used to couple the walls vertically. These strips were designed to dissipate energy when the walls moved relative to each other. Special floor-to-wall connection details were incorporated into the building to avoid any damage caused by the imposed relative vertical displacement expected to develop due to swaying action along the gap between the coupled walls.

The behaviour of the coupled walls and that of the hybrid and pre-tensioned frame connections was excellent. Very little damage was observed during the test even at levels of displacement associated with seismic intensities 50% above the design level [P5]. Post-test residual drifts were very small, as expected from unbonded prestressed structural systems.

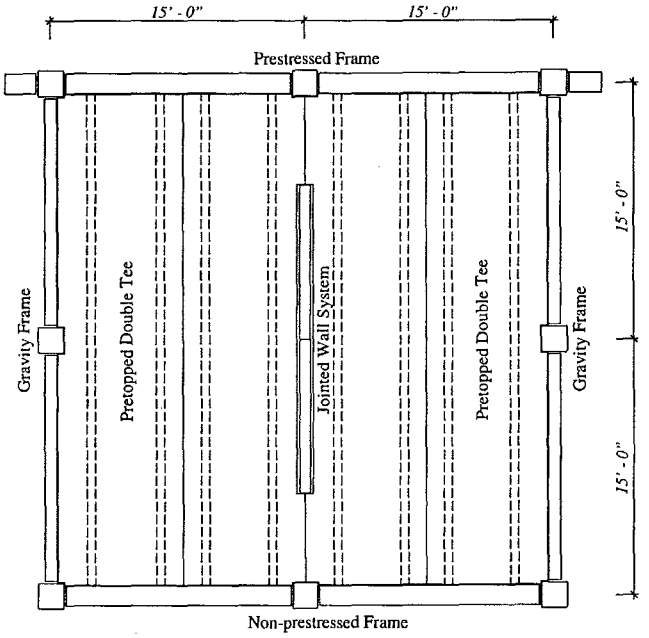

Figure 3.3: Plan view of test building showing lower three floors [P5].

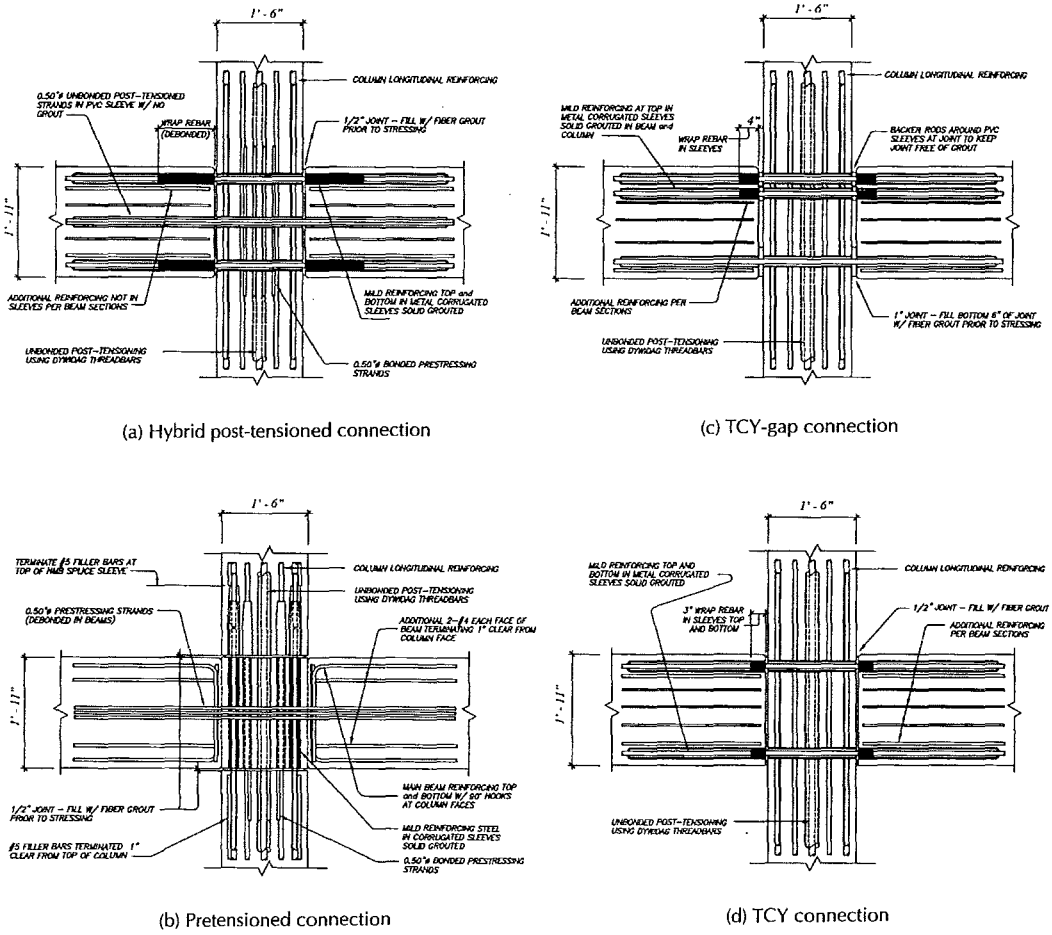

Figure 3.4: Seismic frame types [P5].

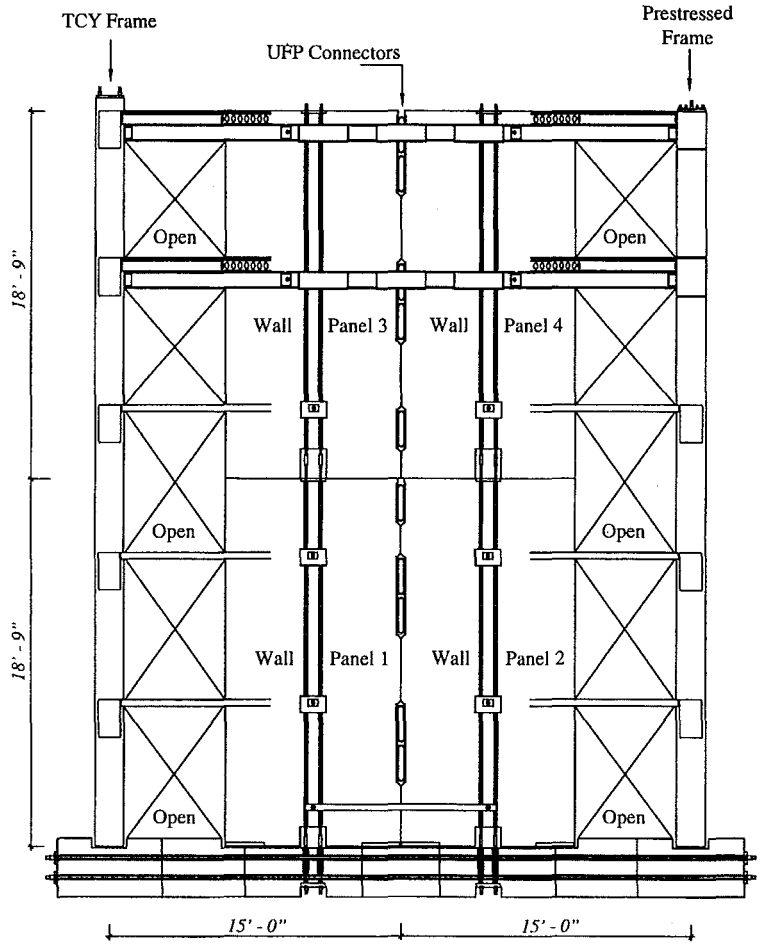

Figure 3.5: Jointed structural wall elevation [P5].

3.3 National Institute for Standards and Technology

An experimental programme at the National Institute for Standards and Technology (NIST) investigated methods of improving the energy dissipation characteristics of this system for precast frame construction [S4]. A hybrid precast connection, see Figure 3.7, was developed in which energy dissipation was provided by bonded mild-strength steel while the prestressing steel provided the clamping and restoring forces. A sufficient unbonded length of the energy dissipating steel on either side of the column prevented the concentration of inelastic response over a small length, thereby delaying failure. The prestressing strands were placed at the mid-depth of the beams, stressed to 0.44 f_{psu}, where f_{psu} is the ultimate tensile strength of the strands, and bonded over the beam mid-span. All four corners of the beam ends were armoured

with steel angels to prevent spalling. Cyclic reversed loading was applied to 1/3-scale precast beam-column units with hybrid connections. High drift levels were attained in the specimens with no damage to the precast units or loss of prestress due to yielding. Excellent behaviour was reported with the development of barely visible cracks that closed upon removal of the applied forces. The results were compared to the performance of comparable monolithic beam-column specimens, which suffered irreparable damage at drift levels lower than those attained by the hybrid connected precast units. A hysteretic model was developed based on these tests and a numerical investigation was conducted in which the behaviour of frame structures of various stories incorporating the hybrid connection at their joints was studied [C1]. Based on these, design guidelines for precast frames with hybrid connections have been proposed [S3].

3.4 Lehigh University, Pennsylvania

The results of the experimental studies conducted at NIST [S4] were utilised by El-Sheikh et al. [E1] in their non-linear static and dynamic time-history analyses of a prototype six-storey office building to develop design recommendations for unbonded post-tensioned precast concrete frames.

A tri-linear idealisation of the connection performance was suggested, see Figure 3.7, and verified in their numerical study. The upper limit of the linear segment of the tri-linear idealisation at which point a reduction in stiffness occurs, V_{II}, Δ_{II} in Figure 3.7, is defined in terms of the minimum value corresponding to either of:

- Concrete softening (defined as an extreme fibre strain of 0.003 assuming an uncracked section with the cover intact), or,

- The opening of the gap at the beam-column interface. This is assumed to occur when the length of the gap exceeds 75% of the section depth.

The yield point, (Δ_y, V_y), is assumed to correspond to the limit of proportionality of the prestressing steel (f_{slp}) at which point spalling of the concrete cover is assumed to have occurred. The final stage of the tri-linear plot is defined by point, (Δ_{ult}, V_{ult}), which corresponds to crushing of the confined concrete at the survival level earthquake. The length of confined concrete in the beam adjacent to the beam-column interface over which concrete crushing occurs, L_{cr}, was assumed to be the smaller of either the confined concrete width or twice the stress block depth.

Design recommendations for precast walls incorporating unbonded post-tensioning bars were proposed by Kurama et al. [K1] based on non-linear static lateral load analyses and dynamic time-history analyses of six-storey prototype walls.

Performance criteria corresponding to design level ground motions (NEHRP [B1] design ground motion with a 500-year return period) were defined as no yielding of the post-tensioning bars or significant damage to the compressed concrete in the precast unit. Failure at the survival level ground motion (corresponding to a 2500-year return period earthquake) was associated with crushing of the compressed confined concrete. The same tri-linear response as El-Sheikh et al. [E1] was identified in the fibre-model analyses.

Based on their parametric studies, the authors recommended a wall height-to-length ratio equal to or larger than three to ensure flexural behaviour under lateral loading conditions. In addition, the location, unbonded length and initial stress of prestressing steel determine the lateral displacement at which yield occurs. Concrete crushing at the ultimate limit state is prevented by providing spiral reinforcement at the ends of wall over a length equal to at least one-quarter of its length and over a height greater than or equal to the height of the first storey of the building. The analyses showed that higher modes did not have a significant influence on the lateral displacements whereas the base shear demands were highly sensitive to these effects. In addition, the length of the gap opening at the wall panel-foundation interface (for a system comprising several precast wall units connected by unbonded prestressing steel) was not dependent on the intensity of the ground motion or the amount of prestress.

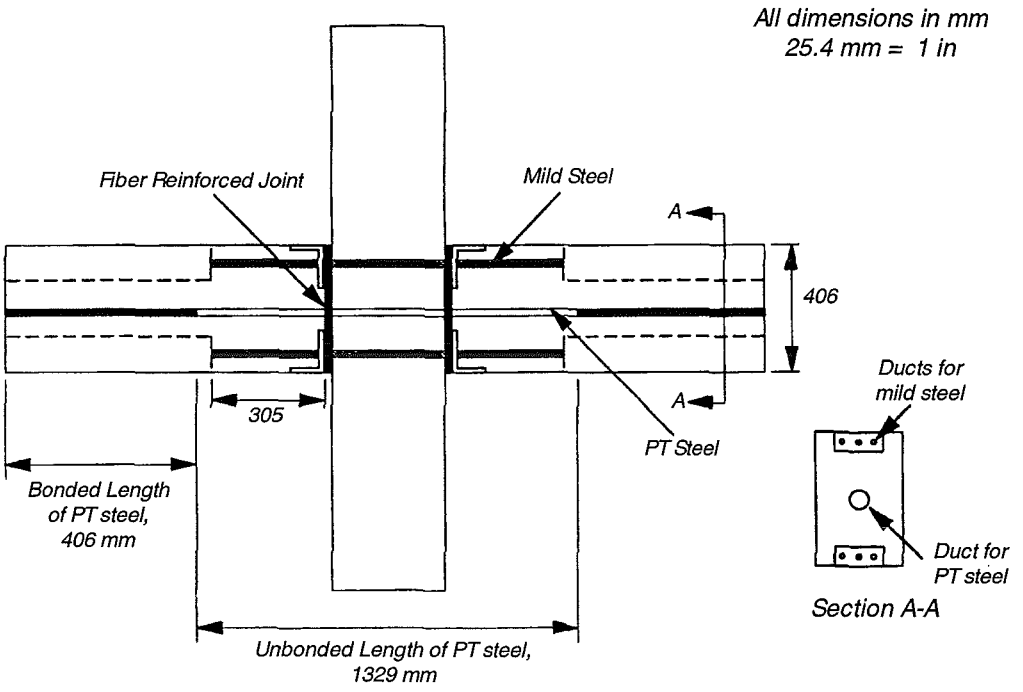

Figure 3.6: Hybrid precast concrete connection for frame systems [S4].

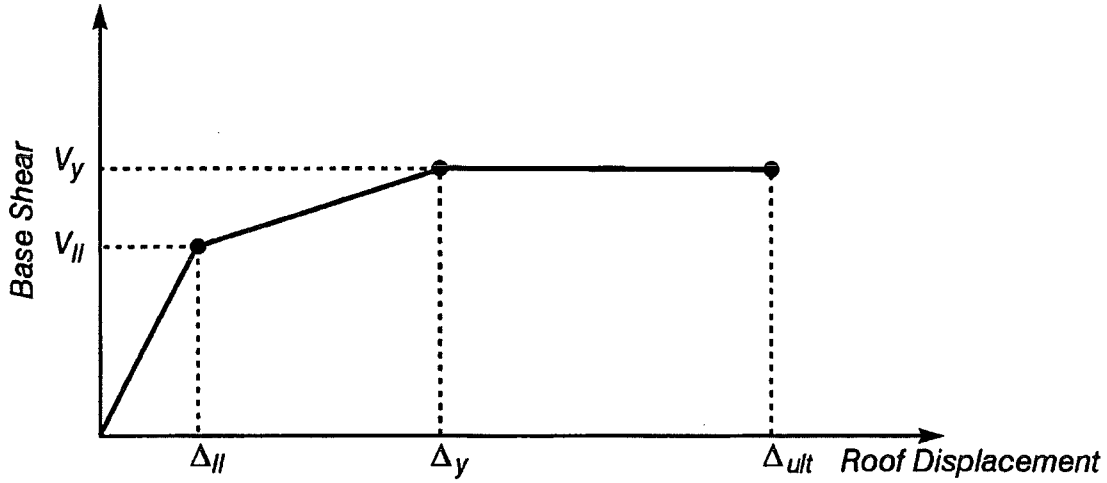

Figure 3.7: Trilinear idealisation of the response of post-tensioned unbonded precast frame system [E1].

3.5 Other Studies

Tests on beam-column subassemblages were conducted by Palmieri et al. [P1] on unbonded prestressing strands and high-strength threaded post-tensioning bars to gradually increasing drift levels under a quasi-static loading regime. Both types of connections, see Figure 3.8, exhibited non-linear elastic behaviour up to drift levels exceeding 3%. Pinching in the hysteretic response occurred upon loss of the post-tensioning force while some energy dissipation was evident upon cracking of the concrete and yielding of the prestressing steel.

In an effort to promote the use of concrete masonry in New Zealand, noteworthy research on the use of unbonded prestressing steel in the post-tensioning of concrete masonry walls is also currently being conducted at the University of Auckland [L1]. In addition to the response of the system, analytical and experimental investigations have been conducted into the behaviour of the constituent materials. Creep and shrinkage of the concrete masonry units result in losses in the prestressing force and must therefore be taken into account during design. Thus, material properties are an important aspect in this type of construction compared to precast concrete.

Rodriguez et al. conducted a series of non-linear dynamic time-history analyses at the University of Canterbury [R2]. The floor acceleration response was studied on three-, six- and twelve- storey buildings incorporating systems emulating monolithic construction and precast concrete wall systems prestressed with unbonded tendons. They found that the non-linear behaviour of the wall system chiefly affects those accelerations associated with the first mode of response. They also found that low-rise multi-storey buildings incorporating walls prestressed with unbonded tendons are significantly affected by the higher modes of response when subjected to a near-fault earthquake with a large velocity pulse. These findings coincide with the observations made of the pseudo-dynamic test of the six-storey building reported by Priestley et al. [P5].

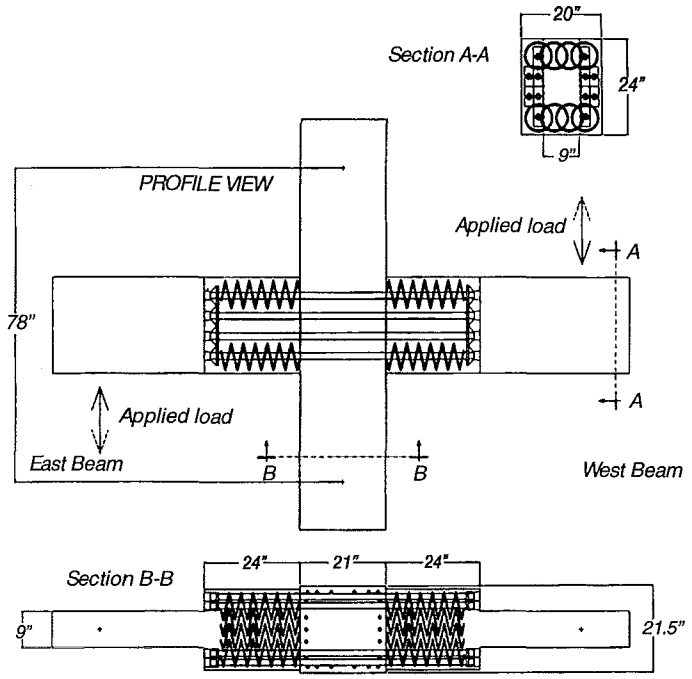

(a) Details of specimen with unbonded prestressing strands.

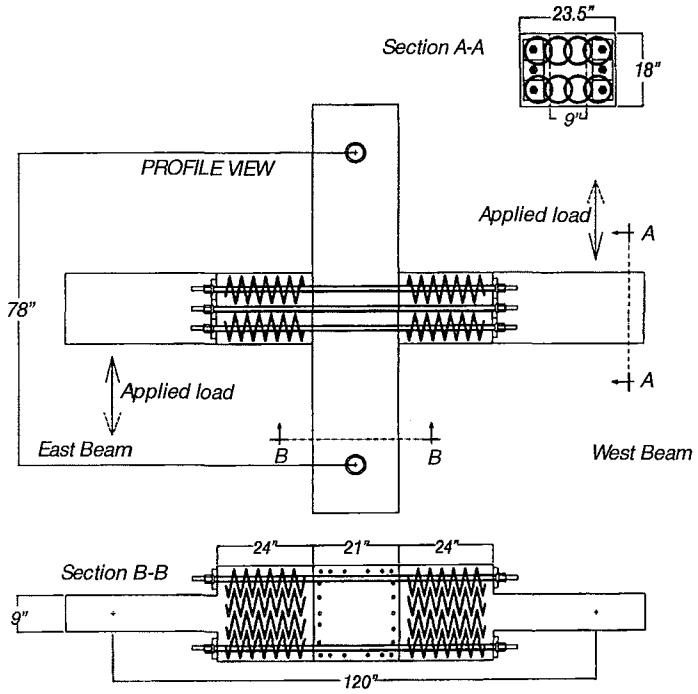

(b) Details of specimen with unbonded post-tensioning bars.

Figure 3.8: Unbonded post-tensioning systems in precast concrete beam-column subassemblages investigated by Palmieri et al. [P1].

4. THEORETICAL CONSIDERATIONS

4.1 General

The fundamental feature of the proposed system is the preclusion of plastic hinges in the precast wall units, with nonlinear response manifested through the development of separation gaps at the horizontal joints between the precast concrete units. The criteria that guarantee the development of this rocking mode of response are presented below.

4.2 Wall Aspect Ratio

The wall aspect ratio is an important factor in effecting a predominantly rocking response mode in systems that rely only on interface friction in resisting the sliding shear. Considering Figure 4.1, the sliding shear resistance of a wall may be determined from equilibrium:

$$F = V_{slide} = \mu_f P \tag{4.1}$$

The lateral force that induces rocking in the wall is given by:

$$H V_{rock} \approx \frac{P L_w}{2} \tag{4.2}$$

For rocking to occur, the shear force capacity at the interface provided by friction must exceed the lateral force which induces rocking:

$$V_{slide} > V_{rock} \tag{4.3}$$

From Equations 4.1 and 4.2:

$$\mu_f P > \frac{P L_w}{2H} \tag{4.4}$$

Therefore, shear sliding may be prevented by designating an aspect ratio of the wall, L_w/H , such that:

$$\frac{L_w}{H} < 2\mu_f \tag{4.5}$$

It must be noted that higher mode effects influence the distribution of the dynamic inertial forces [P6], usually approximated by a static lateral load distribution in the form of an inverted triangle. Therefore, the actual location of the resultant of these inertial forces may be lower than that of the equivalent static load approximation. Thus, the influence of higher mode effects should be accounted for and the value of H in Equation 4.5 taken as the minimum value of M/V, see Figure 4.1. In cases where large ground accelerations are expected, the location of the centroid of the lateral inertial forces including higher mode effects, see Figure 4.2, may be found from [P6]:

$$H_I = \omega_v H \tag{4.6}$$

For buildings up to six stories, the dynamic shear magnification factor, ω_v, for monolithic or precast concrete walls emulating monolithic construction is:

$$\omega_v = 0.9 + \frac{n}{10} \tag{4.7}$$

whereas for buildings over six stories:

$$\omega_v = 1.3 + \frac{n}{30} \tag{4.8}$$

In any case, the value of ω_v must be taken as less than or equal to 1.8 in the above equations.

Dynamic time-history analyses conducted by researchers at Lehigh University [K2] on precast wall systems connected with unbonded prestressing tendons have shown the greater sensitivity of this system to higher mode effects compared to monolithic

cast-in-place concrete walls. Due to this increased sensitivity to higher mode effects, the base shear demands on the proposed system will be higher than a comparable cast-in-place concrete wall. Kurama [K3] describes a method of evaluating the base shear demands considering higher modes effects specifically for this type of system. The maximum base shear demand, V_{max}, is calculated based on the sum of the first mode component, $V_{1,max}$, and a higher mode component, $V_{H,max}$:

$$V_{max} = V_{1,max} + V_{H,max} \tag{4.9}$$

The first mode contribution to to the above equation is determined from the maximum base moment capacity, M_{max}, which is found from a static push-over analysis based on an assumed shape of equivalent lateral forces and the resultant height of the inertia forces, $\bar{x}_1$:

$$V_{1,max} = \frac{M_{max}}{\bar{x}_1} \tag{4.10}$$

The higher mode component of maximum base shear demand, $V_{H,max}$, is estimated from the mass assigned to the wall, M_w, and the peak acceleration for the expected (design level) design ground motion, $\ddot{u}_{o,max}$:

$$V_{H,max} = D_m M_w \ddot{u}_{o,max} \tag{4.11}$$

where coefficient, D_m, is a function of the mode shapes and the mass distribution. This coefficient is given by:

$$D_m = \frac{M_w - M_1 + 0.72 M_2}{M_w} \tag{4.12}$$

The use of linear elastic wall stiffness to calculate D_m is recommended [K3].

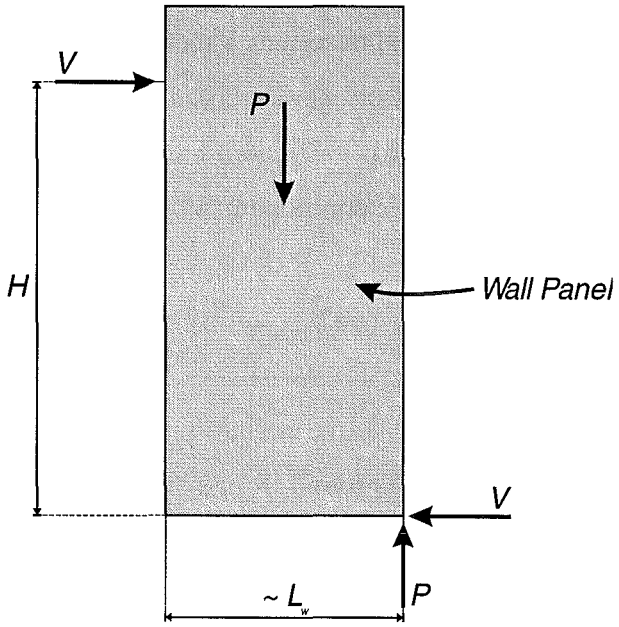

Figure 4.1: Influence of wall aspect ratio on dominance of rocking response.

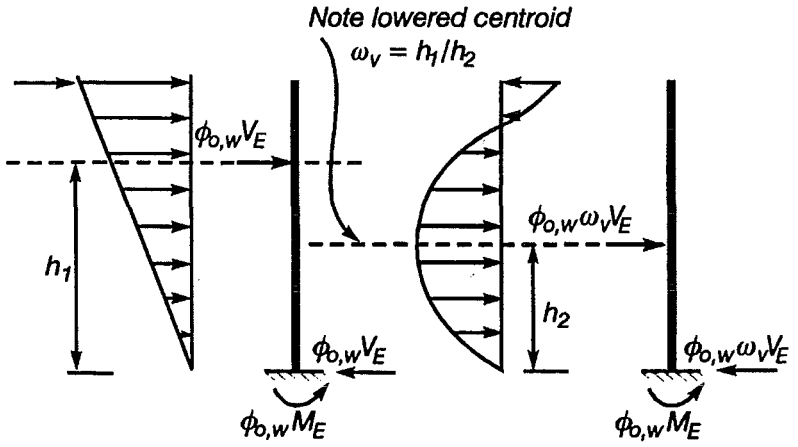

(a) Linear approximation of first mode inertia force distribution.

(b) Dynamic inertial force distribution at higher modes of response.

Figure 4.2: Comparison of equivalent static lateral forces and dynamic forces. [P6]

4.3 Prestressing Force

As a wall is subjected to cyclic reversals under sesimic loading conditions, the forces in the prestressing tendons will increase with the amplitude of the lateral displacement due to the effect caused by the opening of the gap at the wall base. These variations in the prestressing force are dependent on the location of the prestressing tendons within the length of the wall for a given lateral drift. Thus, the optimum location of the prestressing tendons is at midlength of the wall, as this gives the smallest possible elongation in the tendon and maximum wall rotation before reaching the elastic limit in walls expected to be subjected to cyclic load reversals and subjected to concentric axial loading. Since more than one bundle of tendons will be used in practice, it is recommended that these bundles be placed symmetrically within the middle third of the wall.

The expected losses in the prestressing tendons should be accounted for in the determination of the initial prestressing force. These losses include those which are manifested in the tendons during stressing operations (e.g. seating losses), during the normal life of the structure (e.g. relaxation of cable, creep and shrinkage of concrete) and losses arising under seismic loading conditions of the system (e.g. crushing of the mortar bed, spalling of the concrete in the toes of the wall, etc).

The required post-tensioning force (after losses) is determined based on the expected increase in the post-tensioning force due to rocking resulting from elongation of the prestressing tendon furthest from the neutral axis depth at the design level drift, see Figure 4.3:

$$\Delta_{ps} = (d_{ps} - c)\theta_u \tag{4.13}$$

In Equation 4.13, the strength enhancement caused by confinement of the concrete at the ends of the wall, in addition to spalling of the cover concrete, should be considered in calculating the neutral axis depth, c. However, the elongation of the prestressing tendon is insensitive to large variations in the value of the neutral axis depth. From Figure 4.4, the neutral axis depth, c, may be determined from

equilibrium and compatibility requirements at the toe of the wall. The compressive force at the wall toe, C, at the maximum drift is:

$$C = N^* + \eta' F_{lp} + F_{ed} \tag{4.14}$$

where factor η' accounts for the fact that when the tendon furthest from the neutral axis (axis of rotation of the wall) reaches its limit of proportionality, the tendons closest to the neutral axis are below this limit:

$$\eta' = \frac{1}{2}\left(1 + \frac{\left(L_w - d_{ps} - c\right)}{L_{ps}} \frac{E_{ps}}{f_{slp}} \theta_u + \frac{f_{psi}}{f_{slp}}\right) \tag{4.15}$$

From the equivalent stress block for confined concrete, the resultant internal compressive force is:

$$C = \alpha k\, f'_c\, a\, b_e \tag{4.16}$$

The distance from the extreme compressive fibre to the neutral axis is:

$$c \approx a + c_c \tag{4.17}$$

The compression strength of the concrete at the toes of the wall is enhanced through the contribution of the transverse reinforcement and the confining effect of the concrete contact surface (e.g. foundation beam or abutting wall upon which the wall rocks). The compression strength enhancement may be approximated by [P6]:

$$\alpha k\, f'_c \approx 1.4\, f'_c \tag{4.18}$$

Rearranging Equations 4.16 to 4.18 and solving for the neutral axis depth, c:

$$c = \frac{N^* + \eta F_{lp} + F_{ed} + 1.4 f_c' b_e c_c}{1.4 f_c' b_e + \frac{E_{ps} A_{ps}}{2 L_{ps}} \theta_u} \approx \frac{N^* + \eta F_{lp} + F_{ed} + 1.4 f_c' b_e c_c}{1.4 f_c' b_e} \tag{4.19}$$

where:

$$\eta = \left(\eta' - \frac{c}{L_{ps}} \frac{E_{ps}}{f_{slp}} \theta_u \right) \tag{4.20}$$

For the tendons to remain elastic at the collapse prevention limit state, the following inequality should be satisfied:

$$F_{psi} \leq F_{lp} - \Delta F_{ps} \tag{4.21}$$

where:

$$\Delta F_{ps} = E_{ps} A_{ps} \frac{\Delta_{ps}}{L_{ps}} \tag{4.22}$$

A sensitivity analysis was carried out to observe the influence of coefficient η on the neutral axis depth, c, in Equation 4.19. It was found that the neutral axis depth is rather insensitive to this coefficient. As a result, a value of $\eta = 0.9$ is proposed for use in design applications.

Substitution of Equation 4.13 into Equation 4.21 results in:

$$F_{psi} \leq F_{lp} - \frac{E_{ps} A_{ps} \left(d_{ps} - c \right)}{L_{ps}} \theta_u \tag{4.23}$$

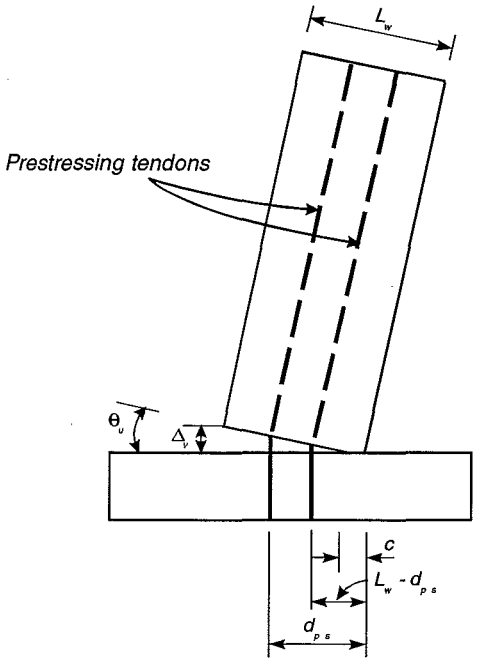

Figure 4.3: Elongation of the prestressing strands due to rocking of the wall.

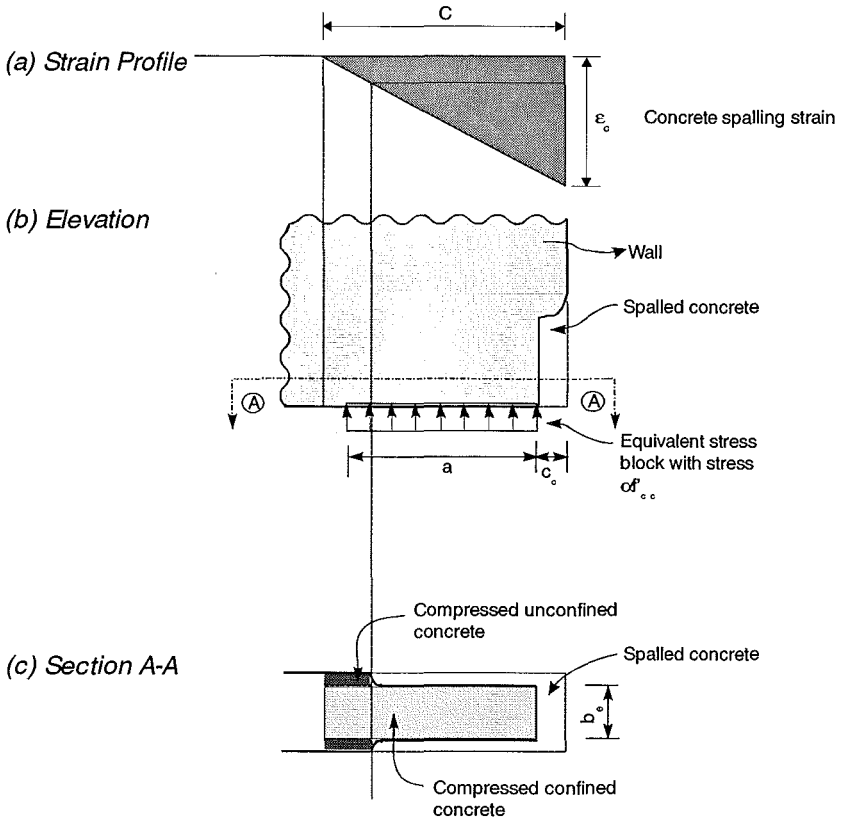

Figure 4.4: Distribution of compression stresses and strains at the toe of the wall during rocking.

4.4 Energy Dissipators

While prevention of damage in precast walls is a desirable feature from the owner's perspective, the non-linearly elastic response of the walls suggests the absence of an energy dissipation capacity. This can significantly influence the response of the system, usually by increasing the lateral displacement demand, the shear forces and the floor accelerations. To improve the energy dissipation capacity, hysteretic energy dissipators in the form of "dog-bones" are proposed in the present study. These energy dissipators can be manufactured from standard steel reinforcing bars that are milled to a smaller diameter over a specified length of the bar, cast into the foundation beam and grouted into the walls after the erection process has been completed. The lengths of the non-milled segments at either end of the milled section of the bar should be such that the full tensile strength of the bar may be developed while the non-milled segments remain elastic. The diameter of the milled segment is selected such that closing of the gap at the horizontal connection is ensured at all times during and after the event (seismic or wind) inducing the dynamic response of the system. Thus, the prestressing force after losses, in addition to the gravity loads, must be sufficient to push the dog-bones to nominally zero strain upon unloading.

The behaviour of New Zealand manufactured low carbon steel cyclically loaded in tension and compression in the tensile strain domain is such that the compressive stress at zero strain after a tensile stress reversal is almost equal to the tensile stress at the reversal point, f_r, see Figure 4.5. In addition, upon unloading from a large displacement excursion that induces tensile strains in the dog-bone of at least one-half of the uniform strain, the associated stress would be approximately similar to the ultimate tensile strength, f_{su}, see Figure 4.6. Hence, the following condition must be satisfied to ensure closure of the gap at the horizontal joint at the base of the wall upon unloading:

$$N^* + F_{psi} \geq F_{ed} \tag{4.24}$$

where

$$F_{ed} = A_{sd}\ \bar{f}_{su} \tag{4.25}$$

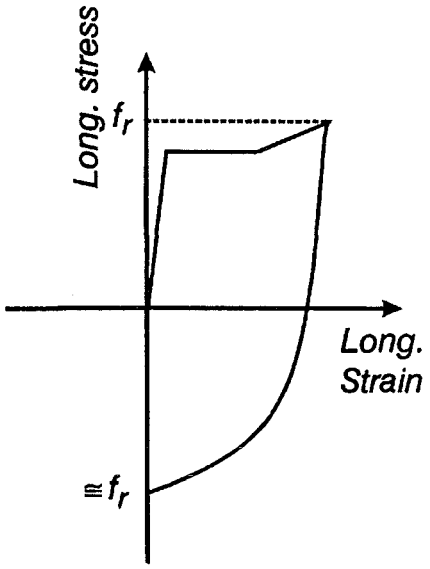

Figure 4.5: Relationship between compressive and tensile stresses in steel reinforcing bars.

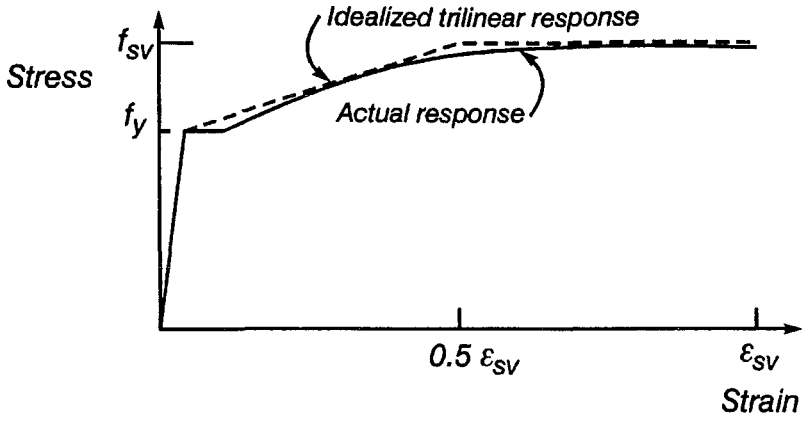

Figure 4.6: Typical stress-strain relationship of standard steel reinforcing bars.

For reinforcement manufactured in New Zealand, the ultimate tensile strength, f_{su} , is not more than 1.40 times the yield strength, f_y. Thus, for a mean yield strength value of:

$$\bar{f}_y = 1.07 f_y \tag{4.26}$$

the expected mean ultimate tensile strength is:

$$\bar{f}_{su} = 1.4 \times 1.07 \times f_y = 1.5 f_y \tag{4.27}$$

Substituting Equations 4.25 and 4.27 in Equation 4.24 and rearranging for A_{sd}:

$$A_{sd} \leq \frac{2}{3} \frac{N^* + F_{psi}}{f_y} \tag{4.28}$$

The length of the milled segment of the energy dissipator, L_e , required to ensure that the strain in the bar at a drift level corresponding to the collapse prevention limit state, θ_u does not exceed 2/3 of the uniform strain, ε_{su} is from geometry:

$$\Delta_{ed} = (d_{ed} - c)\theta_u \tag{4.29}$$

$$\varepsilon_{ed} = \frac{\Delta_{ed}}{L_e} = \frac{(d_{ed} - c)}{L_e} \theta_u \tag{4.30}$$

but

$$\varepsilon_{ed} = \frac{2}{3} \varepsilon_{su} \tag{4.31}$$

Substituting Equation 4.31 into Equation 4.30 and rearranging for L_e:

$$L_e = \frac{3}{2} \frac{\theta_u}{\varepsilon_{su}} (d_{ed} - c) \tag{4.32}$$

The value of the neutral axis depth, c, in Equation 4.32 can be found from Equation 4.19 using $\eta = 0.9$.

4.5 Prediction of the Monotonic Response

Previous studies [K1, E1] have shown the validity of a tri-linear representation of the lateral load-lateral deflection relationship for monotonic response of systems incorporating unbonded prestressing tendons as connections, see Figure 3.7. These studies, however, allow for yielding of the prestressing tendons within the performance limits, albeit within the collapse prevention limit state. The present study proposes that the bi-linear representation of the lateral force-lateral displacement response shown in Figure 3.1 is sufficiently accurate for design purposes. The point at which a softening of the initial stiffness at small amplitude lateral displacements occurs is the first point defining this bi-linear lateral force-displacement relationship. This is the limit of proportionality in precast walls prestressed with unbonded tendons and the yield point in those walls incorporating energy dissipation devices. The second point, corresponding to the collapse prevention limit state, is associated with the threshold of yielding in the critical prestressing tendons. The suggested monotonic loading relationship for predicting the response of these wall types is presented in the next two sections.

4.5.1 Walls Prestressed with Partially Unbonded Tendons

The stress at the base of a precast concrete wall prestressed with partially unbonded tendons, f_b, before lift-off occurs under the loading condition shown in Figure 4.1 is:

$$f_b = \frac{P}{A} \pm \frac{VH}{Z} \tag{4.33}$$

where the first term in Equation 4.33 is the stress due to the axial forces and the second term is the flexural stress due to the resultant lateral force acting on the wall. As the tension capacity at the wall-foundation beam interface is negligible, separation between the wall and the foundation beam is initiated at one end when the flexural (overturning) stress equals the normal stress:

$$\frac{VH}{Z} = \frac{P}{A} \tag{4.34}$$

The lateral force required to initiate decompression of the end of a wall, V_g, is from Equation 4.35:

$$V_g = \left(F_{psi} + N^*\right)\frac{L_w}{6H} \tag{4.35}$$

The limit of proportionality of a wall (Δ_{lp}, V_{lp}) is defined as the point at which a marked reduction of the stiffness occurs. Based on numerical studies of beam-column connections in precast concrete frame subassemblages prestressed with unbonded tendons, it has been shown that a marked change in stiffness occurs when the length of the separation gap is between 50 to 75% of the overall depth of the member [P4, E1]. In this study the limit of proportionality is chosen as the point at which the separation gap has propagated through 75% of the overall depth of the wall. The moment associated with this separation gap is given by:

$$M_{lp} = 2.5\, M_g \tag{4.36}$$

The corresponding lateral force is obtained from Equations 4.35 and 4.36 as follows:

$$V_{lp} = \frac{M_{lp}}{H} = \left(F_{psi} + N^*\right)\frac{L_w}{2.4H} \tag{4.37}$$

The lateral displacement, Δ_{lp}, corresponding at the development of the lateral force, V_{lp}, is approximately obtained by accounting for elastic flexural and shear deformations within the wall unit and ignoring the displacement due to base rotation. For a rectangular wall this results in:

$$\Delta_{lp} = \frac{V_{lp}\, H^3}{3E_c\, I_g}\left(1 + \frac{9I_g}{H^2 A_g}\right) \tag{4.38}$$

In this study, the point corresponding to the collapse prevention limit state, (Δ_u, V_u), is related to the limit of proportionality of the critical tendon, i.e. that furthest from the point of rotation of the wall unit.

The ultimate moment, M_u, is obtained by taking moments about the centroid of the equivalent stress block shown in Figure 4.4. The neutral axis depth, c, is found from Equation 4.19 using $F_{ed} = 0$ and $\eta = 0.9$ and the depth of the equivalent stress block, a, is calculated from Equation 4.17. Thus:

$$M_u = \left(N^* + F_{lp}\right)\frac{\left(L_w - a - 2c_c\right)}{2} \tag{4.39}$$

The lateral force, V_u, is:

$$V_u = \frac{M_u}{H} = \left(N^* + F_{lp}\right)\frac{\left(L_w - a - 2c_c\right)}{2H} \tag{4.40}$$

The ultimate lateral displacement, Δ_u, is found by accounting for flexural and shear deformations in the wall panel plus the additional displacement due to base rotation. This results in,

$$\Delta_u = \frac{V_u H^3}{3E_c I_g}\left(1 + \frac{9I_g}{H^2 A_g}\right) + \frac{H}{d_{ps}}\frac{f_{lp} - f_{psi}}{E_{sp}} L_{ps} \tag{4.41}$$

4.5.2 Walls Prestressed With Partially Unbonded Tendons Incorporating Energy Dissipators

In the present study, the energy dissipation capacity of the precast walls designed in accordance with the previous section will be enhanced through the use of dog-bones. Thus, the lateral displacement, Δ_{lp}, corresponding to the limit of proportionality of the system, may be related to the yield strength of the reinforcement used in the manufacture of these energy dissipators as follows:

$$\Delta_{lp} = \frac{V_{lp} H^3}{3E_c I_g}\left(1 + \frac{9I_g}{H^2 A_g}\right) + \frac{\varepsilon_y L_e}{\frac{L_w}{2} - c} H \tag{4.42}$$

Equation 4.42 takes into account the flexural and shear displacements in the wall panel and the fixed-end rotation at the base. However, this equation is only applicable to those cases where the area of the energy dissipators, ΣA_{sd}, is not less than 60% of the maximum value permitted by Equation 4.28 and the axial load in the wall, P, resulting from gravity loading plus the initial prestressing force, is less or equal to 0.2 $A_g\ f'_c$. For walls having axial loads P > 0.2 $A_g\ f'_c$, a marked reduction in stiffness is expected to result from the non-linear behaviour of the confined concrete and mortar bed compressed at the wall ends.

The bending moment at the limit of proportionality, M_{lp}, can be determined assuming a linear distribution of the compressive stress concrete block. This results in:

$$M_{lp} = \left(N^* + F_{psi} + F_{edy}\right)\left(\frac{L_w}{2} - \frac{c}{3}\right) \tag{4.43}$$

The lateral force, V_{lp}, associated with this moment is:

$$V_{lp} = \left(N^* + F_{psi} + F_{edy}\right)\frac{\left(\frac{L_w}{2} - \frac{c}{3}\right)}{H} \tag{4.44}$$

As in the case of walls without energy dissipators (refer to Section 4.5.1), the point corresponding to the collapse prevention state, (Δ_u , V_u), is related to the limit of proportionality of the critical tendon, i.e. that furthest from the point of rotation of the wall. The ultimate moment, M_u, is determined from the equivalent stress block shown in Figure 4.4 in which the neutral axis depth, c, is given be Equation 4.19 (with η=0.9) and the depth, a, is found from Equation 4.17. Thus:

$$M_u = \left(N^* + F_{lp} + F_{ed}\right)\frac{\left(L_w - a - 2c_c\right)}{2} \tag{4.45}$$

and the corresponding lateral force, V_u, is:

$$V_u = \left(N^* + F_{lp} + F_{ed}\right)\frac{\left(L_w - a - 2c_c\right)}{2H} \tag{4.46}$$

The ultimate lateral displacement, Δ_u, for these types of walls is given by Equation 4.41.

5. EXPERIMENTAL PROGRAMME

5.1 Description of the Test Units

Three identical half-scale precast concrete wall specimens, representative of a four storey building, with the dimensions shown in Figure 5.1 were designed to ensure the nominal limit of proportionality of the tendons would be reached at a drift $\theta_u = 2.5\%$. The nominal limit of proportionality was assumed to be the point corresponding to the 0.2% strain offset obtained from the nominal material specifications, see Table 5.1. The three units were of identical external dimensions with a specified concrete compressive strength, $f'_c = 45MPa$ (maximum aggregate size of 13 mm). The aspect ratio of the walls, $A_r = H_w/L_w$, was equal to 2.96 with the wall height-to-width ratio, H_w/b_w = 30. Units 2 and 3 incorporated energy dissipation devices and additional gravity loads were simulated by means of external post-tensioning to the strong floor in Unit 3.

The longitudinal reinforcement comprised Grade 430 10 mm diameter bars with a reinforcement ratio of $p_l = 0.84\%$, see Figure 5.2. Nominal shear reinforcement was provided in the form of horizontal Grade 485 5.5 mm diameter plain round bars spaced at 150 mm centres vertically giving a transverse reinforcement ratio of p_t = 0.25%. These bars were also used as cross ties. The concrete at the wall ends was confined by Grade 400 5.5 mm diameter plain round bars which differed in vertical and horizontal extent in each of the three walls resulting in the arrangement shown in Figure 5.3 for each wall. The configuration was dictated mainly by the limited spacing between the bars, which hampered assembly of the end confinement. The purpose of these dowels was to prevent slip and longitudinal motion of the wall. Figures 5.7 and 5.8 show the reinforcement details of Units 2 and 3 prior to casting of the concrete.

Each unit was connected to the supporting foundation beam by means of two tendons of 12.7 mm diameter (nominal area = 100 mm^2). The design was carried out in accordance to the method outlined in Section 4.3. Substituting the nominal properties

of the tendons, see Table 5.1, and other relevant values into the equations of Section 4.3, a spacing of 350 mm symmetric about the wall centreline and an initial prestressing force of 94 kN per tendon ($0.5 f_{psu}$) was chosen.

Energy dissipation devices in the form of dog-bones were installed in Units 2 and 3, see Figures 5.4 and 5.5. Based on the theoretical considerations outlined in Section 4.4, reduced diameters of 12 mm and 16 mm for Units 2 Unit 3, respectively, were chosen milled over a 200 mm length of Grade 430 20 mm diameter reinforcing bar, see Table 5.2. In order to enable the development of a force equal to the ultimate tensile force in both tension and compression, a 12 mm thick plate was welded to the lowermost ends of the dissipators, see Figure 5.4. Thus, the compressive force developed in the energy dissipator is transmitted to the anchor block of the tendons in the foundation beam. The topmost part of the energy dissipation devices was anchored with full development length into the wall.

Three types of ducts were incorporated in each test unit, see Figure 5.6. Two standard flat 70x20 mm ducts [V1] were placed longitudinally and spaced at 350 mm centres symmetrically about the centreline in each wall. In order to prevent the ducts from being displaced when the walls were cast, it was necessary to tie the ducts to the main wall reinforcement at regular intervals. The use of flat profile ducts provided clearance for the tendons as the wall rocked, thus precluding friction between the tendons and the inside walls of the ducts and preventing kinking of the tendons at the ends of ducts as the wall rocked. It is to be noted that each duct accommodated one tendon. The plain round 12 mm diameter guide dowels were grouted into 20 mm diameter pre-formed ducts provided in the base of the wall. Standard corrugated ducts of 40 mm diameter [V1] were cast into the precast wall units at 180 mm centres concentric to the wall centreline into which the energy dissipators were subsequently grouted.

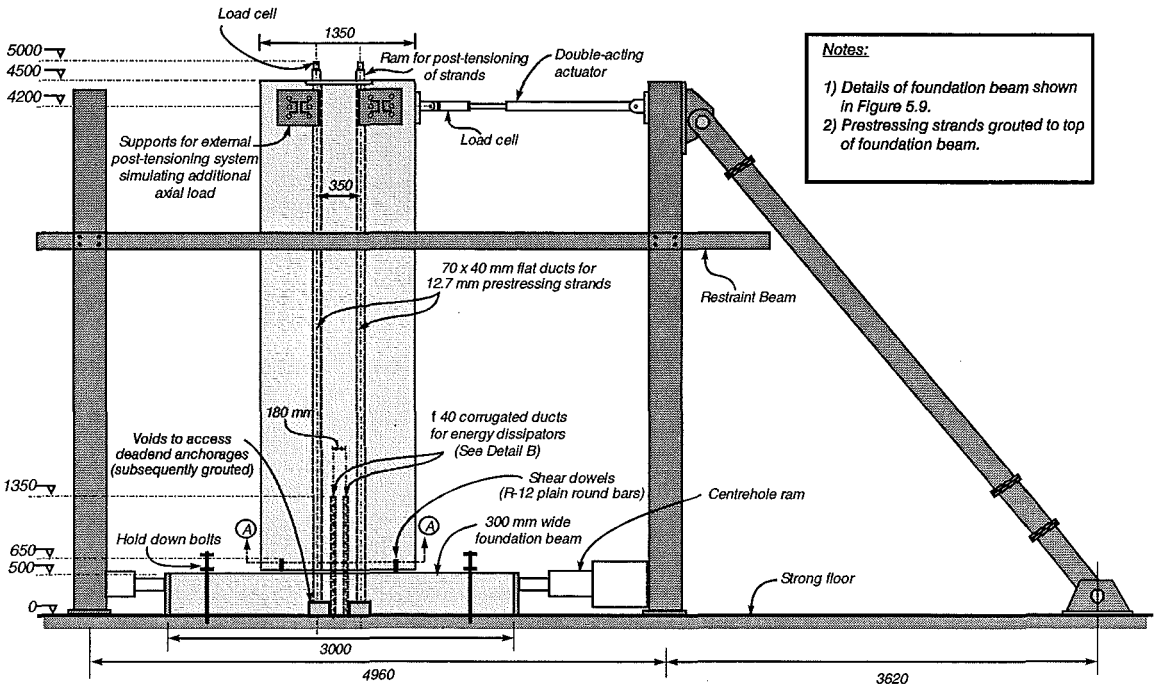

Figure 5.1: Schematic representation of test rig.

Table 5.1: Nominal properties of 12.7 mm diameter low relaxation prestressing strands [V1].

A_{ps} (mm^2)	E_{ps} (GPa)	f_{slp} [(a)] (MPa)	f_{psu} (MPa)
100	180-205	1564	1840

Note:

(a) Derived from the proof load at 0.2% strain offset

Table 5.2: Details of energy dissipation devices used in Units 2 and 3.

Unit	N^* (kN)	F_{psi} (kN)	$\bar{f}_{su}$ [(a)] (MPa)	A_{sd} (mm^2)	
				Eq. 4.28	Provided
2	16	188	690	296	226
3	216	188	690	585	402

Note:

(a) Value determined from Equation 4.27 using $f_y = 430$ MPa

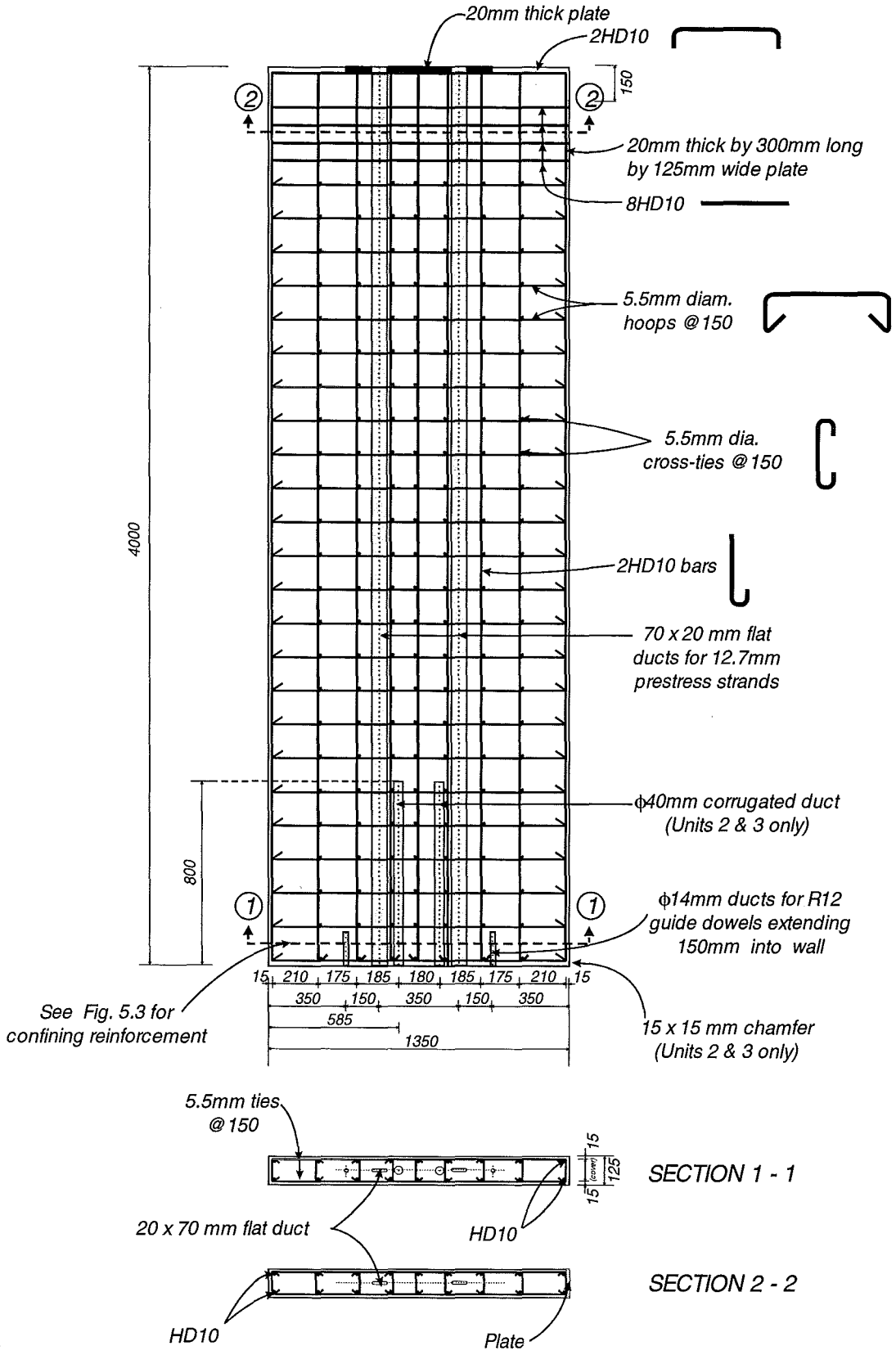

Figure 5.2: Reinforcement details of wall units.

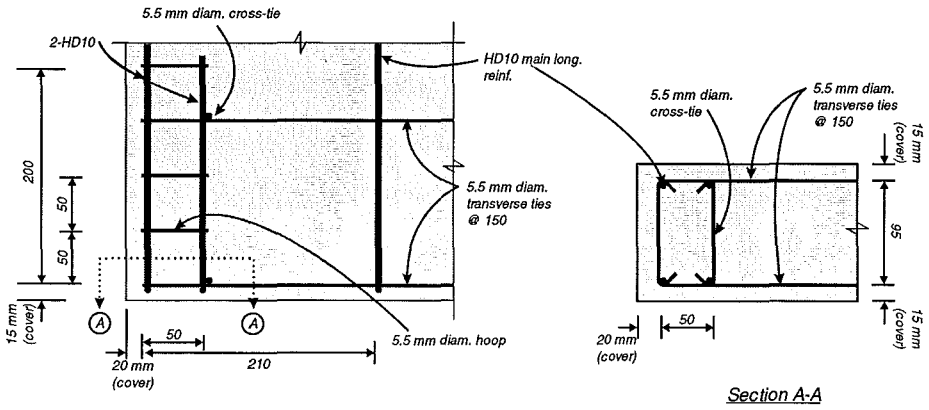

(a) End Confinement Details in Unit 1

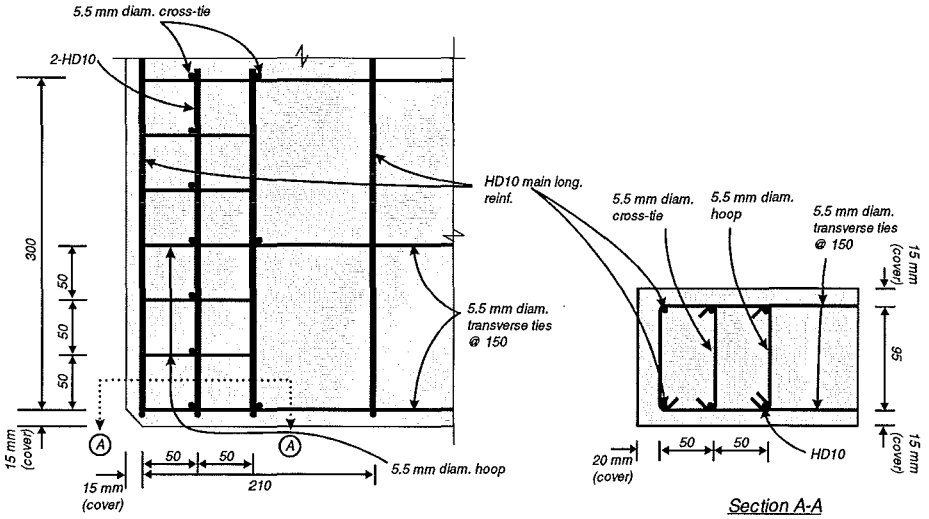

(b) End Confinement Details in Unit 2

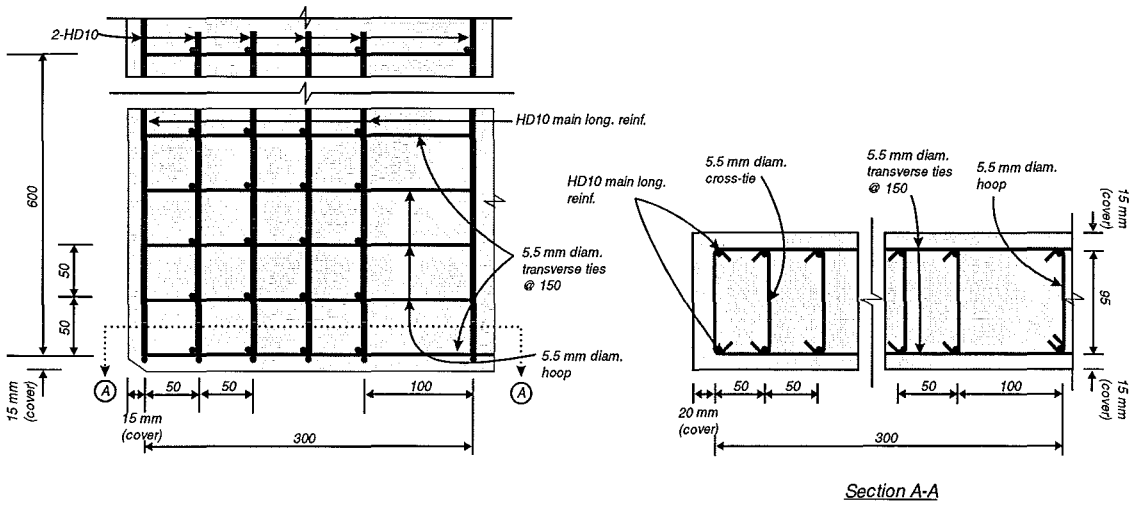

(c) End Confinement Details in Unit 3

Figure 5.3: Details of confinement at the toes of the test units.

A 300 mm wide by 500 mm high foundation beam was built for each unit with the reinforcement arrangement shown in Figure 5.9. These beams were 3 m long, placed between the columns of the loading rig and held down to the strong floor with steel sections. Two pockets were provided at the bottom face of each beam to allow access to the dead-end anchors of the tendons, which were passed through flat ducts cast into the beams. The height of this pockets varied in the second two specimens compared to the first unit. The increased capacity due to the incorporation of the energy dissipators (Units 2 and 3) and the additional gravity load simulated by the external post-tensioning force (Unit 3) necessitated increasing the resistance provided by the foundation beam. This was achieved in the second two specimens by increasing the lever arm of the clamping forces provided by the jacks by raising them further up the height of the beam and lowering the lower set of longitudinal bars in the beam which required decreasing the height of the pockets. The pockets, in addition to the flat ducts in the foundation beam through which the tendons were passed, were grouted after the tendons had been stressed. Two plain round 12 mm diameter reinforcement bars were cast into the foundation beam and grouted 120 mm into the walls to act as guides and to hamper out-of-plane and sliding shear deformations of the walls during the tests, see Figure 5.2.

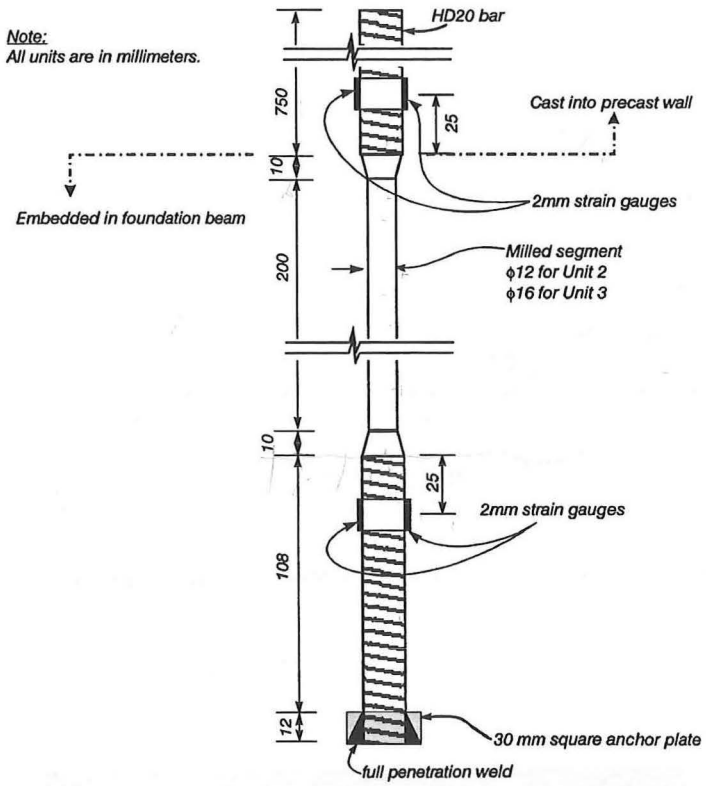

Figure 5.4: Detail of energy dissipator used in Units 2 and 3.

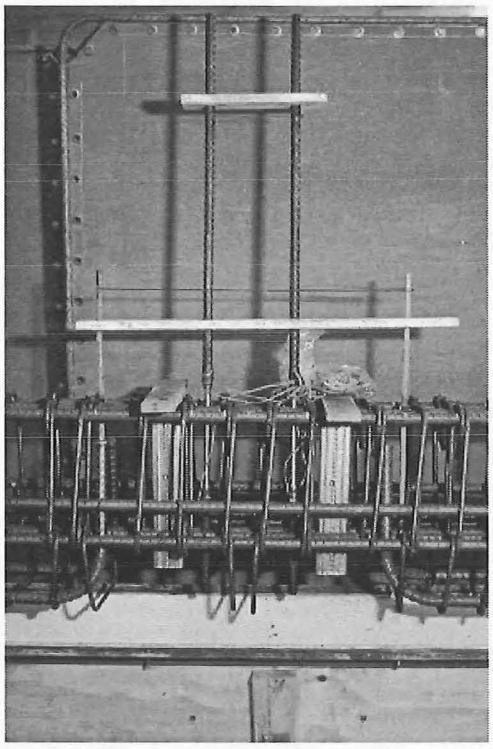

Figure 5.5: Energy dissipators, shear dowels and flat ducts for prestressing strands prior to placing of foundation beam in mould.

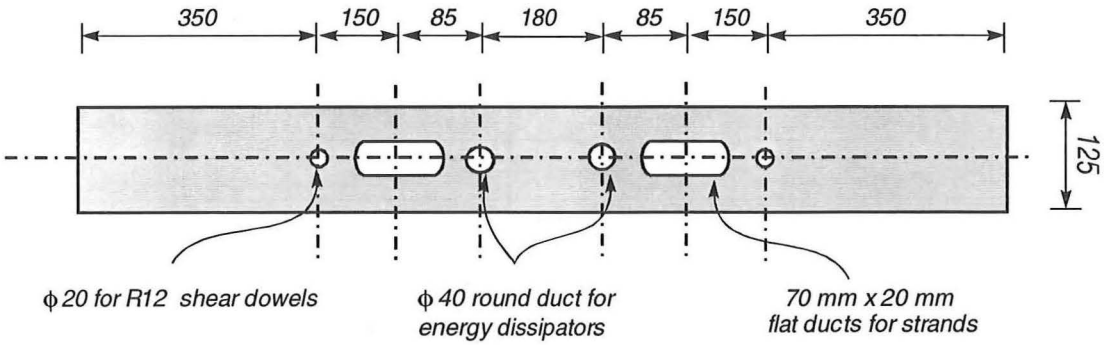

Figure 5.6: Details of duct arrangement in test units.

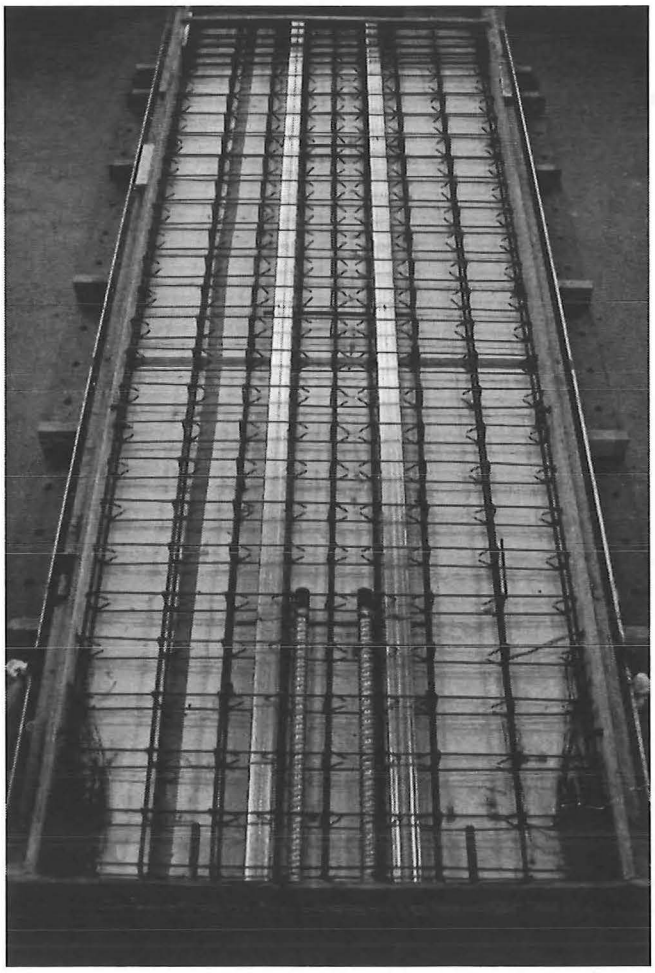

Figure 5.7: Unit 2 prior to casting.

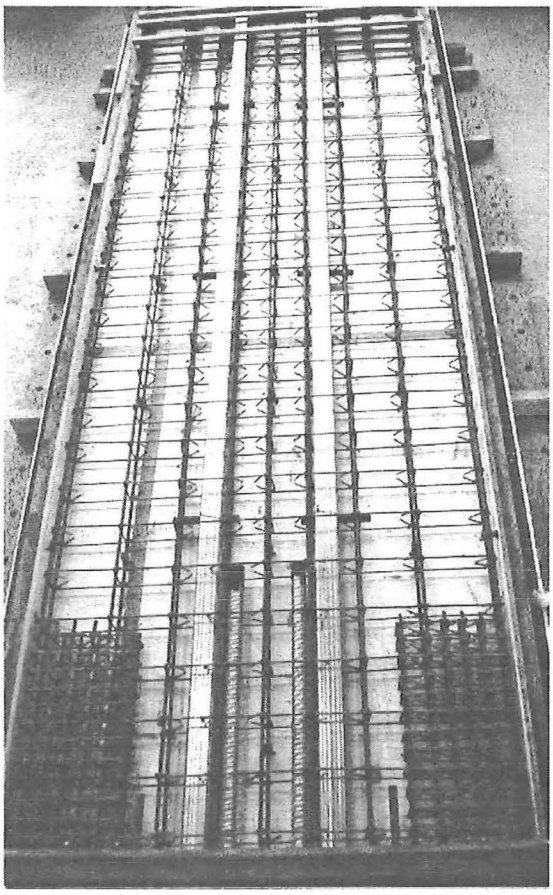

Figure 5.8: Unit 3 prior to casting.

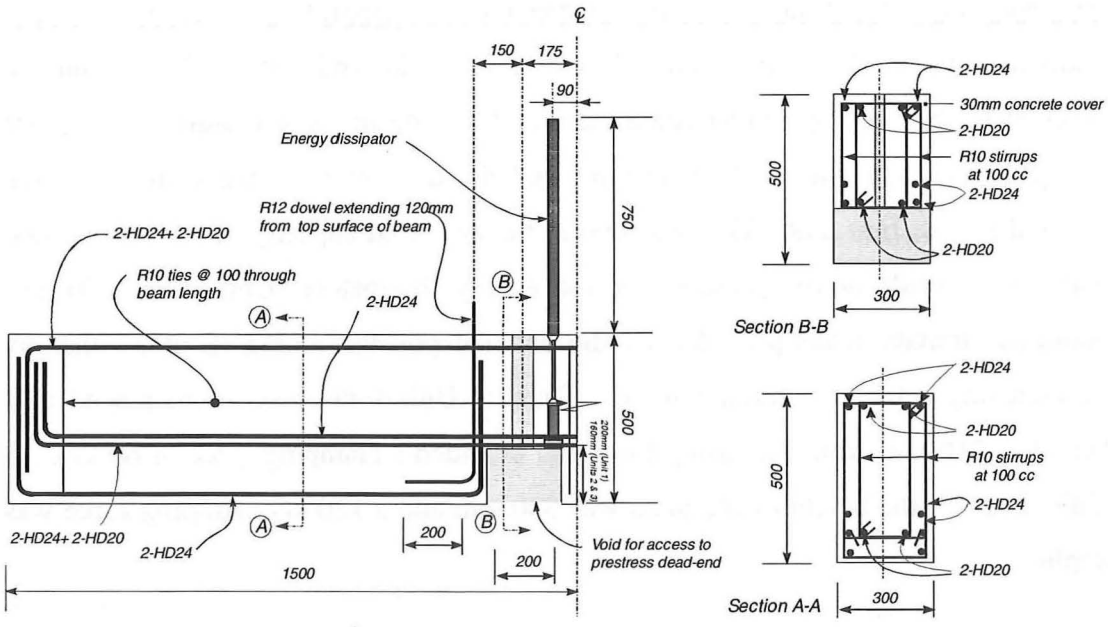

Figure 5.9: Reinforcement details of foundation beam.

5.2 Test Set-Up

Figure 5.1 shows the loading frame used in the tests. Several 38 mm diameter bolts were used to tie down the various components of the rig to the strong floor. Nylon pads were attached to the inside of lateral restraint beams to provide a low friction guiding mechanism to prevent out-of-plane movement of the specimens. Nylon pads were also screwed onto the surface of both (north and south) faces of the specimens, at the level of the guides on the restraint beams, to reduce friction in the event of out-of-plane motion.

A double-acting actuator (330 kN compression and 440 kN tension), bolted to the east column of the testing rig at a height of 4.2 metres from the strong floor, provided the lateral cyclic loading. The diagonal steel brace was bolted at one end to the strong floor and at the other end opposite the actuator on the outside face of the east column. A 20 mm thick plate, to which 8-12 mm diameter reinforcing bars extending the width of the wall were welded, was cast into the wall and provided the connection between the actuator and wall.

The foundation beam was placed between the columns of the loading rig and bolted to the strong floor by means of 38 mm diameter high-strength hold-down bolts spaced 1800 mm apart. Centerhole rams placed between the ends of the beam and the columns of the loading rig restrained the foundation beam against sliding, see Figure 5.1. The vertical position of these rams and the magnitude of the clamping force differed for the first unit. This was due to the increased capacity of the second two walls as a result of the presence of the energy dissipators (Units 2 and 3) and additional gravity loads provided by the external post-tensioning (Unit 3), thereby necessitating a larger clamping force. Thus, in Unit 1 the rams were placed at a height of 210 mm from the strong floor and provided a clamping force of 60 kN. In Units 2 and 3, the height of the rams was 330 mm and a 120 kN clamping force was applied.

External post-tensioning was provided in Unit 3 to simulate gravity load effects by means of two 23 mm diameter threaded high-strength bars, see Figure 5.1 and 5.9

[V1]. A constant axial load of 100 kN per bar was provided by connecting one end of each bar to a hinging mechanism bolted to the strong-floor, see Figure 5.12, with the other end passing through computer-controlled centre-hole hydraulic jacks suspended by the arrangement shown in Figures 5.9 and 5.10. A computer servo-controlled system was utilised to keep the externally applied axial load constant during the test.

5.3 Assemblage

After assembly of the reinforcement cage and positioning in the mould, the concrete was cast and then cured with wet sacking and polyethylene sheeting. Compressive strength tests of standard concrete cylinders conducted 7 days after casting determined the time at which the walls were lifted from the mould. Adhesion of the wall to the mould upon lifting was minimised through application of a debonding agent to the mould prior to casting. Before lifting the precast concrete wall onto the supporting beam, the contact surfaces of both the wall and the beam were mechanically roughened to improve the shear transfer mechanism in this region. In addition, bleed holes were drilled into the wall for subsequent grouting of the energy dissipation devices (Units 2 and 3) and shear dowels. Each wall was lifted by means of lifting points welded into the top plate of the wall onto the foundation beam, see Figure 5.13, with the tendons already inserted into the ducts in the wall and temporarily connected at the top of the wall. The walls were vertically aligned with shims and then lifted once again to place a high-strength Conbextra GP mortar bed on the foundation beam, see Figure 5.14. The wall was temporarily supported to the lateral restraint beam to prevent unintentional movement during curing of the mortar bed and subsequent grouting and prestressing operations. Conbextra GP was also used in the grouting of the energy dissipators into the wall panels for Units 2 and 3, see Figure 5.15.

The tendons were released from the top of the wall and allowed to drop through the flat ducts in the foundation beam. Standard accessories were positioned at the live and dead ends prior to the stressing operations. The prestressing force was provided by means of centre-hole rams placed on the 30 mm thick plates on top of the wall, see Figure 5.1. Each tendon was initially stressed to 94 kN whereupon the force was

released to approximately 0.15 f_{psu} to overcome the anchorage set and the stressing force was reapplied. The elongation corresponding to various force levels up to the maximum post-tensioning force were monitored to determine the actual properties of the tendons. The designated prestressing force was maintained on the tendons for twenty four hours to monitor the data acquisition system and then re-applied prior to testing. It was noticed that losses of up to 15-20% were sustained due to leakage of fluid from the stressing rams. The tendons were grouted in the flat ducts up to the top face of the foundation beam only.

Prior to testing the instrumentation was calibrated and the force level in the tendons was checked and any necessary adjustments made when necessary. Testing commenced at least twenty-four hours after all grouting operations (e.g. grouting of the shear dowels, tendons, mortar bed at the horizontal wall-foundation joint, and the energy dissipation devices in Units 2 and 3). Figure 5.16 shows Unit 3 in the loading frame during testing. A close-up view of the lateral and external axial loading systems is illustrated in Figure 5.17.

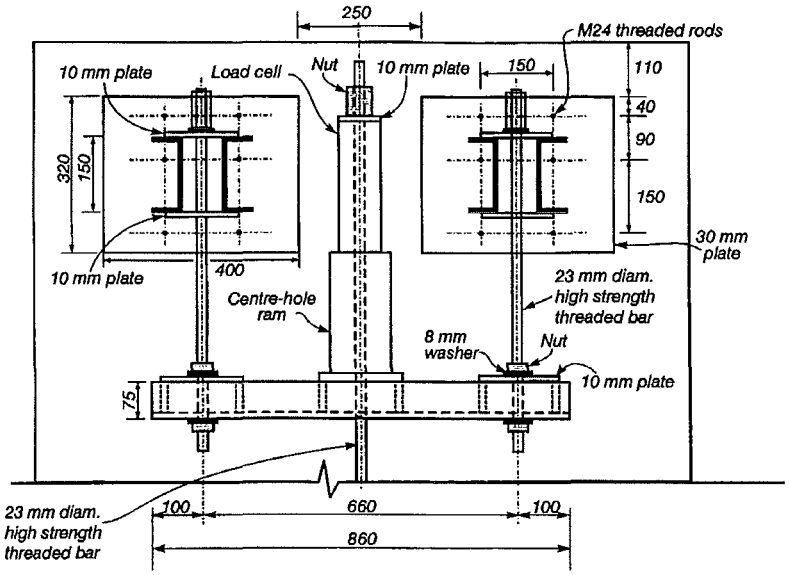

Figure 5.10: Detail of external post-tensioning arrangement used in Unit 3.

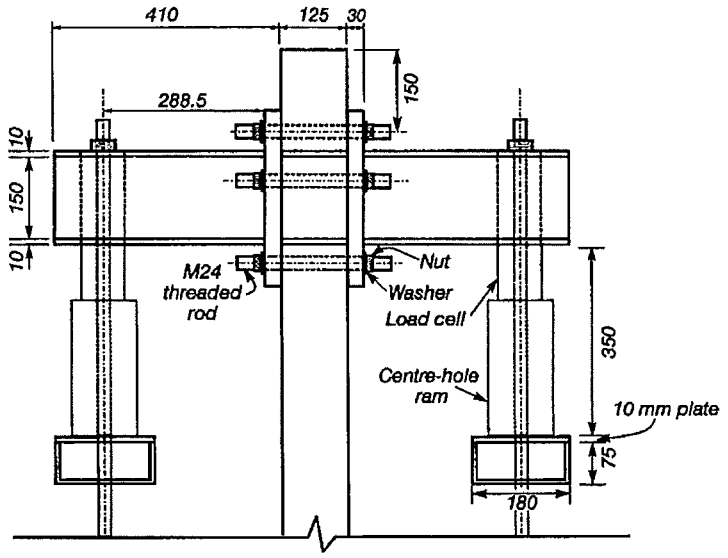

Load frame-wall connection detail

Figure 5.11: Side-view of arrangement at top of Unit 3.

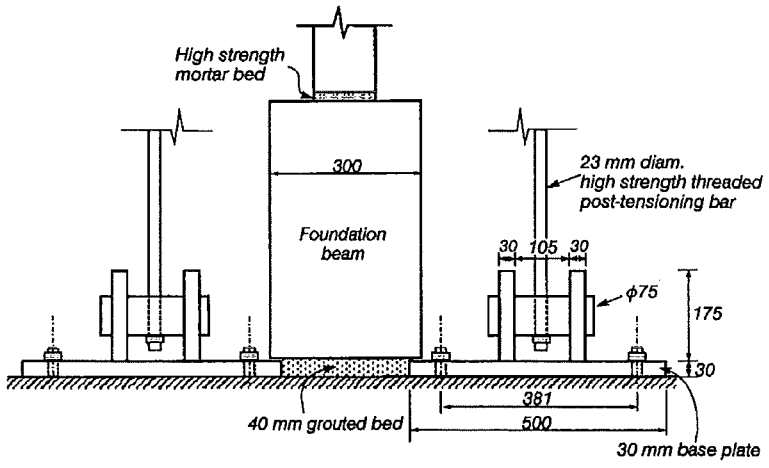

Strong-floor connection detail

Figure 5.12: Details of anchorage of external post-tensioning system with strong floor (Unit 3).

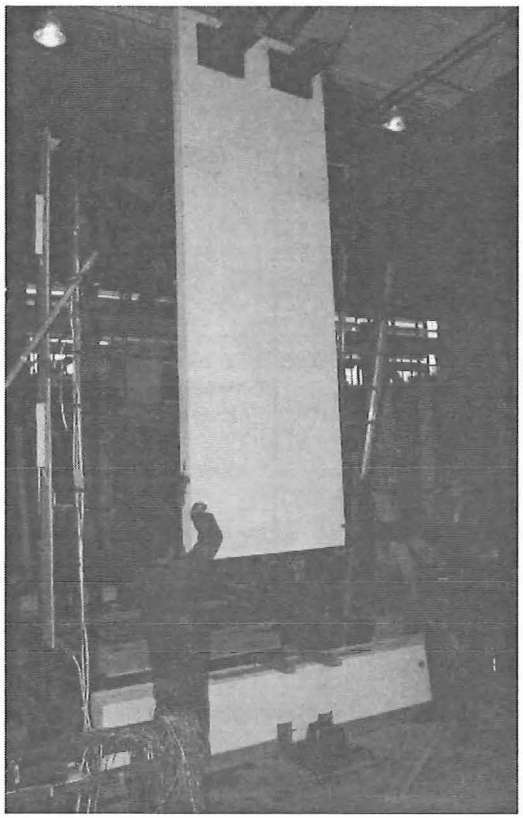

Figure 5.13: Lifting of wall onto foundation beam.

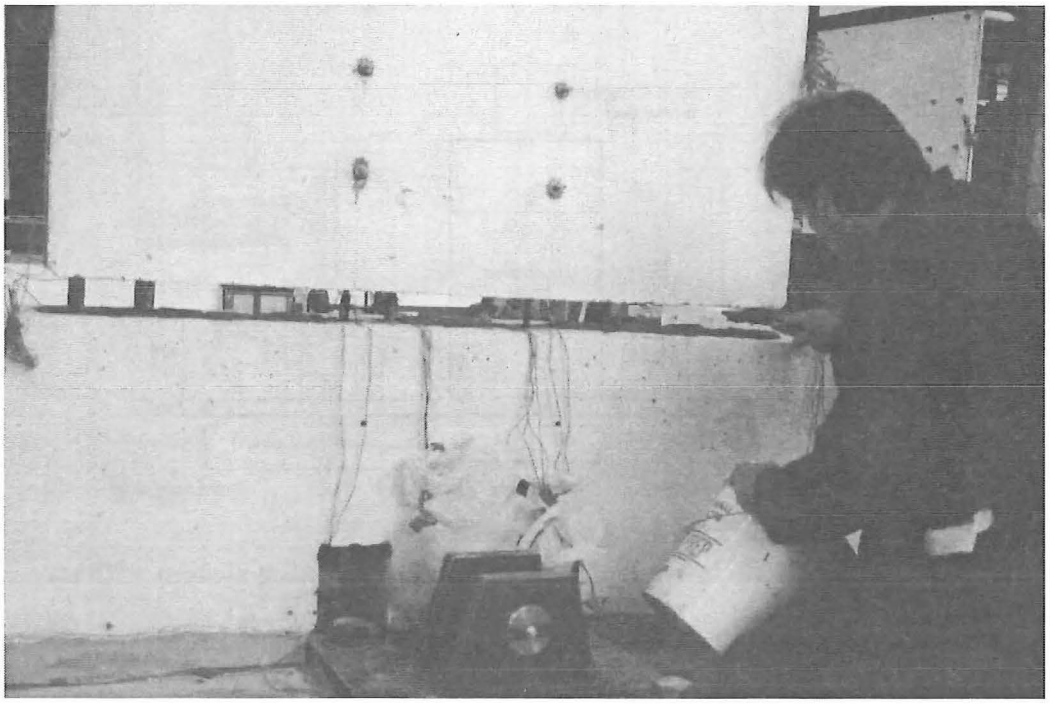

Figure 5.14: Placing of mortar bed at the wall-foundation beam joint after alignment of wall.

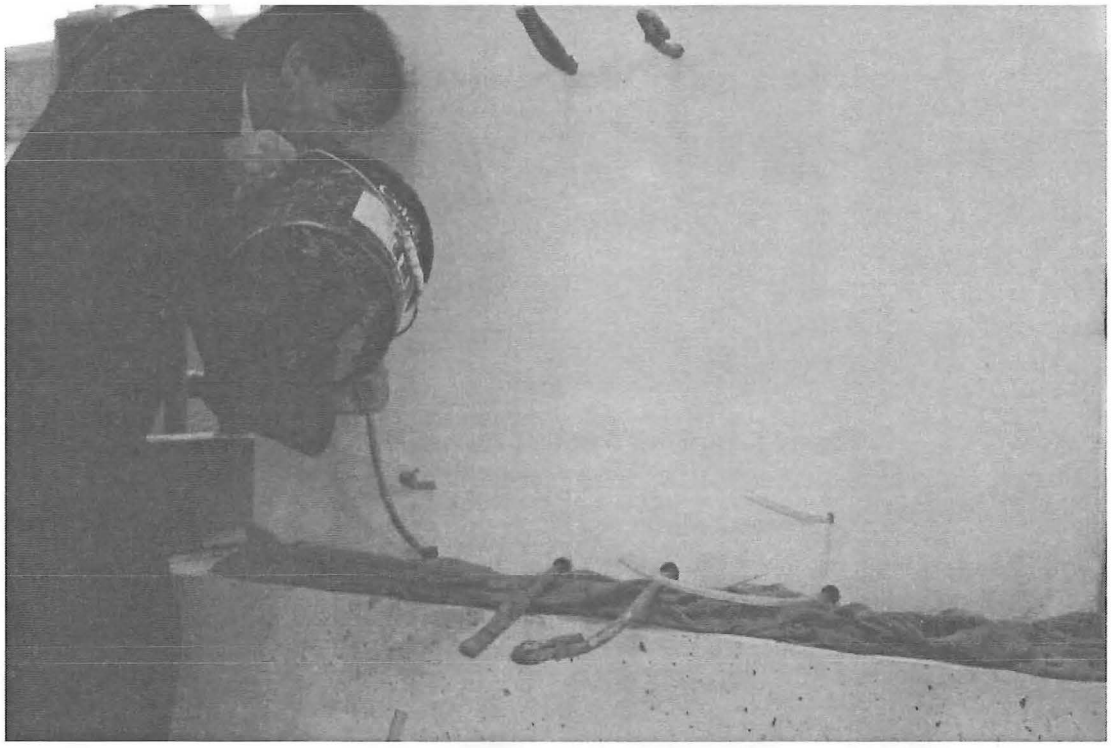

Figure 5.15: Grouting operation of energy dissipators and shear dowels prior to testing.

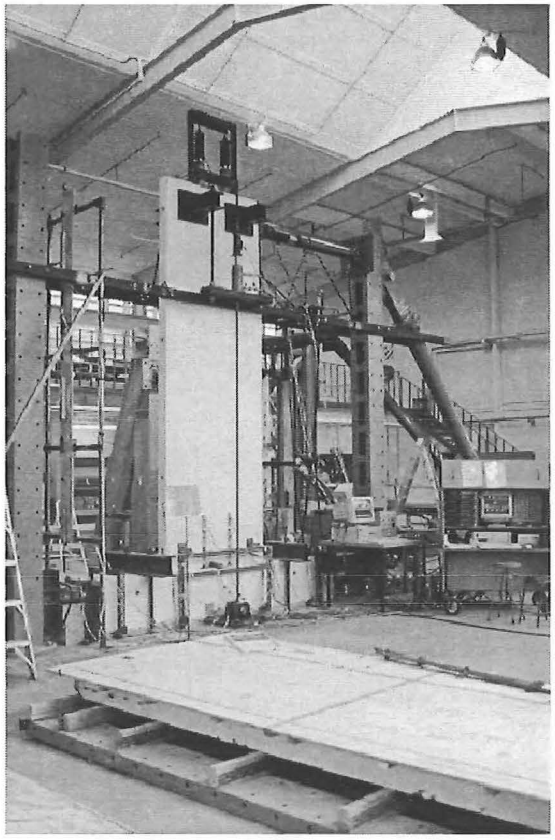

Figure 5.16: Unit 3 in test rig prior to testing.

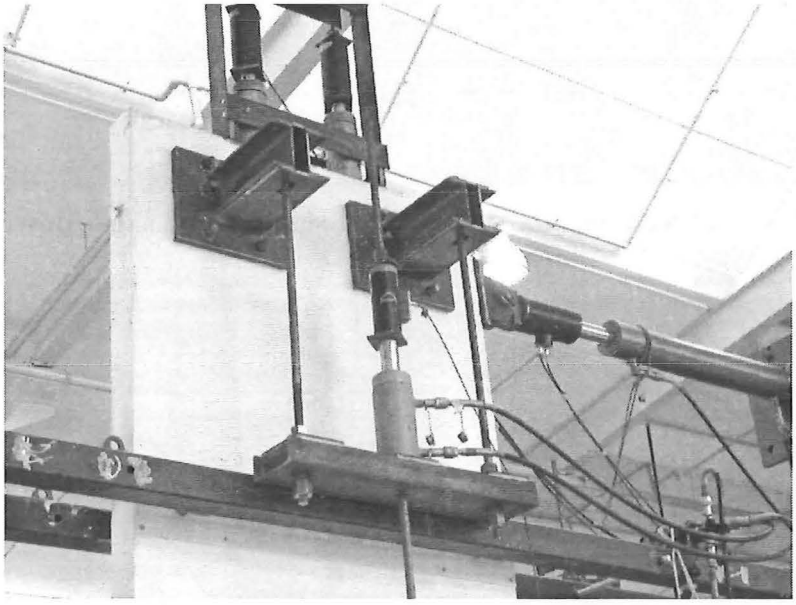

Figure 5.17: Close-up of actuator and prestressing and external post-tensioning arrangements at top of Unit 3.

5.4 Material Properties

Tests were conducted to determine the properties of the concrete, tendons, and steel reinforcement used in the specimens.

To determine the concrete compressive strengths for each wall, nine cylinders of standard dimensions (200 mm high and 100 mm diameter) were cast, cured in a fog room, and tested at 7, 14 and 28 days after casting, with three cylinders tested for each age. An additional three cylinders were placed beside the walls, thus subjecting the cylinders to the same curing conditions as the walls, and tested on the same day of the wall test. Table 5.3 shows the average strengths obtained from the three 28-day cylinders and the three cylinders which were subjected to the same curing conditions as the wall. A general purpose high strength grout (Conbextra GP), with a water/cement ratio of 20% was used in grouting the tendons, shear dowels and energy dissipators. The same material was utilised for preparing the mortar bed at the horizontal joint between the wall and foundation beam using a water/cement ratio of 15%. Small cylinders (100 mm high and 50 mm diameter) were prepared and the average compressive strength of three cylinders per test are indicated in Table 5.4.

All non-prestressed reinforcement (5.5 mm diameter plain round bars, 10mm deformed bars and 20 mm diameter deformed bars) were subjected to tensile strength tests. Table 5.5 indicates the different bars, their application in the tests and their relevant characteristics. The tensile yield strength of the 5.5 mm diameter plain round bars was determined from the average of the 0.2% proof strain of five 500 mm long specimens instrumented with 2 mm long strain gauges. One specimen of the 10 mm diameter reinforcing bar was subjected to a tensile strength test in the determination of its characteristics while four 20 mm diameter bars were tested for the energy dissipators of Units 2 and 3. Each standard length 20 mm diameter bar was cut into two lengths, one for the manufacture of the dissipator and the other for testing. The ultimate tensile strain of the bars was determined by placing notches on two of the test specimens, measuring the initial distances between these notches before the test and the final distances after fracture at the end of the test.

An additional tensile test was conducted on a 20 mm reinforcing bar with a milled segment of 12 mm diameter. This dog-bone was instrumented in a manner similar to the energy dissipation devices used in the tests, see Figure 5.4. The purpose of this test was to establish a relationship between the axial strain developed in the non-milled segments and the axial force applied. This obviated the need for relying on the actual area of the non-milled segments to which the 2 mm strain gauges were attached and enable a calibration of the strain-force relationship to be used during the reduction of data.

Four tests were conducted to determine the properties of the tendons and various methods of strain measurement were employed. Two 20 mm strain gauges were attached to either side of the prepared (cleaned and epoxied) surface of the tendons. In addition, a 500 mm travel potentiometer was attached such that the strain gauges were located in the middle of the potentiometer gauge length. Problems were encountered during the tensile strength tests, which resulted in difficulties in data interpretation. Slippage of the specimens was a common problem in addition to fracture of the tendons caused by the notching effect of the serrated jaws of the testing machine. The use of cushioning material (aluminium foil) was attempted with no success, possibly due to insufficient thickness of the foil. Table 5.6 shows the measured mechanical properties of the tendons.

Table 5.3: Measured cylinder concrete compressive strength. [a]

Unit	Average 28-Day Compressive Strength[b] (MPa)	Age on Day of Test (Days)	Average Compressive Strength at Day of Test[d] (MPa)
1	49 [c]	51	41
2	46	34	48
3	35	41	31

Notes:

[a] Aggregate size = 13 mm
[b] Average of three fog -cured specimens
[c] Strength obtained at 37 days
[d] Average of three specimens with equal curing conditions as the test walls

Table 5.4: Measured cylinder compressive strength of grout [a].

Unit	Age on Day of Test (Days)	Average Compressive Strength at Day of Test (MPa)
1	10	37
2	12	67
3	8	60

Notes:

(a) Water/cement ratio = 15 %.
(b) Values are averages of three specimens.
(c) Specimens subjected to normal curing conditions and tested on day of wall test.

Table 5.5: Measured mechanical properties of non-prestressed reinforcement.

Bar Diameter (mm)	Application	f_y (MPa)	f_{su} (MPa)	ε_{su}
5.5	Wall transverse reinforcement Cross-ties in wall Confinement at wall ends	400	N/A[a]	N/A[a]
10	Wall longitudinal reinforcement	430	570	N/A[a]
20	Energy dissipation devices	460	630	15%

Note:

(a) Designates properties that were not required in design for the particular application.

Table 5.6: Measured mechanical properties of 12.7 mm diameter prestressing strands.

E_{ps} (GPa)	f_{slp} [(a)] (MPa)	f_{psy} [(b)] (MPa)	F_{psu} (MPa)
180	1746	1435	1836

Notes:

[(a)] Defined from the proof load at 0.2% strain offset on a single strand

[(b)] True limit of proportionality, average of two specimens

5.5 Instrumentation

The in-plane lateral displacement of each wall was monitored by three potentiometers placed at regular intervals along the height of the wall (P1 and P2 = 300 mm travel, P3 = 200 mm travel, see Figure 5.18). The topmost potentiometer was aligned to the actuator that provided the cyclic quasi-static lateral force. An additional 30 mm travel linear potentiometer (P16) was attached in parallel to P1 to enable the low amplitude lateral displacements to be monitored with increased resolution. Potential horizontal movement (sliding) of the wall was monitored by a 50 mm travel potentiometer mounted on the top face of the beam at wall mid-length (see P10 in Figure 5.18). Potentiometers P4 to P9 (30 mm travel) were screwed to fittings epoxy-bonded to the south face of the wall and coincided with the centerlines of the tendons. These were utilised to monitor the lift-off of the wall and to measure the elongation in the tendons. In addition, the wall elongation at the level of the energy dissipation devices in Units 2 and 3 were interpolated from the readings of the lowermost pair (P4 and P5). This elongation was used to determine average strains in the milled section of the devices. Out-of-plane motion of the wall was monitored by 50 mm travel potentiometers fixed to a steel frame bolted to the strong floor (see P11 and P12 in Figure 5.18). Potential horizontal movement of the beam relative to the strong floor was monitored by a 50 mm travel potentiometer mounted to a steel frame bolted to the strong floor (see P15 in Figure 5.18). Base rotation of the system (wall and foundation beam) was monitored by vertical, downward directed potentiometers fixed to a steel frame bolted to the strong floor at the ends of the foundation beam (see P13 and P14 in Figure 5.18).

The transverse wall reinforcement and rectangular ties (confinement steel) were instrumented with 2 mm electric foil strain gauges, see Figure 5.18. These were attached at the ends of the first three layers of confining reinforcement in the three test units. Three 20 mm long strain gauges epoxy-bonded to the exterior surface of the walls were placed concentrically to the wall widths at the east and west ends, see Figure 5.19. These were attached along the height of the walls; the first located 50 mm from the lower edge of the wall and the next two spaced at 130 mm and 210 mm, respectively. Unit 1 had an additional strain gauge at 370 mm from the lower edge of the wall.

Two 20 mm long strain gauges were attached to either side of the surface of each tendon at a height corresponding to the lower edge of the wall. The surfaces of the tendons at the appropriate heights were carefully cleaned and then coated with an epoxy resin upon which the strain gauges were attached. In addition, 250 kN load cells situated on top of the centrehole jacks (267 kN capacity), used to prestress the tendons at the top of the wall, measured the forces that developed in the tendons.

Two strain gauges (2 mm long) were attached to either side of the energy dissipators at the top and bottom of the milled segment, see Figure 5.4. The exterior lugs of the Grade 430 (20 mm diameter) reinforcing bars were removed and the strain gauges were attached to the surface. The forces that developed at either end of the dissipators (incorporated in Units 2 and 3) were obtained from these readings.

In addition to the above instrumentation, a graphic plotter was installed as backup and indicated the lateral force-displacement response as measured by the 300 kN load cell attached to the main double-acting (330 kN compression and 438 kN tension) actuator and the corresponding (topmost) potentiometers (see P1 and P16 in Figure 5.18).

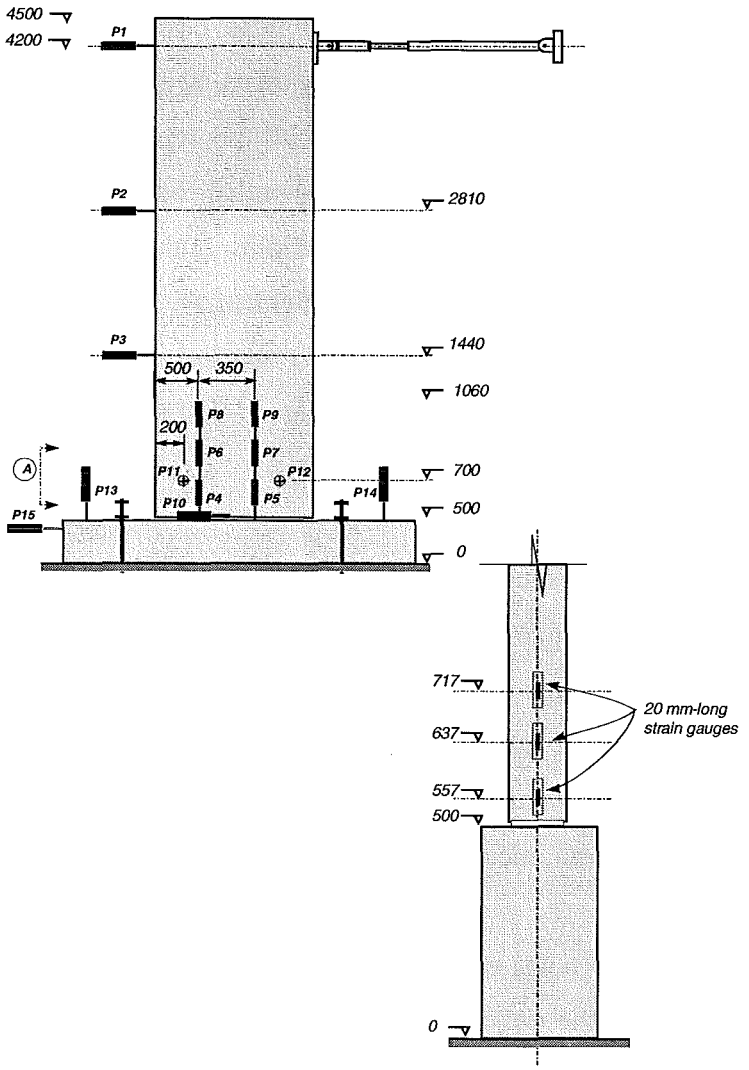

Figure 5.18: Location of external instrumentation on test units.

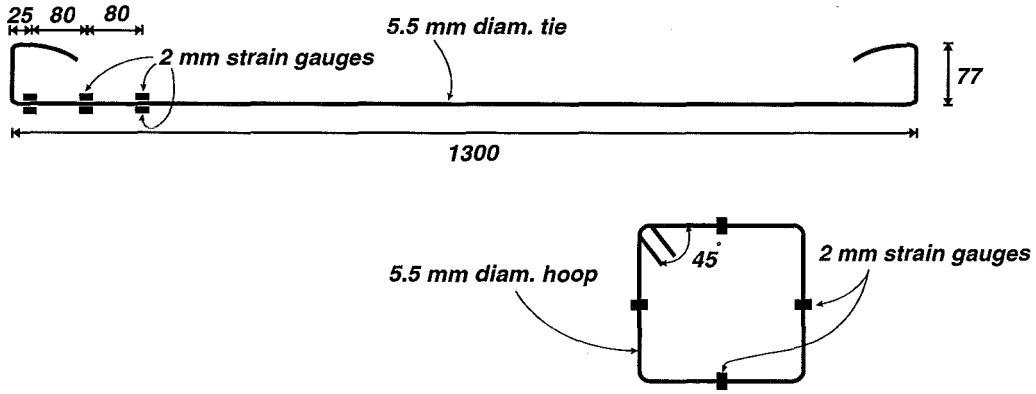

Figure 5.19: Instrumentation of steel reinforcement in test units.

5.6 Loading Regime

A quasi-static cyclic reversed lateral force regime was applied with displacement-based cycles following initial force-based cycles. The amplitude of the force-based cycles corresponded to the following force levels:

a) Initiation of separation between the wall and the foundation beam (gapping). This occurs when the flexural stress at the base of the wall (due to the lateral force) equals the stress provided by the restoring forces (represented by the sum of the axial forces) as outlined in Section 4.5.

b) Twice the force level determined by (a) above.

c) The theoretical lateral force required to induce flexural cracking in the wall panel V_{cr}, which is determined from the modulus of rupture of the concrete, f_{cr}, [S2] as follows:

$$V_{cr} = \frac{f_{cr} Z}{H} \tag{5.1}$$

Subsequent cycles comprised two large-amplitude cycles followed by one cycle at a level corresponding to the last lower drift level. The loading history applied to each unit is presented in section 6.

6. TEST RESULTS

6.1 Unit 1

The applied quasi-static loading for Unit 1 test is shown in Figure 6.1 and is also tabulated in Table 6.1. It is to be noted that the drift amplitudes applied in the negative and positive directions were not equal, due to difficulties of monitoring the level of lateral displacement during the test.

Separation of the wall from the mortar bed occurred at 0.2% drift. Damage in the wall at the end of the test was limited to some spalling at the end regions though it did not extend more than 60 mm up the height of the wall, see Figure 6.2. A separation gap of 30 mm was sustained at the ends of the wall during the last stages of the test, but this closed completely upon removal of the lateral force.

The lateral force-drift response of Unit 1 is shown in Figure 6.3. The non-linear elastic response is clearly evident in this figure. No residual lateral displacements were recorded during the response, even after the application of drift levels to 2.8%. It is to be noted that no energy dissipators were installed in this unit. The initial stiffness of the wall at small drifts was maintained, even after excursions to large drifts. In addition, no degradation in the capacity occurred with the progressively increasing drift demands.

Figure 6.4 shows the vertical displacements of the wall base measured by the lowest pair of 30 mm potentiometers on the south face of the wall (see P4 and P5 in Figure 5.18). Base rotation, determined as the slope of the lines in Figure 6.4, was the dominant mode of deformation in the response of Unit 1. For example, in cycle 18 to 1.8% drift, base rotation accounted for 98% of the applied lateral displacement. Sliding of the wall and foundation beam, foundation beam rotation and out-of-plane wall displacements were all insignificant (less than 1 mm).

The position of the neutral axis depth was determined by extrapolation of the lines joining the data from potentiometers P4 and P5 in Figure 6.4. The depth, measured from the extreme compressive fibre, varied between 71 and 93 mm for the cycles to positive drifts at or exceeding 1.4% drift. In the cycles to negative drifts at or exceeding 1.2% drift, the neutral axis depth was found to range between 87 and 108 mm.

Figure 6.5 shows the variation of the forces developed in the tendons as measured by the load cells at the live ends, see Figure 5.1. The forces recorded at the peak of each cycle are shown in Figure 6.6. Notable increases in the prestressing force commenced only at cycles 6 (0.6% drift) and 9 (0.7% drift) in the west and east tendons, respectively. The elongation in the east and west tendons corresponding to these drift levels (as measured by the lower pair of 30 mm potentiometers on the wall face) were 4.3 and 3.2 mm, respectively.

The force corresponding to the true limit of proportionality of the tendons (143.5 kN) was attained at 2% drift, as may be seen in Figure 6.6 (cycles 17 and 12 for the east and west tendons, respectively). The loss of the prestressing force was noted upon unloading from the cycles exceeding 2% drift, see Figure 6.6. The maximum forces developed in the east and west tendons of 158 and 155 kN, respectively, occurred at 2.7% drift (cycle 21 for the east tendon and 20 for the west tendon).

Incipient crushing of the concrete cover was observed to occur at the peak of cycle 16 at 2% drift. Nonetheless, spalling of the concrete cover only took place in cycle 25 at 2.8% drift. Spalling took place over a 60 mm square region, see Figure 6.2.

The compressive strains developed at the ends of Unit 1 are depicted in Figure 6.7. Data from the lower strain gauges were discarded at the higher drift levels due to incipient crushing of the concrete cover. The increase in strains with progressive increase in drift is evident in Figure 6.7. However, the magnitude of the strains is quite low at the levels recorded. This suggests that large strains were mainly concentrated in the wall near the wall-foundation beam interface and in the mortar bed.

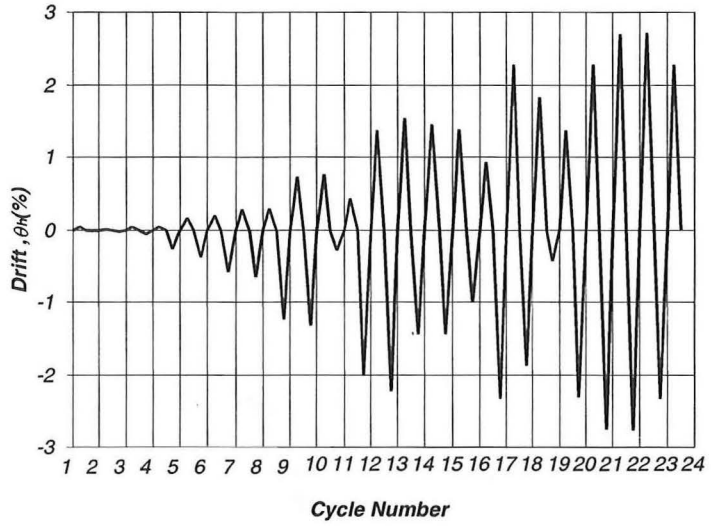

Figure 6.1: Loading regime applied in testing of Unit 1.

Table 6.1: Peak drifts monitored during the test of Unit 1.

	Cycle	1	2	3	4	5	6	7	8	9	10	11	12	13-14	15
Drift %	+ve	0.05	0.02	0.04	0.04	0.2	0.2	0.3	0.3	0.7	0.8	0.4	1.4	1.5	1.4
	-ve	0.01	0.02	0.06	0.25	0.4	0.6	0.65	1.2	1.3	0.3	2.0	2.2	1.4	1.0

	Cycle	16	17	18	19	20	21	22	23
Drift %	+ve	0.9	2.3	1.8	1.4	2.3	2.7	2.7	2.3
	-ve	2.3	1.9	0.4	2.3	2.7	2.8	2.3	0

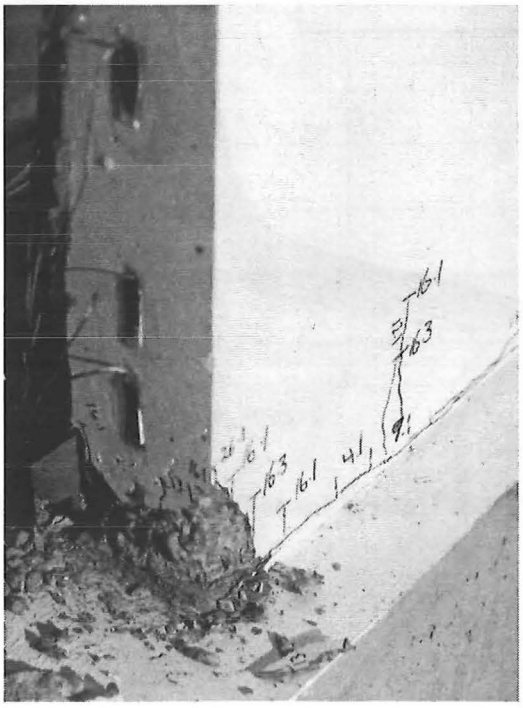

Figure 6.2: East end of Unit 1 at end of test.

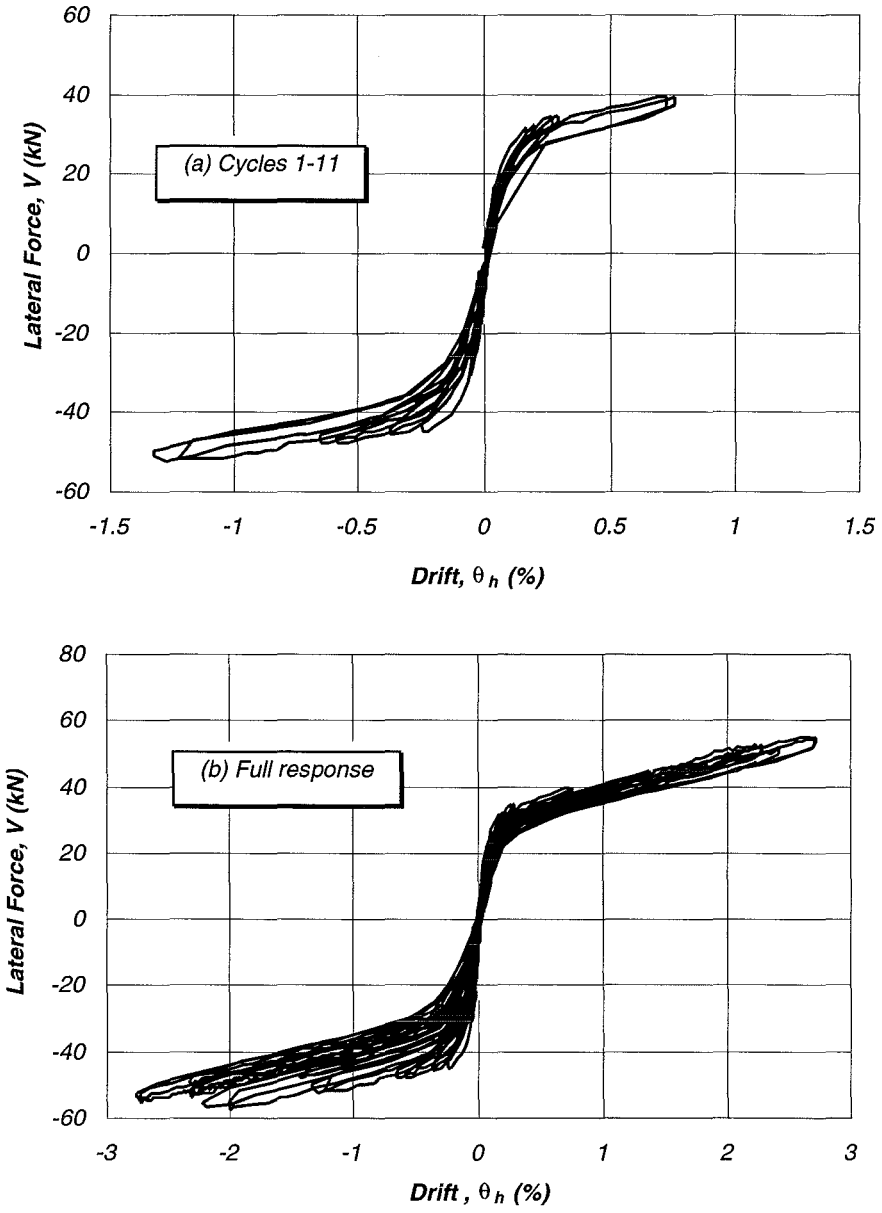

Figure 6.3: Lateral force-drift response of Unit 1.

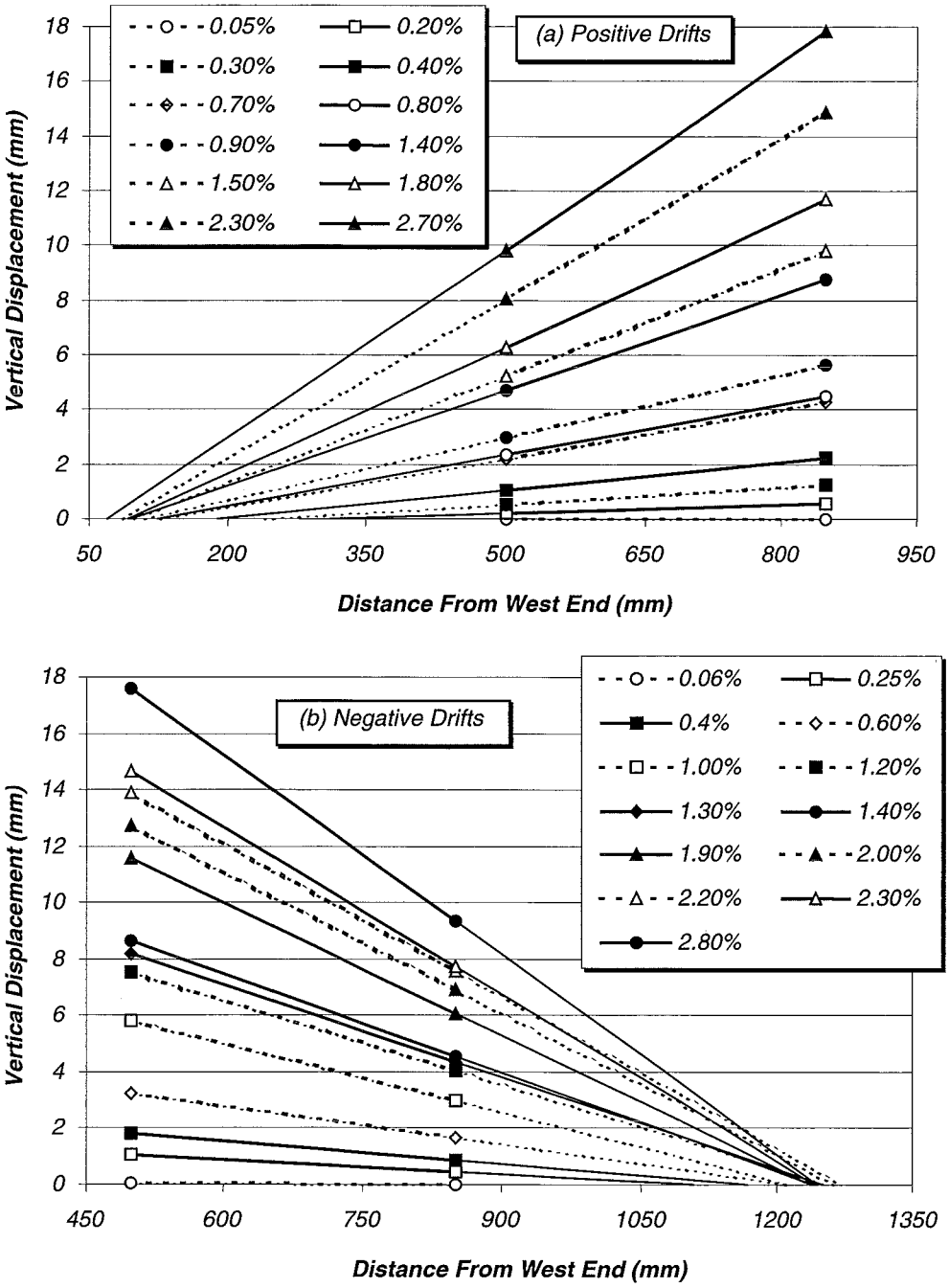

Figure 6.4: Vertical displacement of Unit 1 at the construction joint corresponding to different lateral drift levels.

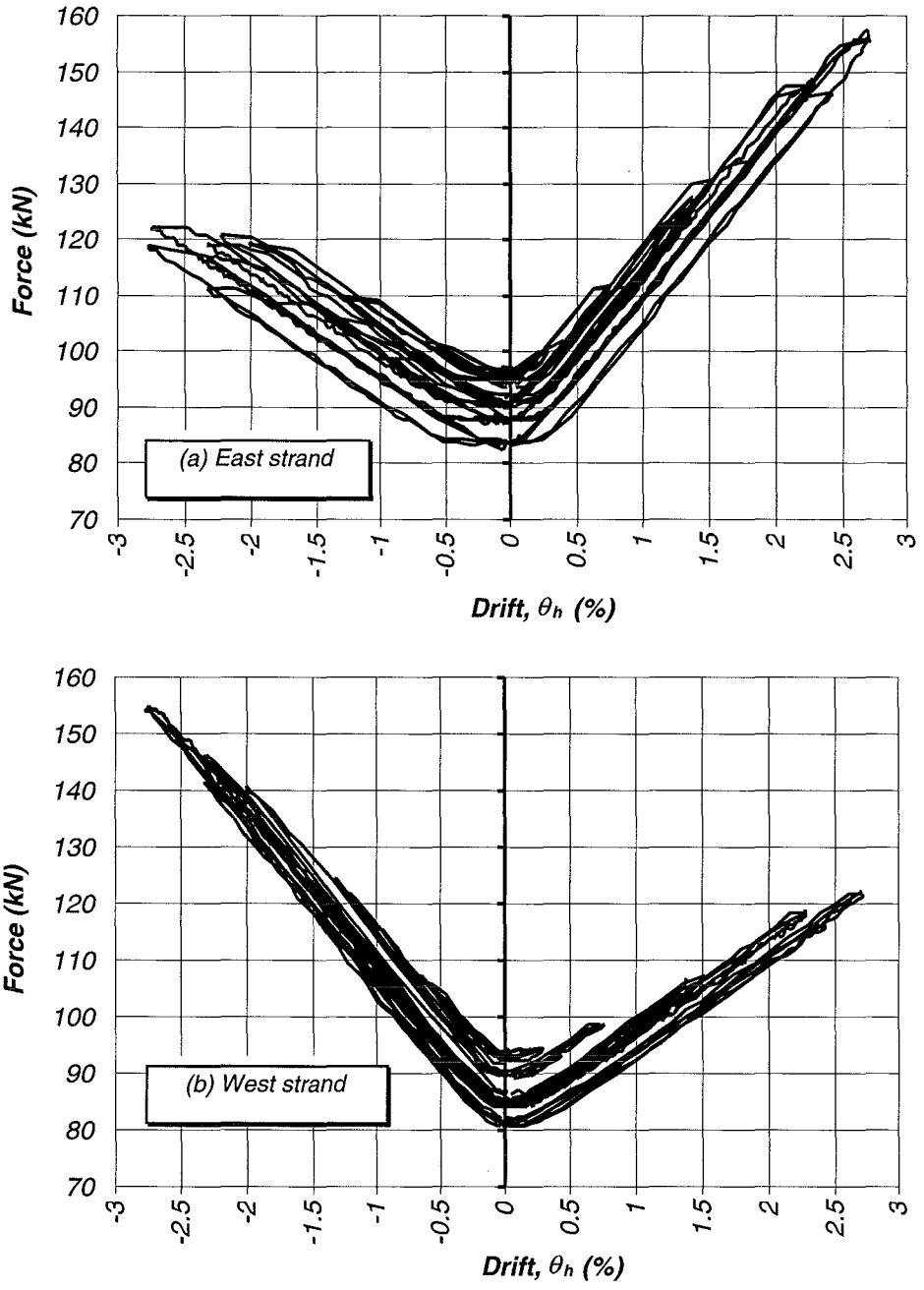

Figure 6.5: Forces developed in prestressing strands of Unit 1 at various drift levels.

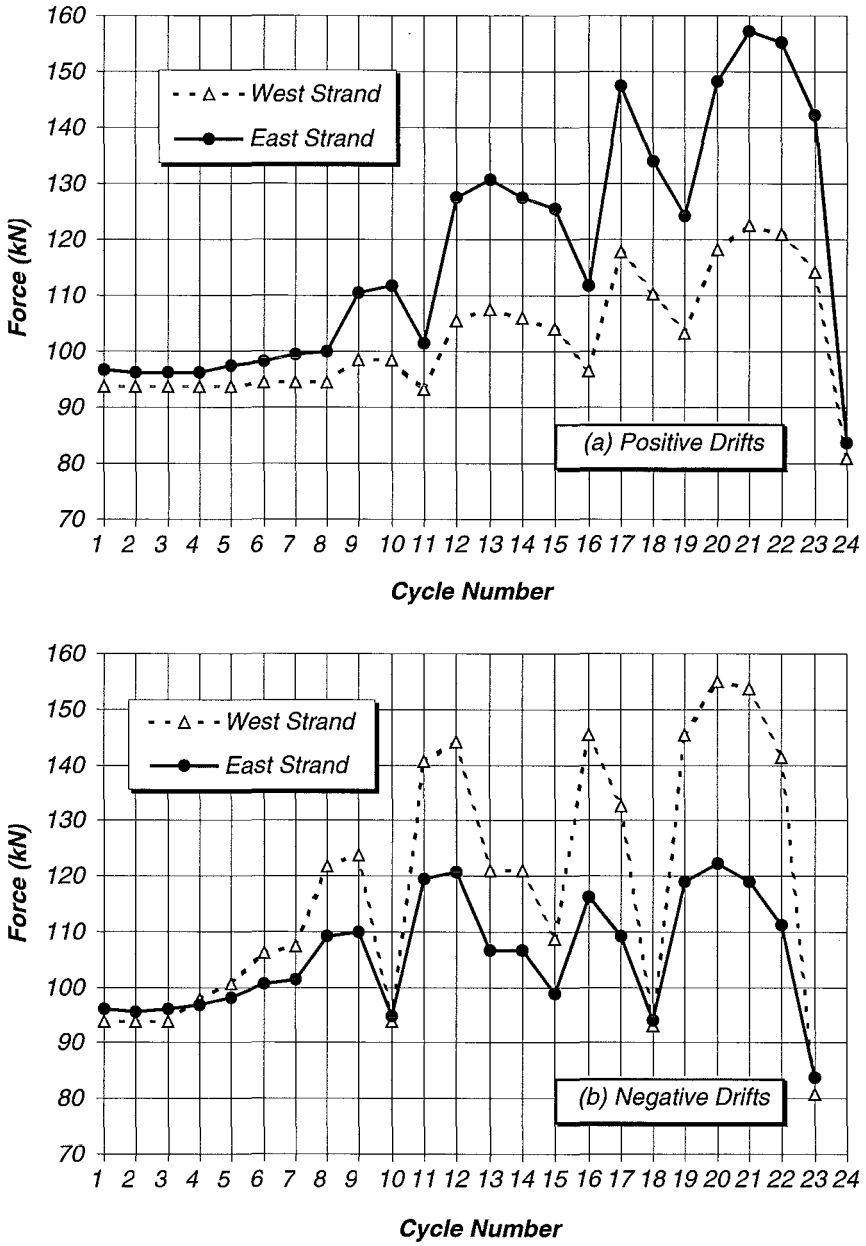

Figure 6.6: Maximum forces in prestressing strands of Unit 1 at the different loading cycles.

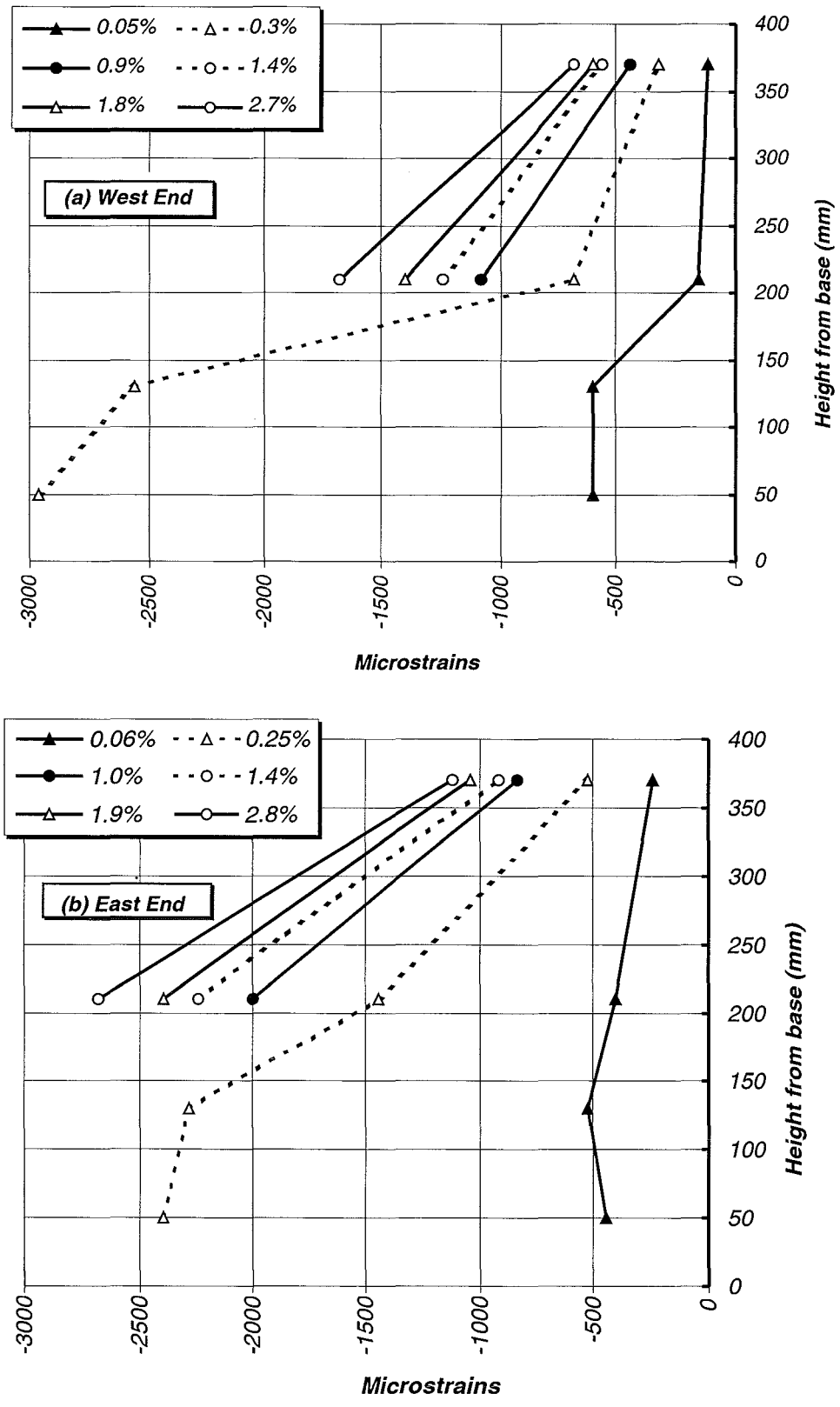

Figure 6.7: Concrete strains at ends of Unit 1.

6.2 Unit 2

Chamfers (15x15 mm) were provided at the ends of the wall panel in this unit as a simple method to reduce the cosmetic damage observed during the test of Unit 1. Unit 2 also incorporated two energy dissipators. The dissipators were designed as outlined in Section 4.4, resulting in a 12 mm diameter for the milled segment of the dissipator.

Minor damage was inflicted to the concrete at the base of the wall during the lifting operation. The damage was repaired during the preparation of the mortar bed. This damage did not influence the response obtained for this unit.

The loading regime applied for the testing of Unit 2 is shown in Figure 6.8 and is also tabulated in Table 6.2. Complete data for only the last nine cycles of loading are available due to electronic data corruption.

The crack between the wall and mortar bed extended nearly the full length of the wall at 0.2% drift. At cycle 22 to 2.5% drift, a single flexural hairline crack developed at the west end of the wall at a height of 1.65 m. This crack extended 350-400 mm towards the centre of the wall along both faces. A similar crack developed at the same level in the east end during the following half cycle, see Figure 6.9. Flexural cracks also developed at 2.0 metres from the base of the wall during subsequent loading cycles but were of shorter lengths than the lower cracks. A single hairline crack developed on either face of the wall at 0.2% drift. This crack started at the base at a location corresponding to the east energy dissipator, see Figure 6.14. The crack on the north face progressed horizontally for 350 mm before diverging sharply towards the west dissipator at 1% drift. The corresponding crack on the south face bifurcated at a 0.25% drift with one branch extending towards the west dissipator for a distance of 250 mm. The increase in lengths of both branches ceased at a drift of 1% at which stage the east branch was approximately 50 mm long.

Visual damage in the wall was confined to the wall ends where spalling extended between 150-200 mm in the vertical direction, see Figure 6.10. Incipient crushing

these regions commenced at a drift of 1%. Nonetheless, spalling of the concrete cover only occurred at about 2% drift, spalling in the horizontal direction along the bottom edge of the wall less than 80 mm. At the conclusion of the test the crack at the wall-foundation beam joint remained open, see Figure 6.14. This was attributed to the presence of debris from the mortar bed, which had detached from the top of the foundation beam at some locations, and to the loss of the prestressing force after the tendons reached the limit of proportionality.

A loud sound was heard during the second excursion to 3% drift. This was due to the rupture of the west energy dissipator. At the end of the test this was found to have fractured at the topmost of the milled segment.

Figures 6.11 (a) and (b) plot the lateral force-drift response of Unit 2. Figure 6.11 (a) shows the response during cycles 7, 11, 13, and 16. To obtain this response, points were digitised from the x-y plot used as a back up measure during the test. For completion, the response shown in Figure 6.11 (a) has been superimposed with the data obtained electronically. Figure 6.11 (b) shows the response of this unit during cycles 7, 11, 13, 16 and cycles 23 to 31. It can be seen that the response of this unit is characterised by very small residual drifts in those cycles before the rupture of the energy dissipator. The presence of the energy dissipators is evident in the hysteretic response. Pinching of the response near the origin in the final stages of the test suggests the wall slid, although the linear potentiometer monitoring sliding at the base of the wall indicated a maximum displacement of 1.7 mm at 3% drift. It is believed that sliding of the wall concentrated the inelastic deformations in the energy dissipators within a very small length, which resulted in the fracture the west dissipator. The gradual degradation in stiffness observed in Figure 6.11 is primarily due to unrecoverable residual compressive strains in the concrete of the wall ends and in the mortar bed.

Figure 6.12 shows the hysteretic response of the east energy dissipator for the available output (cycles 19-21) derived from the lower pair of strain gauges depicted in Figure 5.4. Data from the upper strain gauges in the east dissipator and the upper and lower strain gauges for the west dissipator was discarded due to incoherence. The

axial force in the dissipator plotted in the vertical axis of Figure 6.12 was computed from the average strain gauge readings following the calibration of a similar dissipator in a universal testing machine. The longitudinal strain shown in Figure 6.12 was derived from the vertical displacement at the level of the dissipator, obtained by interpolation from linear potentiometers P4 and P5 (refer to Figure 5.18), divided by 200 mm, which was the length of the milled segment. This implies that the strains plotted in this figure are only approximate and should be considered to be average values. It is to be recalled that the dissipators were designed such that yielding would occur both in tension and compression as shown in Figure 4.5. This is the overall behaviour obtained during this test, as Figure 6.12 shows.

The tensile forces computed at the peak of each cycle for the west dissipator are shown in Figure 6.13. It appears from the data obtained that the force in the dissipators was less than the yield force of 52 kN calculated from the tensile tests. This contrasts with the large hysteresis shown in Figure 6.12. The main reason for the discrepancy is that the axial tensile force derived from the lowermost pair of strain gauges is expected to be smaller than the force resisted in the milled section of the dissipator due to the anchorage forces that develop at the lower taper end. This effect will become obvious when data from Unit 3 is presented in the following section.

The equivalent viscous damping, ζ_{eq} was determined from the energy dissipated by hysteresis, E_D, measured by the area under the hysteretic response per cycle in Figure 6.15, and the maximum strain energy, E_{so} [C2], as follows:

$$\zeta_{eq} = \frac{E_D}{4\pi E_{so}} \tag{6.1}$$

Figure 6.15 shows the equivalent viscous damping in the system at various cycles. Equivalent viscous damping values ranging between 11% and 14% were calculated for Unit 2 for the cycles with drifts ranging between 0.5% and 3%. The loss of the west energy dissipator in cycle 25 (3% drift) is apparent in the 50% drop in the equivalent viscous damping at the subsequent cycle to the same drift level.

The vertical displacements measured by the lowest pair of 30 mm potentiometers on the south face of the wall (see P4 and P5 in Figure 5.18) are shown in Figure 6.16. By integrating the rotation obtained from these potentiometers, it was found that base rotation provided over 90% of the total applied lateral displacements in cycles 19 and beyond. Figure 6.16 also indicates that, in the cycles near the end of the test, the neutral axis depth remained fairly constant and was located at about 150 mm from the wall ends.

Figure 6.17 shows the strain readings recorded by strain gauges at the concrete surface at the wall ends. The lowest strain gauge reading is not shown as data from this gauge was only obtained for the final cycles of the test, when crushing of the concrete had already been observed. The strains recorded at a distance of 150 mm and greater were reasonably small. This suggests that the largest strains were concentrated in a small region at the base of the wall.

The strain readings obtained from the confining reinforcement are plotted in Figure 6.18. These readings are consistent with the strains obtained on the concrete at the wall ends. The strains in the reinforcement were all significantly less than the yield strain.

Load cells at the top of the wall monitored the force in the tendons, see Figure 5.1. Figure 6.19 plots the force versus drift for both tendons. The maximum values recorded at each cycle are shown in Figure 6.20. The force corresponding to the true limit of proportionality of the prestressing tendons (143.5 kN) had been attained in cycle 19 with the first excursion to 2% drift. The loss of the data prior to this cycle did not permit the determination of the cycle at which the true limit of proportionality had been obtained. Losses of 5% and 12% of the initial prestress force were sustained by the west and east tendons, respectively, in the final cycles of the test. The maximum recorded forces were 169 and 163 kN for the east and west tendons, respectively.

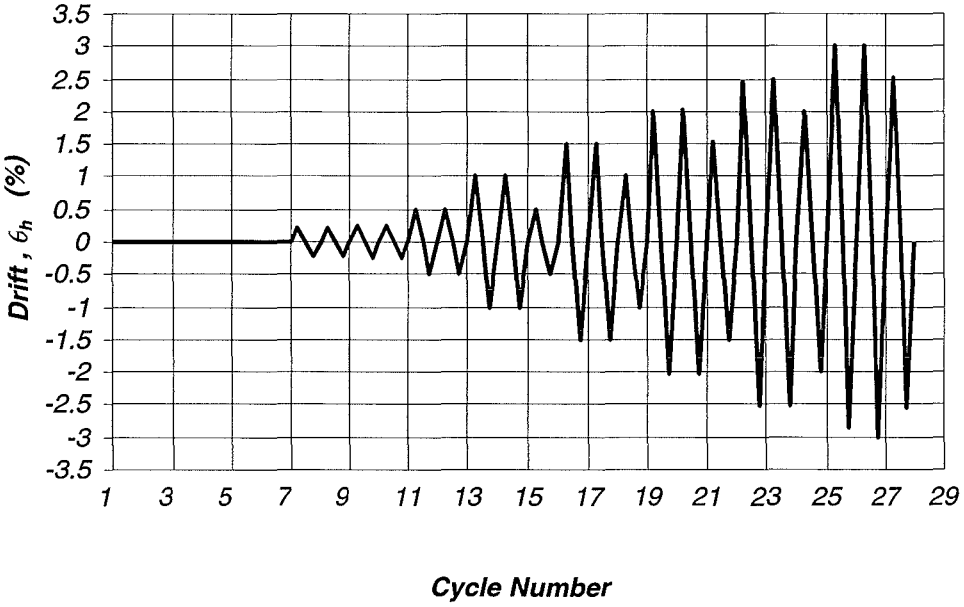

Figure 6.8: Loading regime applied in testing of Unit 2.

Table 6.2: Peak drifts monitored during the test of Unit 2.

	Cycle	1-2	3-4	5-6	7-8	9-10	11-12	13-14	15
Drift %	+ve	0.008	0.002	0.01	0.2	0.25	0.5	1.0	0.5
	-ve	0.008	0.002	0.01	0.2	0.25	0.5	1.0	0.5
	Cycle	**16-17**	**18**	**19-20**	**21**	**22-23**	**24**	**25-26**	**27**
Drift %	+ve	1.5	1.0	2.0	1.5	2.5	2.0	3.0	2.5
	-ve	1.5	1.0	2.0	1.5	2.5	2.0	3.0	2.5

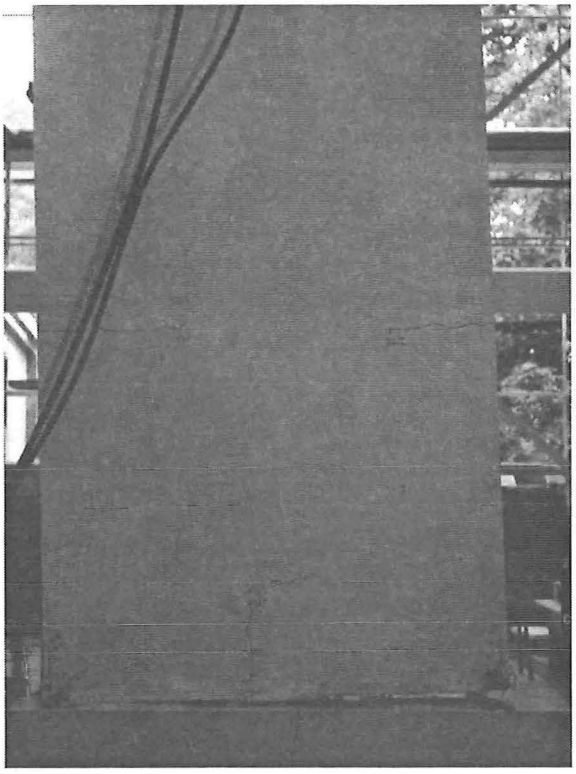

Figure 6.9: Unit 2 at 3% drift. North face.

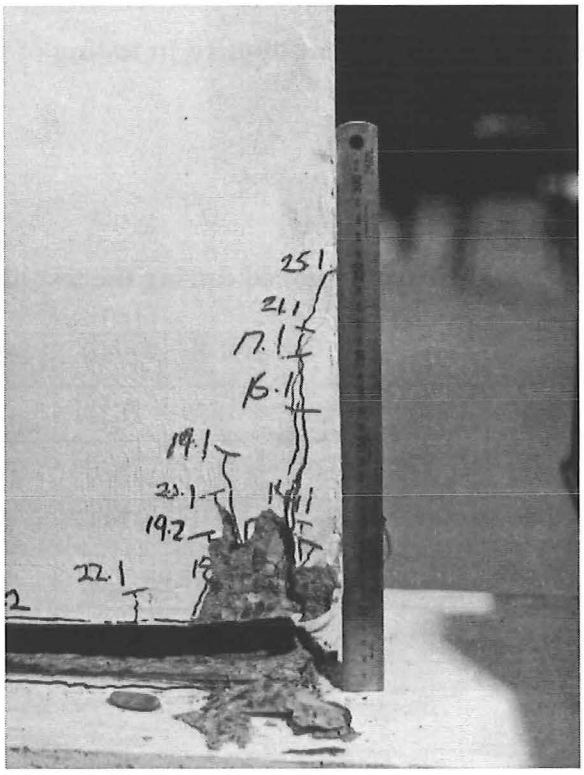

Figure 6.10: Unit 2 at 3% drift (second half-cycle). West edge (north face).

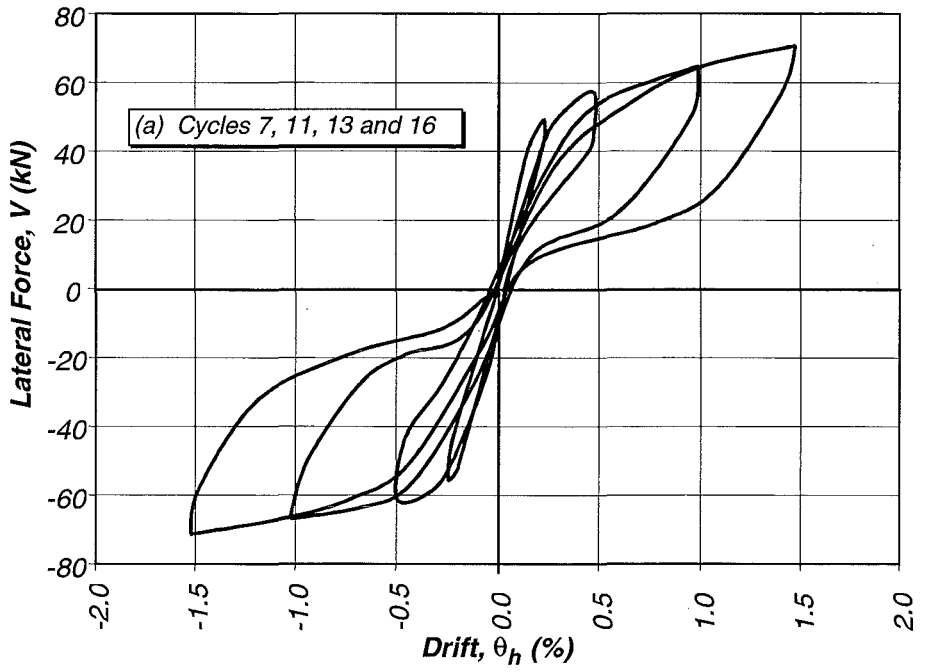

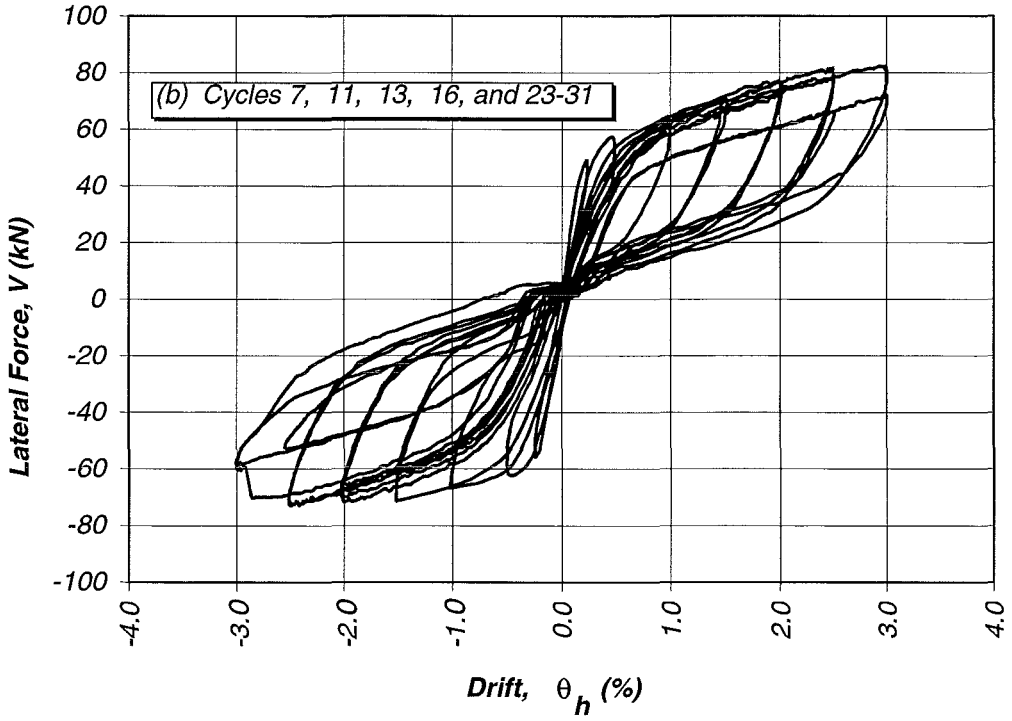

Figure 6.11: Lateral force-drift response of Unit 2.

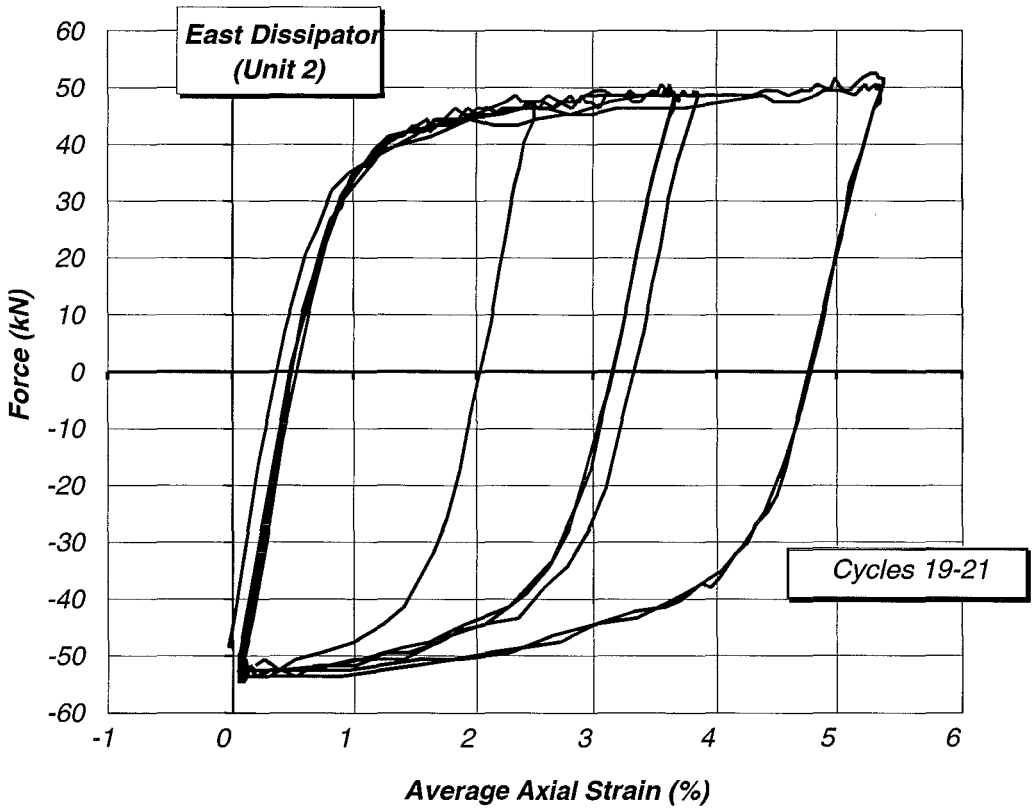

Figure 6.12: Hysteretic response of energy dissipator (east) in Unit 2.

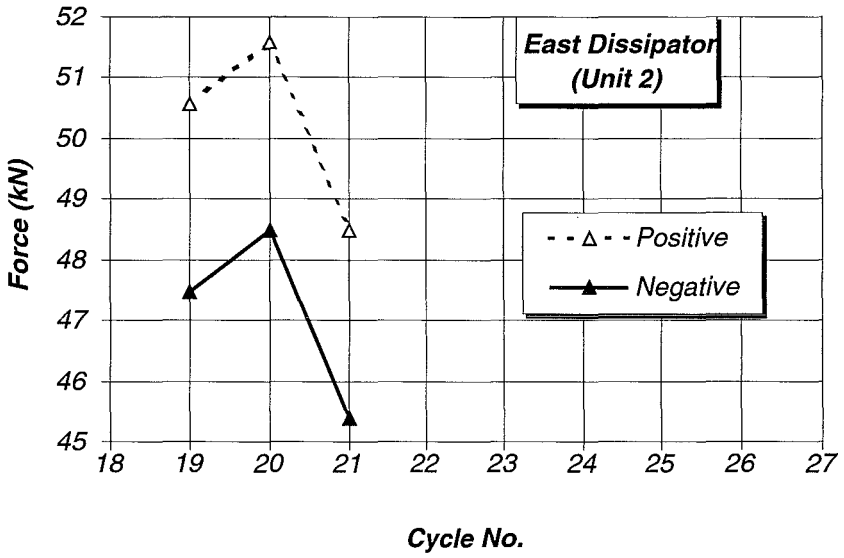

Figure 6.13: Maximum forces developed in the east energy dissipator (Unit 2).

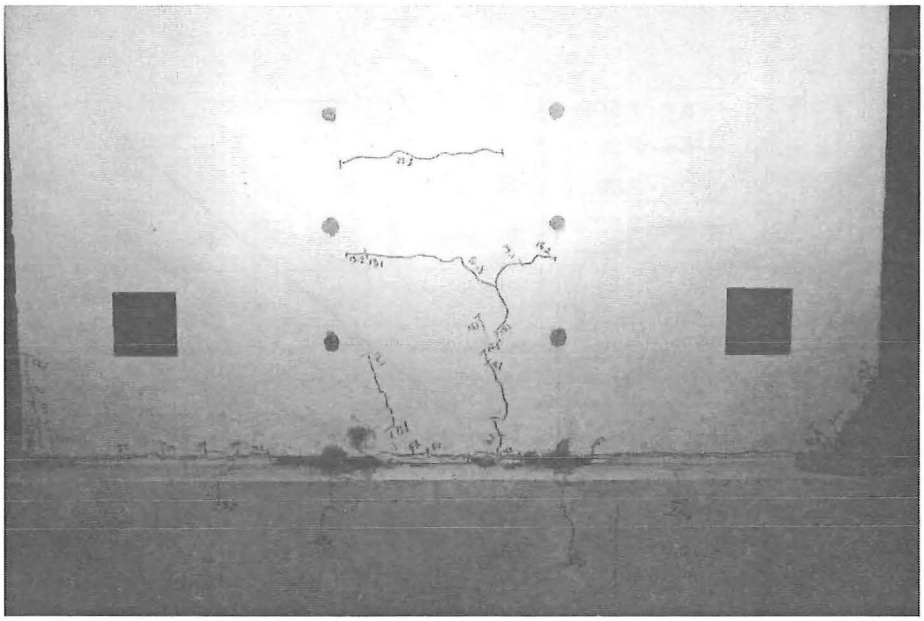

Figure 6.14: Unit 2 at end of test. South face.

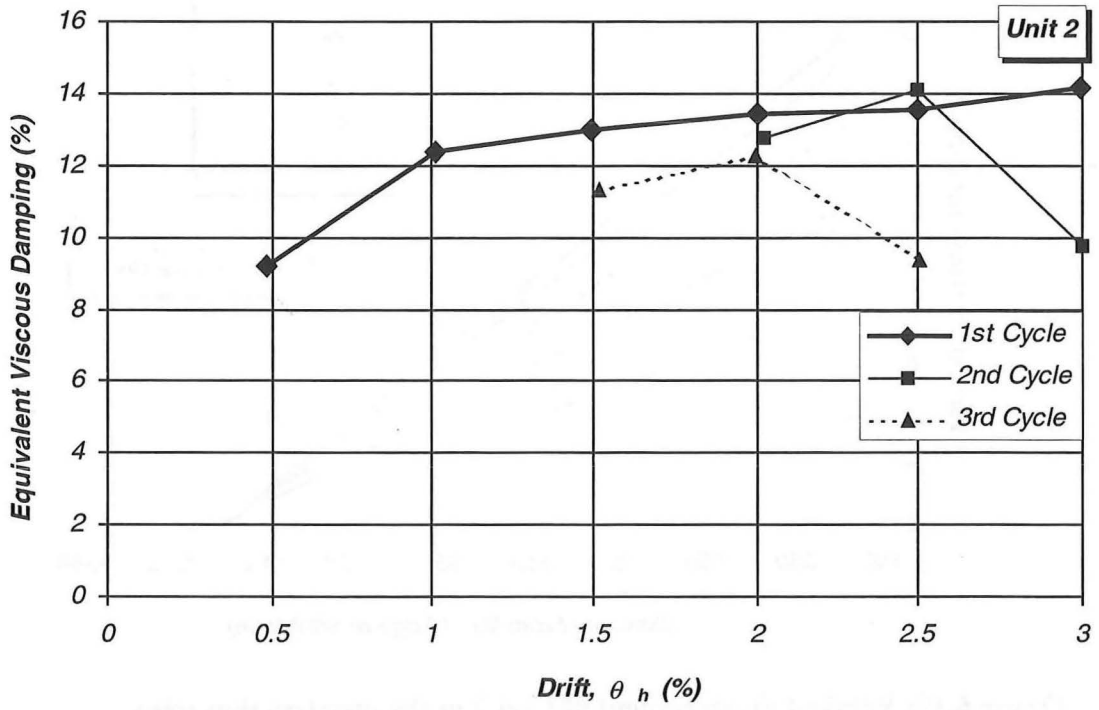

Figure 6.15: Equivalent viscous damping provided by the energy dissipators in Unit 2.

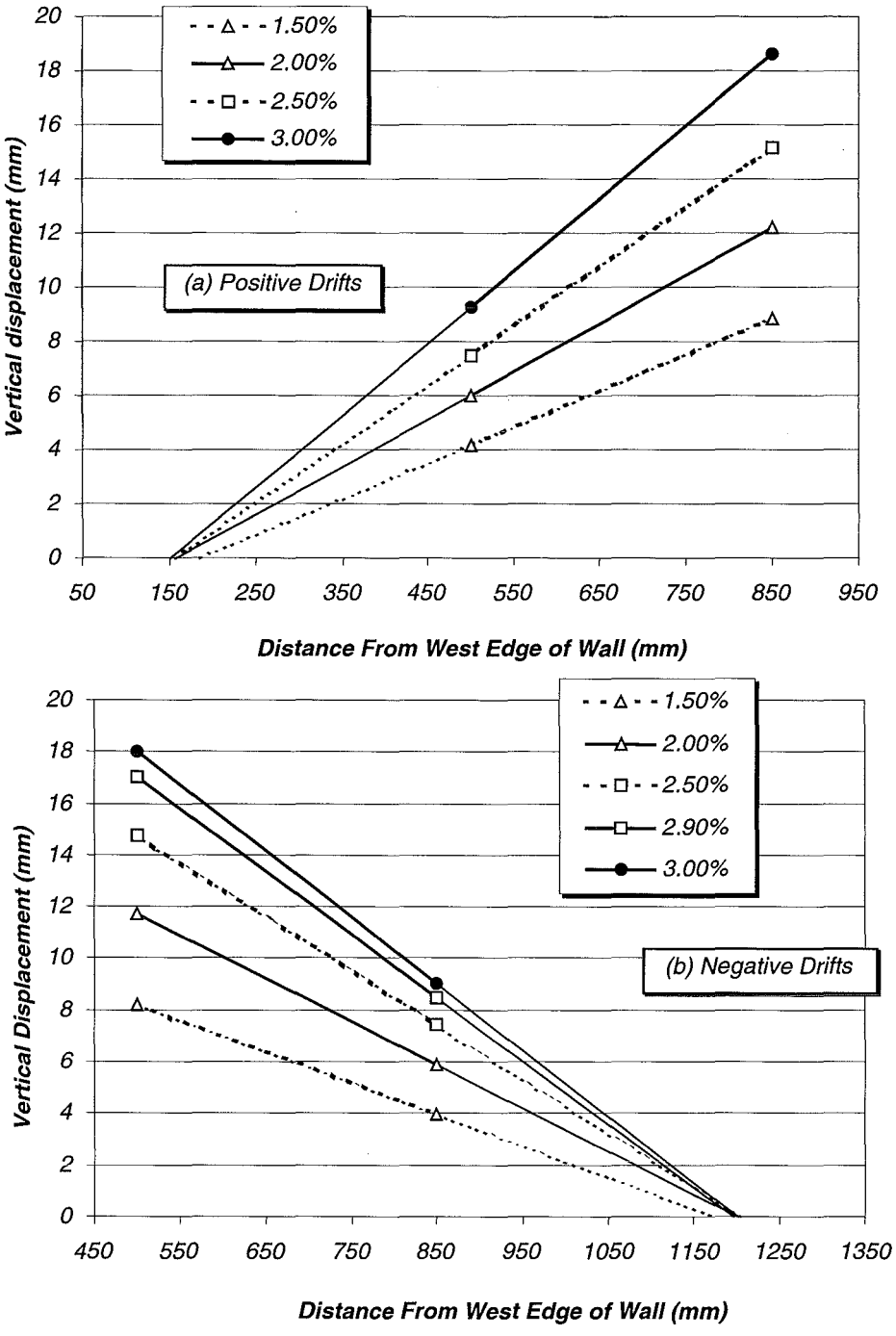

Figure 6.16: Vertical displacement of Unit 2 at the construction joint corresponding to different lateral drift levels.

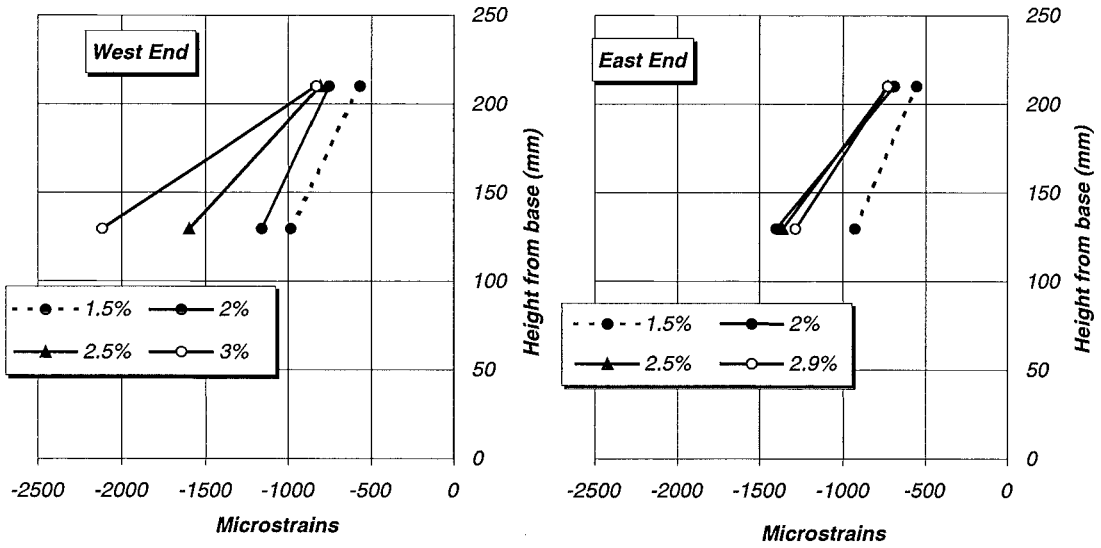

Figure 6.17: Concrete compressive strains at ends of Unit 2.

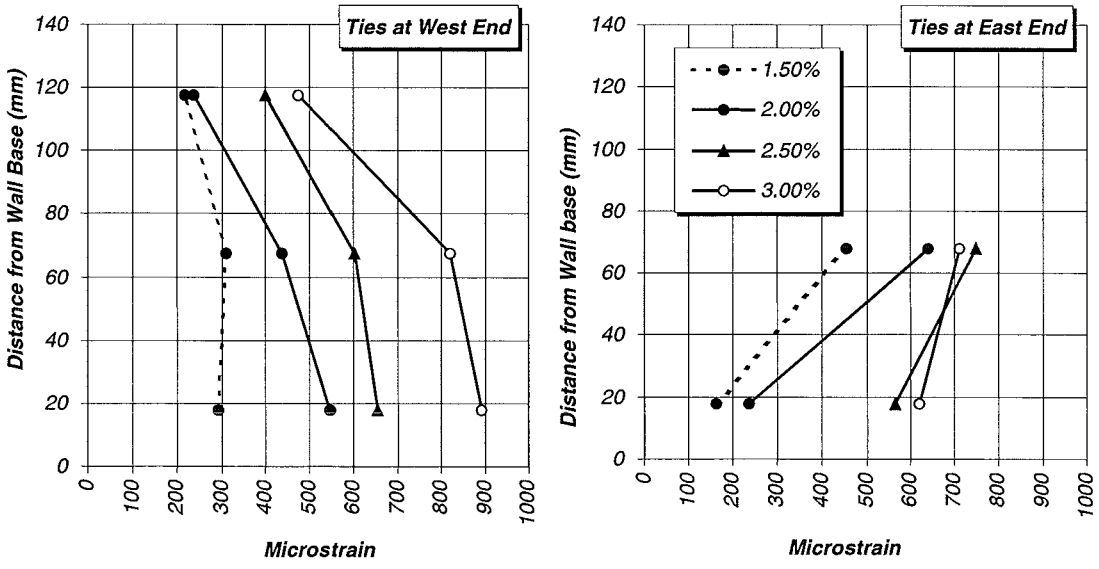

Figure 6.18: Tensile strains in confining ties at ends of Unit 2.

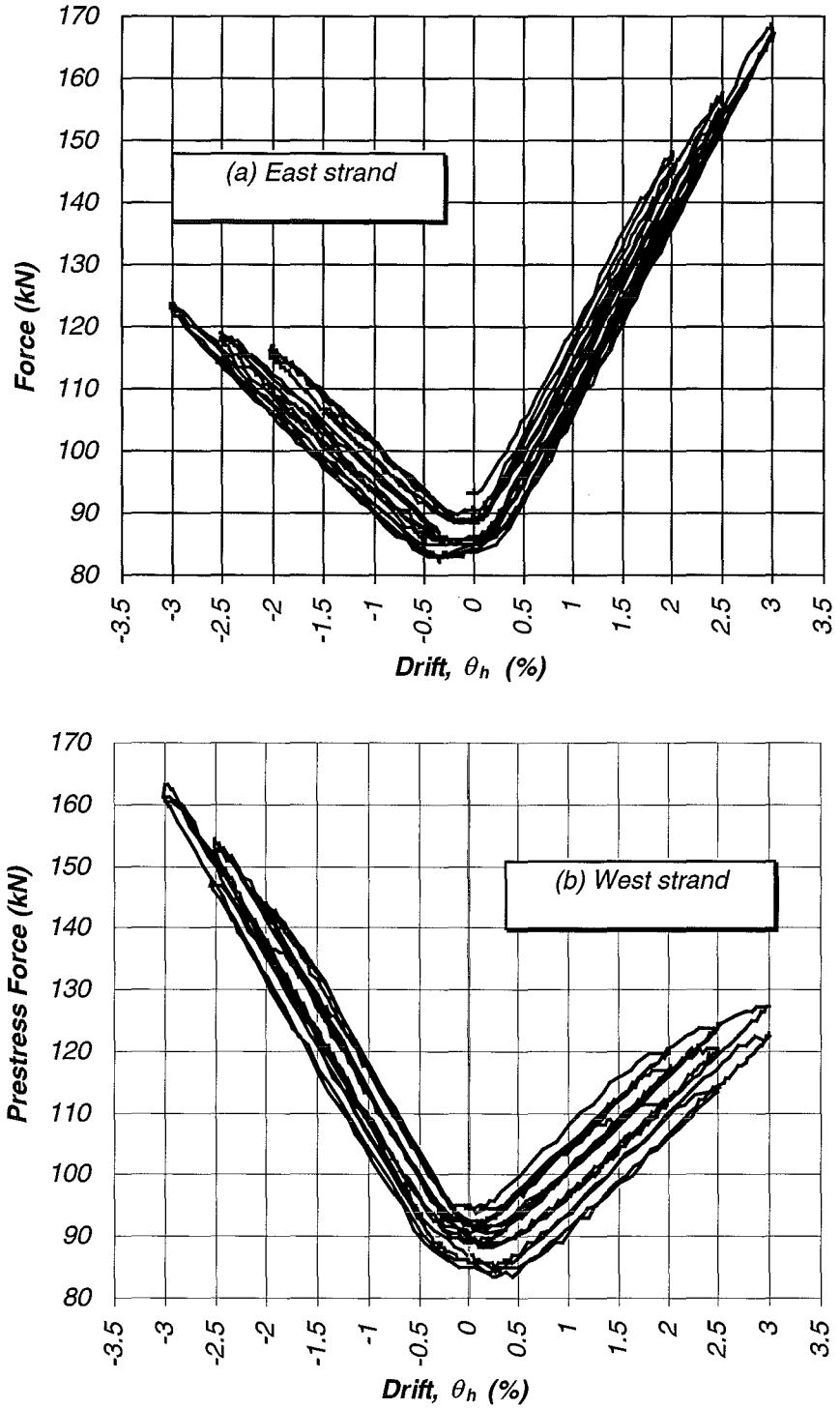

Figure 6.19: Forces developed in prestressing strands during testing of Unit 2.

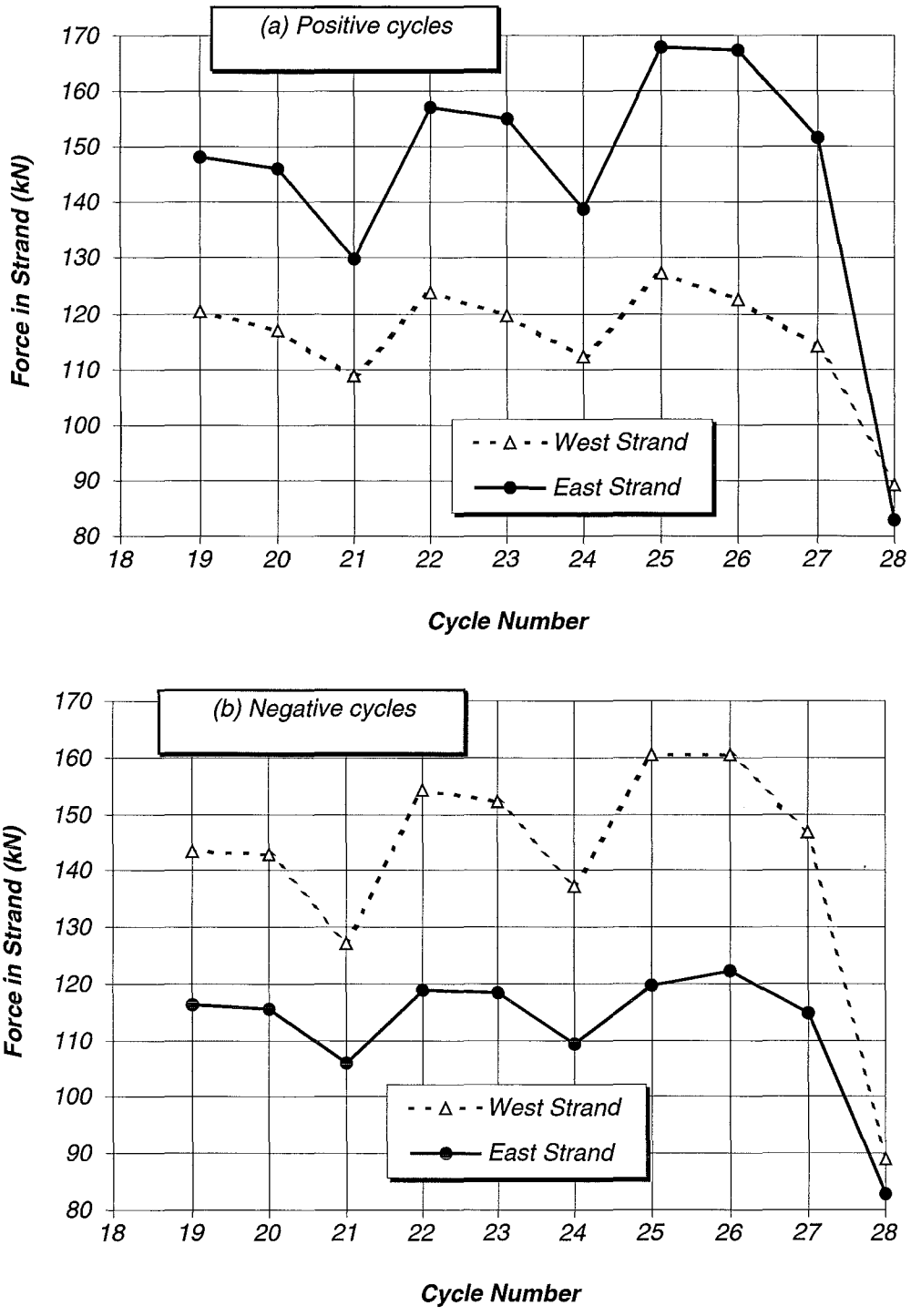

Figure 6.20: Maximum forces in prestressing strands of Unit 2 at the different loading cycles.

6.3 Unit 3

A constant axial load of 200 kN was applied to Unit 3 by means of two external 23 mm diameter post-tensioning bars connected to the strong floor, see Figures 5.9 to 5.11. Two energy dissipators were incorporated in this unit. The dissipators were designed following Section 4.5, which resulted in a milled segment with a diameter of 16 mm. The wall was built with a 15 mm x 15 mm chamfer at the ends in an effort to reduce the cosmetic damage expected to occur as a result of rocking.

The reversed cyclic quasi-static loading history applied to Unit 3 is shown in Figure 6.21 and is also tabulated in Table 6.3. Two cycles of an excursion to a large drift level was followed by one cycle to a lower level of drift.

A crack at the wall-foundation beam interface extended near the full length of the wall at 0.2% drift at which point lift-off was considered to have occurred. In addition, vertical hairline cracks developed on both faces of the wall at this stage at the location of the east energy dissipator, see Figure 6.22. Similar cracks developed at the west dissipator at the next drift level (0.25%) extending approximately 250 mm vertically. Horizontal hairline cracks developed on the west edge 1260 mm from the base of the wall during the second excursion into cycle 11 (0.24% drift) and extended along the south face. A corresponding horizontal crack developed on the east edge extending 400-500 mm along both faces at the next cycle of loading (being the first excursion to 0.5%). Spalling of the concrete the wall ends commenced at 0.5% drift (cycle 13). The end regions where concrete spalled off were confined to within 200 mm vertically and horizontally at the conclusion of the test, see Figures 6.22 and 6.23. A network of inter-connected hairline cracks developed on both faces of the wall spanning the distance between the energy dissipators, see Figure 6.22. These cracks are attributed to the tensile forces induced in the concrete arising from anchorage of the dissipators.

The presence of the energy dissipators is evidenced by the hysteretic lateral force-drift response of Unit 3 shown in Figure 6.24. The response shows that no strength degradation occurred before 3% drift and that the degradation that followed was small and occurred gradually as the drift applied increased. The prestressing force together

with the externally applied compressive axial force provided a restoring force that enabled the wall to return its original position after unloading. The apparent loss of stiffness at large drifts seen in Figure 6.24 is associated with unrecoverable compressive strains developed in the concrete and the mortar bed at the wall ends.

The axial force versus average longitudinal strain response estimated for the east energy dissipator is plotted in Figure 6.25. The force shown in the vertical axis of Figure 6.25 (a) was derived from the upper pair of strain gauges whereas the force shown in the vertical axis in Figure 6.25 (b) was obtained from the lower pair of strain gauges. The compressive forces derived from the upper and lower strain gauge readings are very similar, except only in the initial cycles of response where the forces derived from the lower strain gauges is smaller than that derived from the upper gauges. In contrast, the tensile forces obtained from the lower strain gauges are consistently smaller than those derived from the upper gauges. This is because anchorage forces developed at the lower tapered end of the milled segment. Thus, forces transferred to the weld-plate, and monitored by the lower strain gauges, were found to be smaller. Note that the response obtained from the energy dissipators is in excellent agreement with the conceptualised behaviour depicted in Figure 4.5 used for establishing the design equations in Section 4.4.

The tensile forces obtained for the east dissipator at the peak of each cycle are plotted in Figure 6.26. The yield force, 92.5 kN, for the 16 mm diameter milled segment of was attained at 1% drift (cycles 14 and 15).

Figure 6.27 shows the equivalent viscous damping ratios obtained from the hysteretic response of Unit 3. The equivalent viscous damping was derived using Equation 6.1. The equivalent viscous damping ratio was relatively high during loading cycles to less than 0.1% drift. This ratio decreased and reached a minimum during the loading cycles to 0.2% as cracking developed in the wall panel and in the foundation beam. Further cycles to greater drifts resulted in an increase in the damping ratio. This was chiefly due to yielding of the energy dissipators. The damping ratio was observed to be smaller in the second and third cycles to the same drift level. This is mainly because during the first cycle of loading some energy had been dissipated through the

concrete in compression at the wall ends.

The vertical displacements of the lowest pair of 30 mm potentiometers at the base of the wall (see P4 and P5 in Figure 5.18), are shown in Figure 6.28. The base rotation, obtained from the slope of these lines, dominated the response of this unit. For example, base rotation accounted for up to 80% of the applied lateral displacements at the peak of the cycles to 3% drift.

The position of the neutral axis depth, obtained from the intersection with the x-axis of the lines shown in Figure 6.28, varied between 220 and 250 mm during the cycles to positive drifts at 1% and 3% drift, respectively. Similar values, 200 and 250 mm, were deduced for the cycles to negative drifts for the same drift.

The initial forces in the prestressing tendons directly prior to testing were 92.5 kN (50.4% f_{psu}) and 91 kN (49.6% f_{psu}) in the west and east tendons, respectively. The variation of the forces in the tendons with the applied drifts is presented in Figure 6.29 with the maximum force in each cycle shown in Figure 6.30. The force corresponding to the true limit of proportionality of the prestressing tendons of 143.5 kN was first exceeded during cycle 23 at 2.4% and 2.5% drift in the positive and negative directions of loading. The west and east tendons sustained losses of 12.5% and 19.3%, respectively, at the end of the test as may be seen in Figure 6.30.

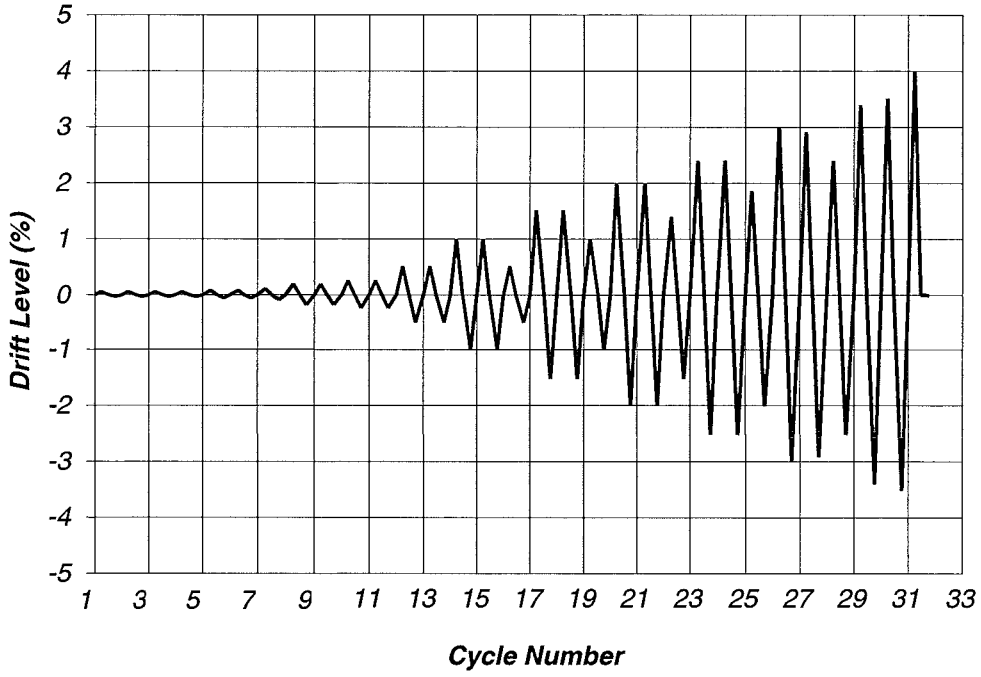

Figure 6.21: Loading regime applied in testing of Unit 3.

Table 6.3: Peak drifts monitored during the test of Unit 3.

	Cycle	1-2	3-4	5-6	7	8-9	10	11	12-13	14-15	16	17-18	19
Drift	+ve	0.03	0.04	0.06	0.09	0.20	0.25	0.24	0.50	1.0	0.5	1.5	1.0
	-ve	0.05	0.05	0.08	0.10	0.20	0.24	0.24	0.50	1.0	0.5	1.5	1.0
	Cycle	20-21	22	23-24	25	26	27	28	29	30	31		
Drift	+ve	2.0	1.4	2.4	1.9	3.0	2.9	2.4	3.4	3.5	4.0		
	-ve	2.0	1.5	2.5	2.0	3.0	2.9	2.5	3.4	3.5	0.0		

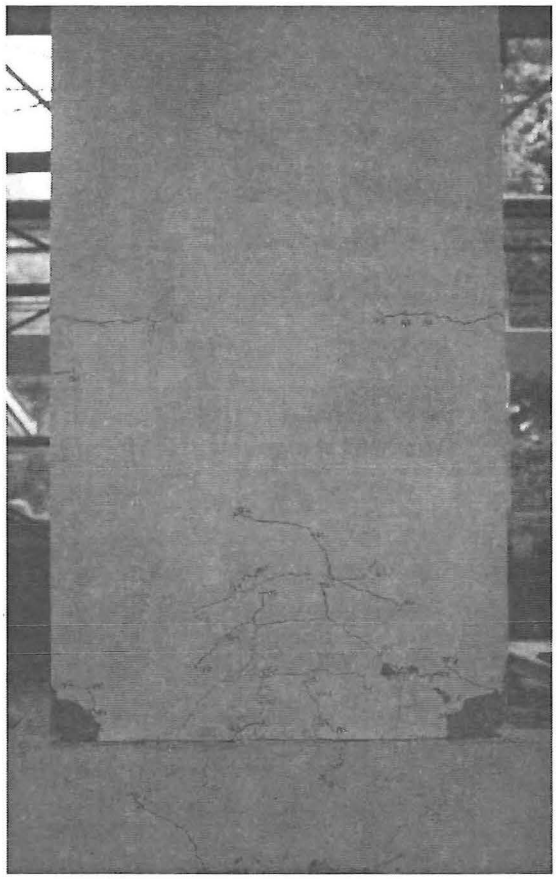

Figure 6.22: North face of Unit 3 at end of test.

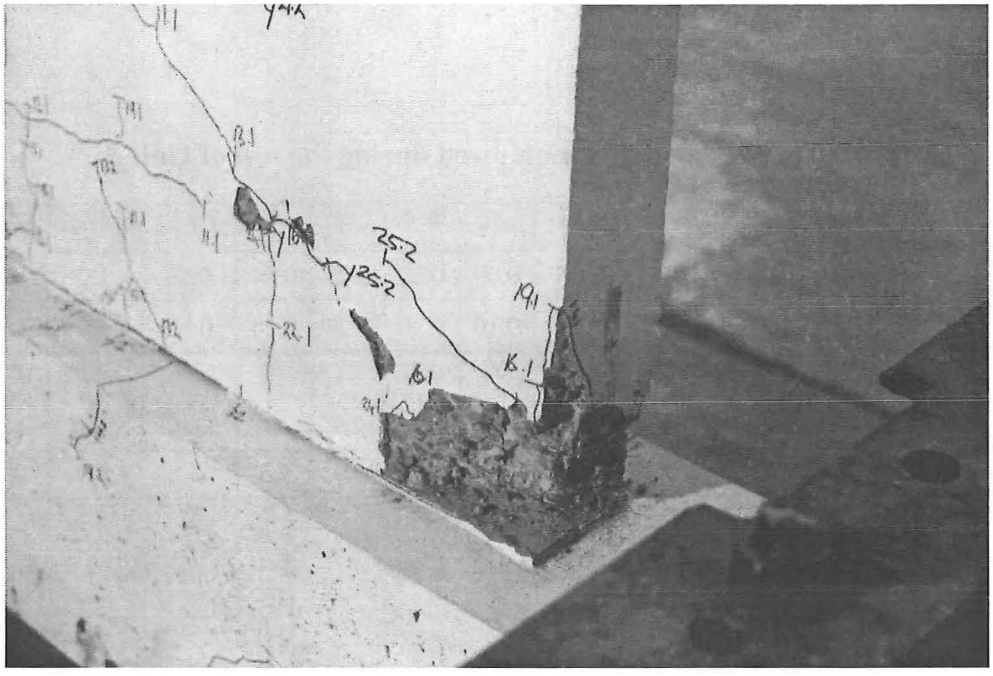

Figure 6.23: North face (west end) of Unit 3 at end of test.

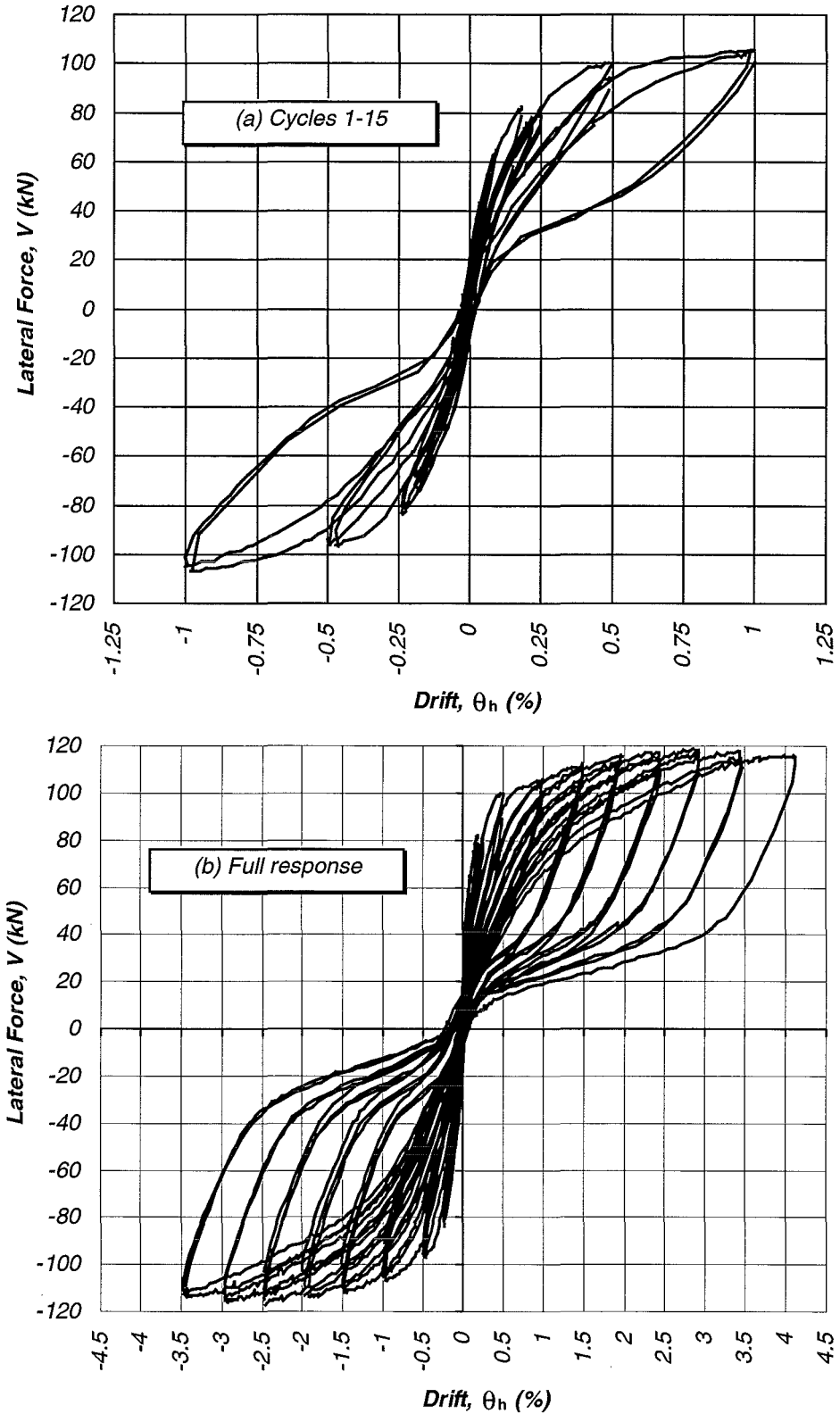

Figure 6.24: Lateral force-drift response of Unit 3.

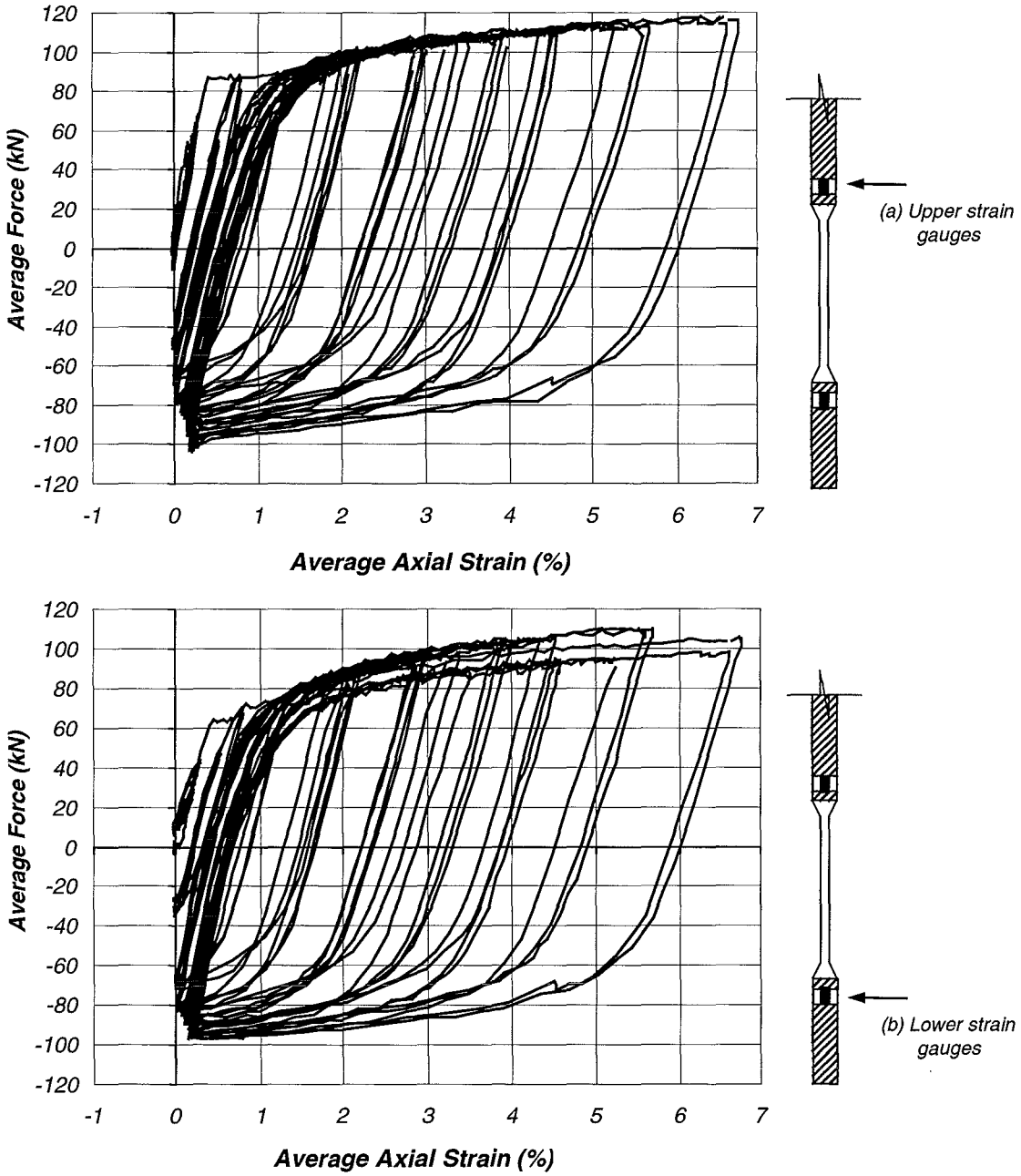

Figure 6.25: Force-strain characteristics of (east) energy dissipator in Unit 3.

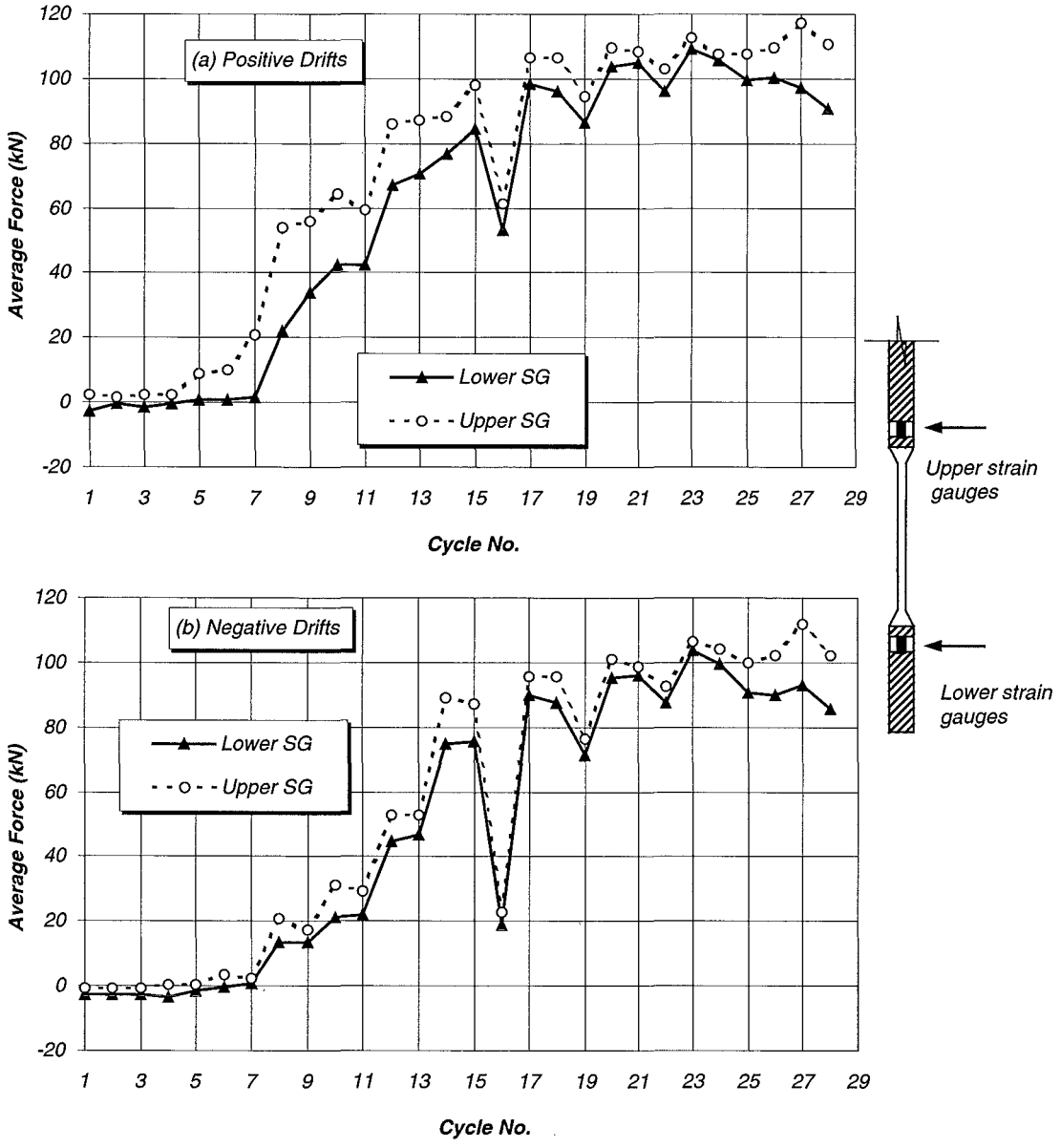

Figure 6.26: Maximum forces developed in (east) energy dissipator in Unit 3.

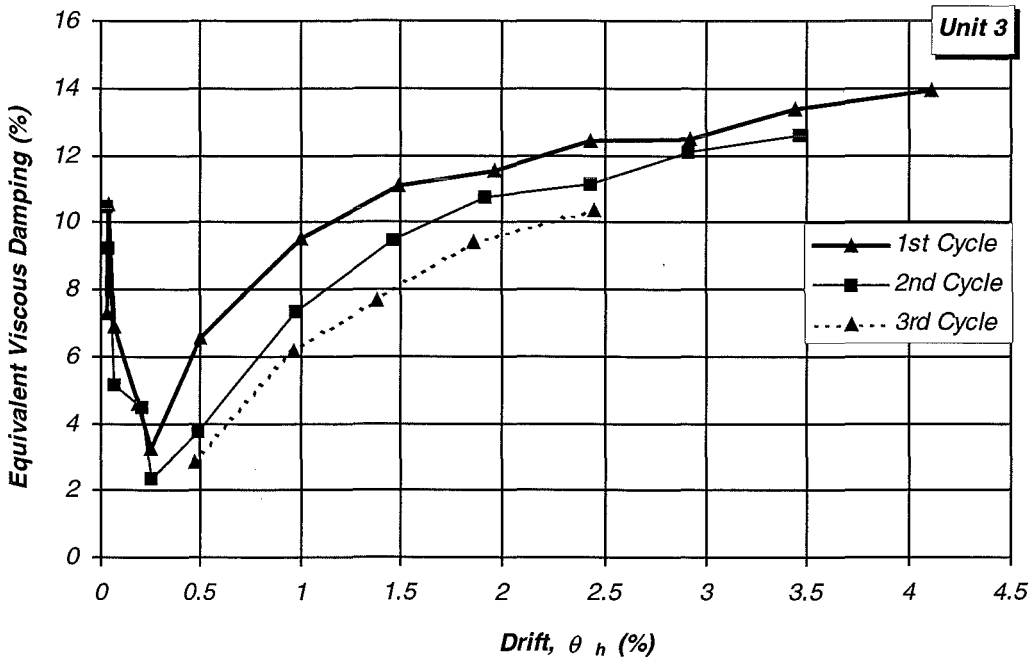

Figure 6.27: Equivalent viscous damping per cycle provided by energy dissipators in Unit 3.

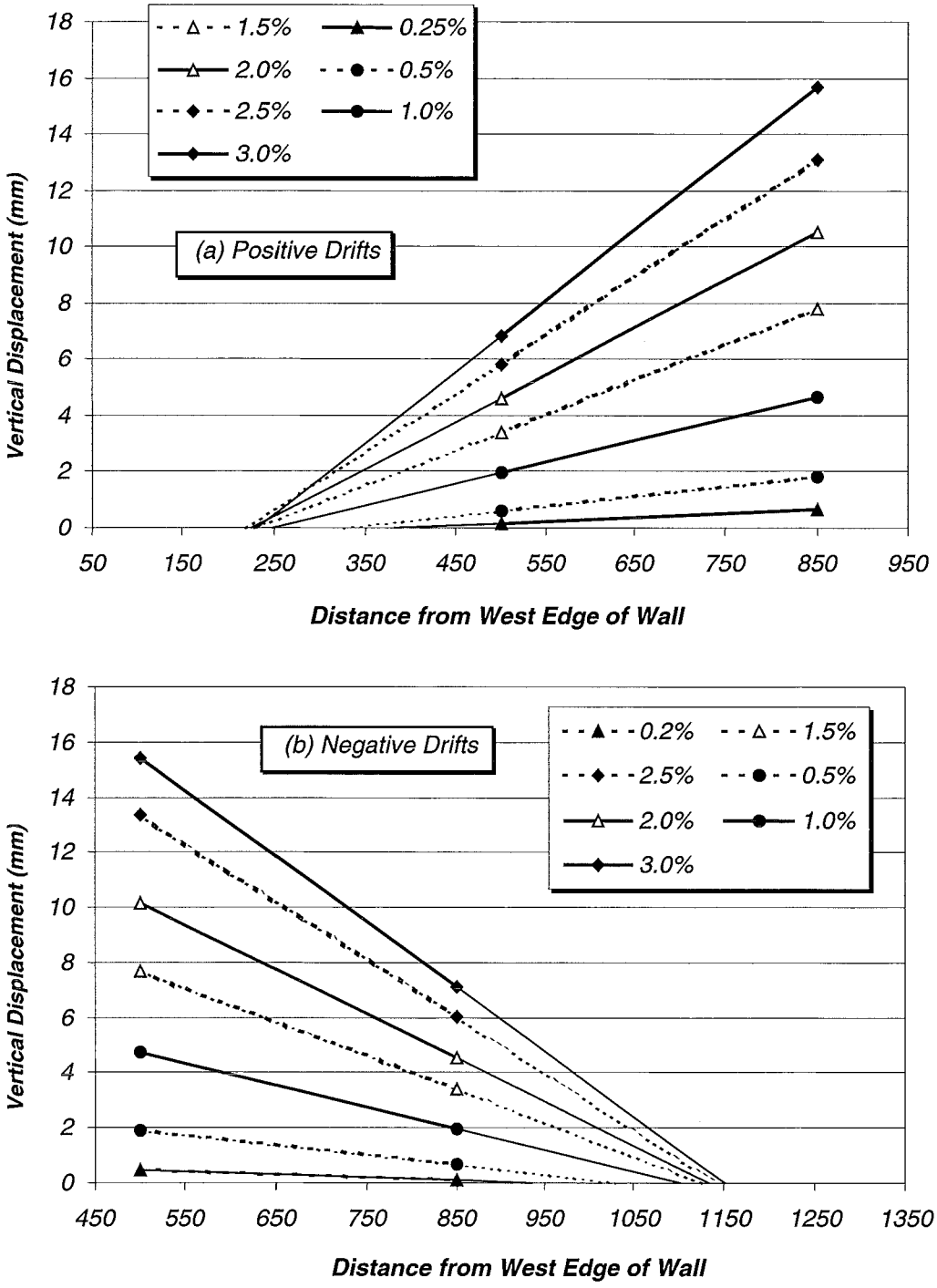

Figure 6.28: Vertical displacement of Unit 3 at the construction joint corresponding to different lateral drift levels.

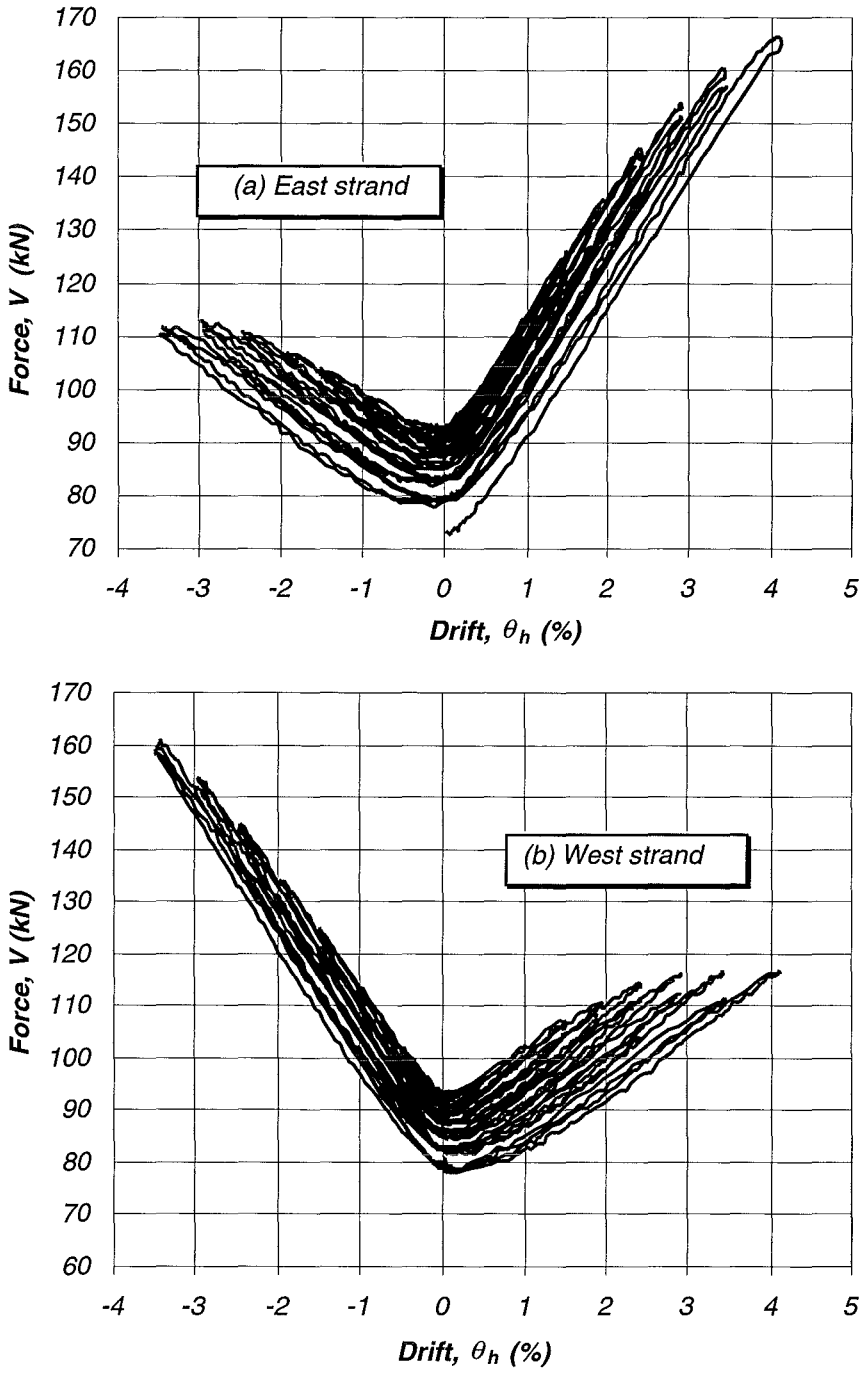

Figure 6.29: Forces developed in prestressing strands during testing of Unit 3.

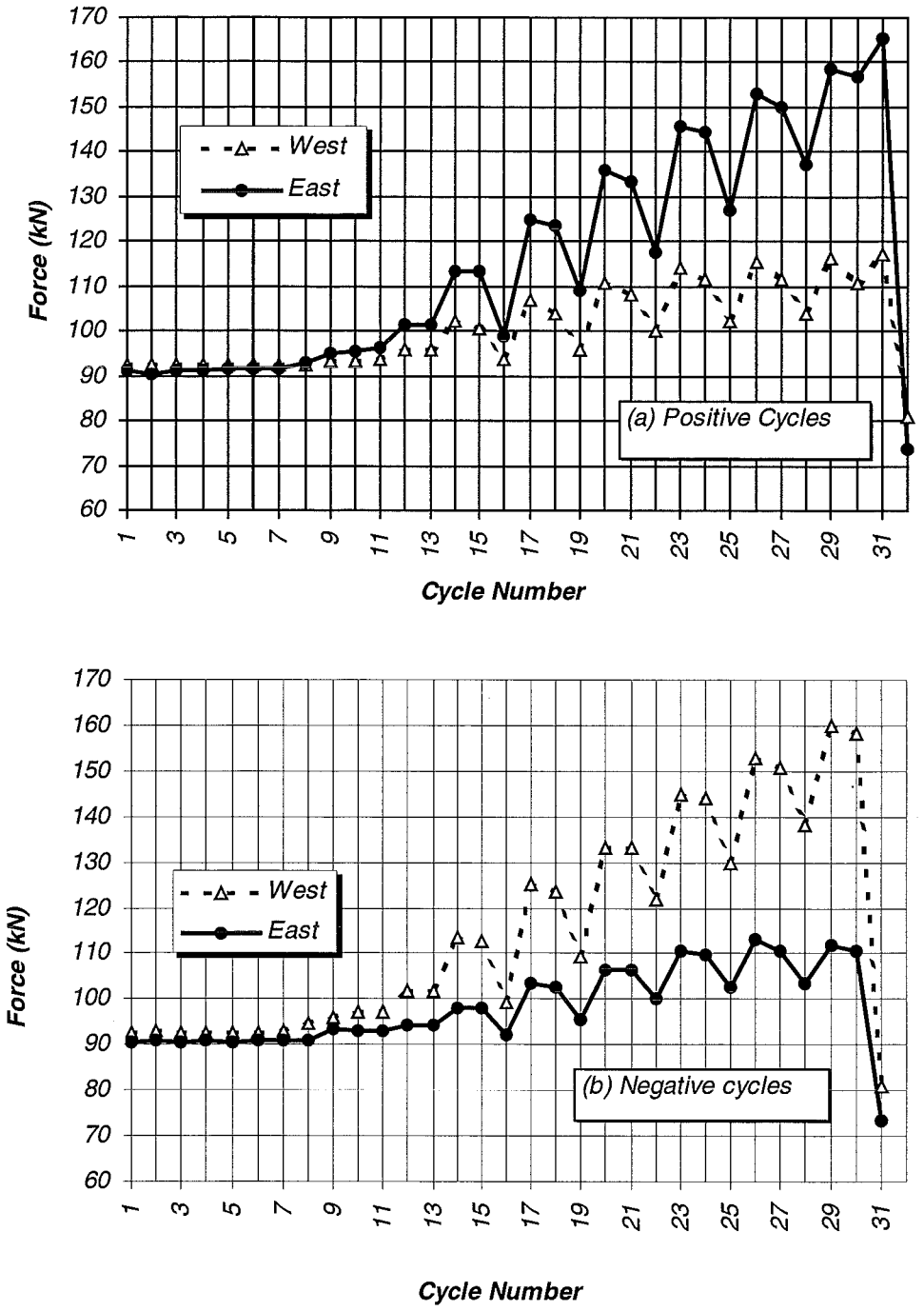

Figure 6.30: Maximum forces in prestressing strands of Unit 3 at the different loading cycles.

7. DISCUSSION

7.1 Overall Response

The precast concrete wall system relying on unbonded prestressing tendons investigated in this study showed unique non-linear elastic response characteristics, namely, origin-centred response under the experimentally-applied quasi-static loading. The limited energy dissipation, distinctive of these types of systems, was augmented through the addition of simple devices that relied on the yielding characteristics of standard steel reinforcing bars. The experimental work conducted on three half-scale precast concrete walls indicates minimal damage and minimal residual drifts when subjected to drift levels in excess of 2.5%.

Elastic response of the prestressing tendons up to the design drift level guarantees a self-centering mechanism for the rocking walls. The main advantage of this type of system is the reduction of repair costs for the owner and elimination of business downtime after a major and/or moderate seismic event. In light of current labour-intensive practices expended in the connections of precast concrete elements, which are necessary to fulfil code requirements, it is envisaged that a reduction in construction time, and thus initial costs, can be achieved with the proposed system.

7.2 Prediction of the Response

The lateral force-drift response of a system utilising the proposed connection mechanism may be characterised by a bi-linearly elastic response as outlined in Section 4.5.

Figure 7.1 plots the response of the three test units in terms of lateral force-drift recorded at the peak lateral-displacement cycles. The theoretical response, determined using the procedures outlined in Section 4.5, is plotted using two different definitions for the yield strength of the tendons. The first definition is associated with

the true limit of proportionality of the tendons as determined from a tensile test. The second definition for the yield strength is associated with the tendon stress corresponding to 0.2% offset strain.

The response of the test units is in good agreement with the theoretical prediction, apparently except for the response of Unit 1 when loaded in the negative direction, see Figure 7.1 (a). Figure 7.1 (a) shows the load response envelope obtained from Unit 1 based on overturning moment calculated at the base of the wall. The overturning moment was computed using data from the load cells monitoring the force in the tendons and accounting for the weight of the wall unit. In the calculations, it was assumed the resulting compressive force act at the corner of the wall. Consequently, the overturning moment obtained is the greatest that could have developed. The lateral force lateral displacement response obtained from this calculation is in excellent agreement with the theoretical response. This suggest that the force measured by the load cell placed in series with the horizontal actuator at the top of the wall unit recorded was greater than that inducing the overturning moment at the base of the wall. Such disparity could possibly be attributed at frictional forces developing in restraint beam due to misalignment.

Figure 7.1 shows conclusively that the theoretical lateral displacement capacity obtained from Equation 4.41 is quite sensitive to the stress value chosen for the limit of proportionality of the tendon, f_{lp}. When the yield strength is associated with the true limit of proportionality, the lateral displacement capacity is greatly underestimated. An excellent prediction is obtained when the stress associated with 0.2% offset strain is used as the tendon's yield strength. However, use of the latter value in design implies loss in the prestressing force at deformation levels exceeding those corresponding to the true limit of proportionality in the tendons. For this reason, it is recommended that the true limit of proportionality be used in design for checking the collapse prevention limit state.

7.3 Other Considerations

Limited non-linear response of the compressed concrete in the toes of the walls and mortar bed at the wall ends contributed to the degradation in the stiffness of the walls. This was particularly evident in Unit 3, which incorporated large-diameter energy dissipators and an additional axial load applied at the top of the wall. It is believed that such degradation can by minimised by externally armouring the wall ends and/or by increasing the amount of confining reinforcement in this region.

The fracture of an energy dissipator in Unit 2 at 2% drift necessitates further investigation to establish the main reason for the unexpected behaviour. Inaccuracies in the milling process and small-amplitude sliding shear between the wall unit and the foundation beam during wall rocking could have accelerated the fracturing process.

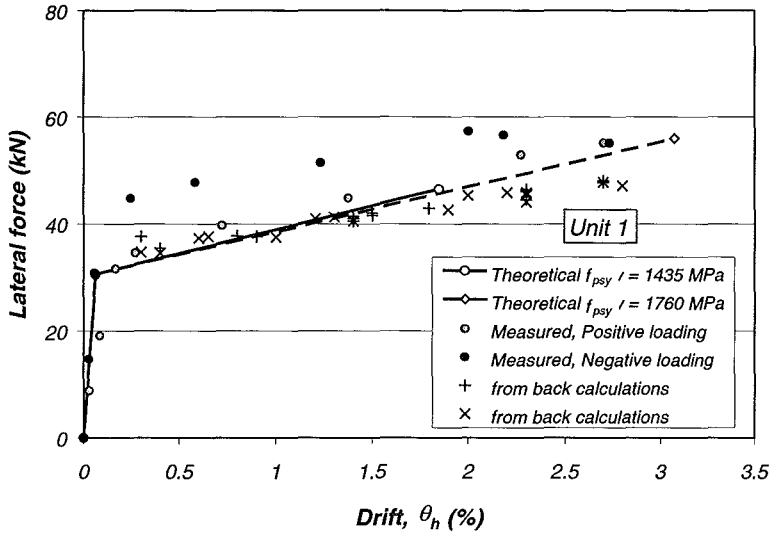

(a) Unit 1

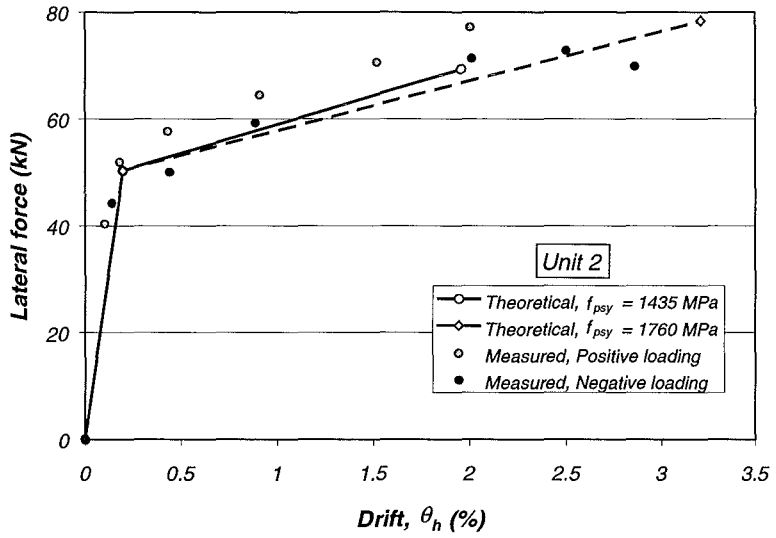

(b) Unit 2

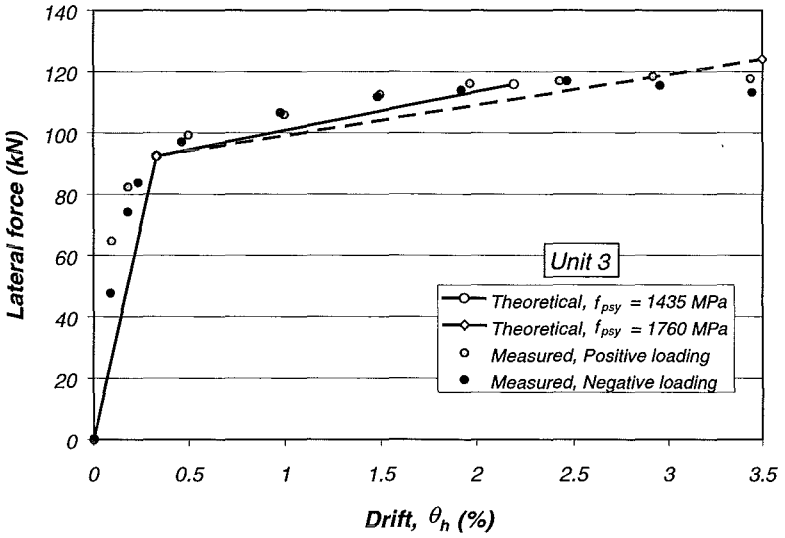

(c) Unit 3

Figure 7.1: Measured versus predicted lateral force-drift response of Units 1, 2 and 3, respectively.

8. CONCLUSIONS

1. The unique response characteristics of a precast concrete cantilever wall system that relies on unbonded prestressing tendons as a connection mechanism were investigated in this study. The proposed system ensures minimal structural damage during a major or moderate seismic event in addition to the absence of post-earthquake residual drifts in the system. Elastic response of the prestressing tendons up to design level lateral loading demands guarantees a self-centering mechanism for the wall system.

   An advantage of the system investigated is the reduction of repair costs for the owner and practical elimination of business downtime after a major and/or moderate seismic event. In addition, it is envisaged that a reduction in construction time, and thus initial costs, can be achieved with this type of system compared to conventional precast and cast-in-place systems currently used.

2. The lateral load-displacement response of a system utilising the proposed connection mechanism may be characterised by a bilinearly elastic response. When the overturning moment due to the lateral forces equals the moment due to the stabilising forces, decompression occurs at the horizontal joint at one end of the wall. A gap forms at this end and extends along the horizontal joint with increasing magnitude of the lateral force. The limit of proportionality, at which a reduction in the lateral stiffness of the system occurs, is attained when this gap extends a sufficient distance along the length of the horizontal joint.

   As a result of this bilinearly elastic response, limited energy can be dissipated due to impacting of the wall against the foundation structure and through radiation to the soil. Damage in the precast concrete wall unit is limited to spalling of the cover concrete at the toes of the wall and no residual post-earthquake drifts are expected to occur before the tendons reach the limit of proportionality.

3. Energy dissipation capacity can be incorporated into the system through the use of mild steel bars with a milled segment in the form of a "dog-bone", which resemble the starter bars currently in wide use in precast concrete construction. These "dog-bones" are cast in the foundation and then grouted into the wall. Energy

dissipation is effected through extensive yielding of these "dog-bones" in tension and compression in the tensile strain domain within the milled portion of the bar. Buckling in the dissipators is unlikely to occur as the milled portion of the bar is surrounded by the concrete grout. The diameter of the milled segment is selected such that closing of the gap at the horizontal connection is ensured upon unloading. Thus, the prestressing force after losses, in addition to the gravity loads, must be sufficient to ram the "dog-bones" to nominally zero strain upon unloading. Consequently, no residual displacements will ever occur. The lengths of the non-milled segments are such that the full tensile strength of the bar may be developed in the milled segment while the non-milled segments remain elastic.

4. Preliminary theoretical investigations were conducted as part of the current project to ascertain the dimensions of the wall units to ensure predominately rocking response, to determine the necessary amount of prestressing reinforcement, establish the dimensions of the energy dissipators and to predict the lateral force-lateral displacement response of the wall units. The location of the prestressing strands along the wall length and the prestressing force after losses were selected such that the prestressing strands would maintain their elastic response characteristics at 2.5% drift.

5. Tests conducted as part of this research work involved three half-scale reinforced concrete walls connected to a supporting reinforced concrete foundation beam by means of unbonded prestressing strands. Two of the specimens (Units 2 and 3) incorporated hysteretic energy dissipators in the form of dog-bones while gravity load effects were simulated by means of external post-tensioning on one of these specimens (Unit 3). End confinement at the toes of the precast walls was provided in the form of hoops, which differed in extent due to the differing strength capacities of the walls. Various levels of quasi-static lateral drifts were applied in which two large amplitude loading cycles were followed by a smaller amplitude cycle to the previous lower drift level.

6. The lateral load-displacement response of Unit 1 (no energy dissipation device or externally applied gravity loads) was characterised by a bilinearly elastic relationship. The horizontal extension of the separation gap between the wall and supporting foundation beam, in addition to limited inelastic response of the

concrete at the compression ends of the wall, effected a reduction in the initial stiffness (measured at small amplitude lateral displacements) of the precast concrete wall. A separation gap developed at the horizontal joint between the wall and the supporting foundation beam as the wall responded to the applied lateral drifts in a predominately rigid body rotation mode. Consequently, the precast concrete wall units sustained very little damage and no residual deformations occurred at the end of the tests. Damage was limited to spalling of the cover concrete at the ends of the walls. The initial stiffness was maintained even after a number of excursions to large lateral drift levels. The response of this unit showed little energy dissipation capacity, as was expected.

7. Units 2 and 3, which included energy dissipators, were also characterised by the lack of residual drifts and damage to the precast wall units after the test. The hysteretic response of the units was origin-centered with energy being dissipated by the milled bars between the wall panel and the foundation beam. The efficacy of the energy dissipators was clearly demonstrated, with a 14 percent equivalent viscous damping ratio attained in both tests.

8. Damage that was sustained by all three specimens was cosmetic and manifested itself as spalling of the concrete cover at the ends of the walls at relatively large drifts. Spalling of the concrete took place due to the large compressive strains, which developed at the ends of the wall due to rocking. The preclusion of plastic hinges at the base of the wall to provide the lateral drift capacity and energy dissipation mechanism resulted in the absence of damage to the wall panels. The lack of damage confirms that no special provisions are required with regards to either the transverse reinforcement or main longitudinal reinforcement as in the design of conventional cast-in-place wall panels.

9. While the energy dissipators incorporated into Units 2 and 3 met the desired objectives in terms of improving the energy dissipation characteristics of the system, the unexpected fracture of an energy dissipator at 2% drift in Unit 2 prompts the need for further study of the behaviour of such device. The machining process and tolerances as well as the possible detrimental effect that small sliding shear of the wall unit relative to the foundation beam should be further investigated.

REFERENCES

[B1] Building Seismic Safety Council, *NEHRP Recommended Provisions for Development of Seismic Regulations for New Buildings*, BSSC, Washington, D.C., 1994.

[C1] Cheok, G.S., Stone, W.C. and Kunnath, S.K., "Seismic Response of Precast Concrete Frames with Hybrid Connections", *ACI Structural Journal*, Vol. 95(5), September-October 1998, pp. 527-539.

[C2] Chopra, A.K., *Dynamics of Structures: Theory and Applications to Earthquake Engineering*, Prentice Hall, Inc., N.J., 1995.

[C3] Collins, M.P. and Mitchell, D., *Prestressed Concrete Structures*, Response Publications, Toronto, Canada, 1997.

[E1] El-Sheikh, M.T., Sause, R., Pessiki, S. and Lu, L-.W., "Seismic Behaviour and Design of Unbonded Post-Tensioned Precast Concrete Frames", *PCI Journal*, Vol.44(3), May-June 1999, pp. 54-71.

[G1] *Guidelines for the Use of Precast Concrete in Buildings*, Report of a Study Group of the New Zealand Concrete Society and the New Zealand Society for Earthquake Engineering, (ed.) A.W. Charleson, The Printery, University of Canterbury, Christchurch, New Zealand, August 1991.

[K1] Kurama, Y., Sause, R., Pessiki, S. and Lu, L-.W., "Lateral Load Behavior and Seismic Design of Unbonded Post-Tensioned Precast Concrete Walls", *ACI Structural Journal*, Vol. 96(4), July-August 1999, pp. 622-632.

[K2] Kurama, Y., Sause, R., Pessiki, S., Lu, L-.W. and El-Sheikh, M., *Seismic Design and Response of Unbonded Post-Tensioned Precast Concrete Walls*, PRESSS Report No. 98/03 (LU Report No. EQ-97-01), Department of Civil and Environmental Engineering, Lehigh University, Bethlehem, Pennsylvania, USA, 1998.

[K3] Kurama, Y. *Seismic Analysis, Behavior, and Design of Unbonded Post-Tensioned Precast Concrete Walls*, PhD Dissertation, Department of Civil and Environmental Engineering, Lehigh University, Bethlehem, Pennsylvania, USA, May 1997.

[L1] Laursen, P. and Ingham, J., "Design of Prestressed Concrete Masonry Walls", *Journal of the New Zealand Structural Engineering Society*, Vol. 12(2), September 1999, pp.21-39.

[M1] MacRae, G.A. and Priestley, M.J.N., *Precast Post-Tensioned Ungrouted Concrete Beam-Column Subassemblage Tests*, Report No. SSRP-94/10, Department of Applied Mechanics and Engineering Sciences, University of California, San Diego, California, USA, 1994.

[M2] McMenamin, A., *The performance of slender precast reinforced concrete cantilever walls with roof level lateral displacement restraint under simulated in-plane seismic loading*, Civil Engineering Research Report 99/4, Department of Civil Engineering, University of Canterbury, Christchurch, New Zealand, March 1999.

[N1] Nakaki, S.D., Stanton, J.F. and Sritharan, S., "An Overview of the PRESSS Five-Story Precast Test Building", *PCI Journal*, Vol. 44(2), March-April 1999, pp. 26-39.

[P1] Palmieri, L., Saqan, E., French, C. and Kreger, M., "Ductile Connections for Precast Concrete Frame Systems", *Proceedings Mete A. Sozen Symposium*, SP 162-13, (eds.) J.K. Wight and M.E. Kreger, American Concrete Institute, Farmington Hills, Mich., USA, 1996, pp.313-355.

[P2] *Performance based seismic engineering of buildings*, prepared by Structural Engineers Association of California, Vision 2000 Committee, (ed.) J. Soulages, Sacramento, Calif., USA, 1995.

[P3] Priestley, M.J.N., "Overview of PRESSS Research Program", *PCI Journal*, Vol. 36(4), July-August 1991, pp. 50-57.

[P4] Priestley, M.J.N. and Tao, J.R.T., "Seismic Response of Precast Prestressed Concrete Frames with Partially Debonded Tendons", *PCI Journal*, Vol. 38(1), January-February 1993, pp. 58-69.

[P5] Priestley, M.J.N., Sritharan, S., Conley, J.R. and Pampanin, S., "Preliminary Results and Conclusions From the PRESSS Five-Story Precast Concrete Test Building", *PCI Journal*, Vol.44(6), November-December, 1999, pp.42-67.

[P6] Paulay, T. and Priestley, M.J.N. *Seismic Design of Reinforced Concrete and Masonry Buildings*, John Wiley and Sons, Inc., NY, USA, 1992.

[R1] Restrepo, J.I., Crisafulli, F.J. and Park, R., *Earthquake Resistance of Structures: The Design and Construction of Tilt-Up Reinforced Concrete Buildings*; Research Report 96-11, Department of Civil Engineering, University of Canterbury, Christchurch, New Zealand, Sept. 1996.

[S1] Standards New Zealand, NZS 4203: 1992 (Parts 1 and 2), *Code of Practice for General Structural Design Loadings for Buildings and Commentary*, Wellington, New Zealand, 1992.

[S2] Standards New Zealand, NZS 3101: 1995 (Parts 1 and 2), *Concrete Structures Standard and Commentary*, Wellington, New Zealand, 1995.

[S3] Stanton, J.F., Stone, W.C. and Cheok, G.S., "A Hybrid Reinforced Precast Frame for Seismic Regions", *PCI Journal*, Vol. 42(2), March-April 1997, pp. 20-32.

[S4] Stone, W.C., Cheok, G.S. and Stanton, J.F., "Performance of Hybrid Moment-Resisting Precast Beam-Column Concrete Connections Subjected to Cyclic Loading", *ACI Structural Journal*, Vol. 91(2), March-April 1995, pp. 229-249.

[S5] Standards Association of Australia, AS 1311: 1987, *Steel Tendons for Prestressed Concrete- 7-Wire Stress Relieved Steel Strand for Tendons in Prestressed Concrete,* Australia, 1987.

[V1] *VSL Construction Systems*, VSL Prestressing (Aust.) Pty. Ltd., 1995.